

Acronym: FLARE  
Project full title: Flooding Accident REsponse  
Grant agreement No. 814753  
Coordinator: BALance Technology Consulting GmbH

---



## Deliverable 4.3



The project has received funding from the European's Horizon 2020 research and innovation programme (Contract No.: 814753)

Duration: 36 months - Project Start: 01/06/2019 - Project End: 31/05/2022

## Deliverable data

<b>Deliverable No</b>	4.3
<b>Deliverable Title</b>	Results of benchmarking
<b>Work Package no: title</b>	WP4.3

<b>Dissemination level</b>	Public	<b>Deliverable type</b>	Report
<b>Lead beneficiary</b>	NAPA		
<b>Responsible author</b>	Pekka Ruponen (NAPA)		
<b>Co-authors</b>	Markus Tompuri (NAPA) & Daniel Lindroth (NAPA)		
<b>Date of delivery</b>	30-04-2021		
<b>Approved</b>	<b>Name (partner)</b>	<b>Date [DD-MM-YYYY]</b>	
Peer reviewer 1	Apostolos Papanikolaou (NTUA), advisor	23-04-2021	
Peer reviewer 2	Anna-Lea Routi (Meyer Turku)	27-04-2021	

## Document history

Version	Date	Description
1.0	21-04-2021	First version for peer review
1.1	30-04-2021	Revised version based on reviewer and participant feedback

*The research leading to these results has received funding from the European Union Horizon 2020 Program under grant agreement n° 814753.*

*This report reflects only the author's view. INEA is not responsible for any use that may be made of the information it contains.*

The information contained in this report is subject to change without notice and should not be construed as a commitment by any members of the FLARE Consortium. In the event of any software or algorithms being described in this report, the FLARE Consortium assumes no responsibility for the use or inability to use any of its software or algorithms. The information is provided without any warranty of any kind and the FLARE Consortium expressly disclaims all implied warranties, including but not limited to the implied warranties of merchantability and fitness for a particular use.

©COPYRIGHT 2019 The FLARE consortium

*This document may not be copied, reproduced, or modified in whole or in part for any purpose without written permission from the FLARE Consortium. In addition, to such written permission to copy, acknowledgement of the authors of the document and all applicable portions of the copyright notice must be clearly referenced. All rights reserved.*

**CONTENTS**

**List of symbols and abbreviations.....6**

**1 EXECUTIVE SUMMARY.....7**

1.1 Problem definition.....7

1.2 Technical approach and work plan.....7

1.3 Results.....8

1.4 Conclusions and recommendation.....8

1.5 Recommendations for FLARE project.....9

**2 INTRODUCTION.....11**

**3 PREVIOUS BENCHMARK STUDIES.....12**

3.1 ITTC Benchmark on the Capsizing of a Damaged Ro-Ro/Pass. Ship in Waves (2001) 12

3.2 ITTC Benchmark on Numerical Prediction of Damage Ship Stability in Waves (2005) 13

3.3 ITTC Benchmark on Time-to-Flood – Phase 1 (2007).....14

3.4 ITTC Benchmark on Time-to-Flood – Phase 2 (2008).....16

3.5 SAFEDOR Benchmark (2008).....17

3.6 Summary of recommendations.....17

**4 FLARE BENCHMARK OVERVIEW.....19**

4.1 Objectives and Structure.....19

4.2 Schedule.....19

4.3 Material.....20

4.4 Participants.....21

**5 FLARE BENCHMARK A – FLOODING FUNDAMENTALS.....24**

5.1 Overview.....24

5.2 Discharge Coefficients.....24

5.3 Case A1 – Up-Flooding.....25

5.3.1 Description.....25

5.3.2 Results.....26

5.4 Case A2 – Down-Flooding.....28

5.4.1 Description.....28

5.4.2 Results.....29

5.5 Case A3 – Effect of Waves on Cross-Flooding.....32

5.5.1 Description.....32

5.5.2 Results.....33

5.6 Case A4 – Progressive Flooding on Deck.....37

5.6.1 Description.....37



5.6.2	Results.....	40
5.6.3	Computational performance .....	49
<b>6</b>	<b>FLARE BENCHMARK B – CRUISE SHIP FLOODING .....</b>	<b>51</b>
6.1	Model Geometry.....	51
6.2	Comparison of Hydrostatics.....	54
6.3	Roll Decay for Intact Ship .....	56
6.4	Case B1 – Transient Flooding in Calm Water .....	58
6.4.1	Description.....	58
6.4.2	Results.....	58
6.5	Case B2 – Transient and Progressive Flooding in Waves .....	63
6.5.1	Description.....	63
6.5.2	Results.....	64
6.5.3	On the Effects of Drifting.....	70
6.6	Case B3 – Progressive Flooding in Calm Water .....	72
6.6.1	Description.....	72
6.6.2	Results.....	73
6.7	Computational Performance .....	77
6.8	Analysis on Air Compression Effects .....	78
<b>7</b>	<b>FLARE BENCHMARK C – ROPAX SHIP FLOODING .....</b>	<b>81</b>
7.1	Model Geometry.....	81
7.2	Comparison of Hydrostatics.....	83
7.3	Notes on Applied Simulation Codes .....	84
7.4	Case C1 – Transient Flooding in Calm Water .....	85
7.4.1	Description.....	85
7.4.2	Results.....	87
7.5	Case C2 – Transient Flooding in Waves .....	91
7.5.1	Description.....	91
7.5.2	Results.....	92
7.6	Case C3 – Gradual Flooding in Waves.....	95
7.6.1	Description.....	95
7.6.2	Results.....	96
7.7	Computational Performance .....	99
<b>8</b>	<b>SUMMARY AND CONCLUSIONS .....</b>	<b>100</b>
<b>9</b>	<b>ACKNOWLEDGEMENTS .....</b>	<b>103</b>



10 REFERENCES .....104

11 ANNEXES .....107

11.1 Annex A: Public summary.....107

11.2 Annex B: Sensitivity Analyses for Cruise Ship Flooding Cases .....108



## List of symbols and abbreviations

<b>CFD</b>	computational fluid dynamics
<b>CL</b>	centerline
<b>DOF</b>	degree-of-freedom
<b>ITTC</b>	International Towing Tank Conference
<b>RANS</b>	Reynolds-Averaged Navier-Stokes
<b>SWE</b>	shallow water equations
<b>TTC</b>	time-to-capsize
<b>TTF</b>	time-to-flood
<b>VOF</b>	volume of fluid



# 1 EXECUTIVE SUMMARY

## 1.1 Problem definition

Over the past two decades several simulation tools have been developed for time-domain analyses of flooding and motions of damaged ships, both in calm water and in waves. Methods based on hydraulics (Bernoulli's equation) are most common due to computational efficiency. However, recently also CFD (Computational Fluid Dynamics) methods have been applied for a more detailed assessment of the flooding process.

Several Benchmark studies were organized by the International Towing Tank Conference (ITTC), and in addition, many individual validation studies have been published. However, there has not been a wide benchmark study for validation and analyses of the available simulation tools since 2007. The aim of this FLARE Benchmark study is to fill this gap.

Some partners in the FLARE consortium have developed their own flooding simulation codes, but it was recognized that these do not cover the whole range of different approaches for codes that have been implemented. Therefore, participants outside the FLARE consortium were also invited to this Benchmark, in order to get a good overview of the characteristics and capabilities of as many simulation codes as possible. All invited participants have published new innovative approaches to flooding simulation during the recent years.

## 1.2 Technical approach and work plan

Flooding of a damaged passenger ship is a complex process, especially if it happens in waves. Therefore, the benchmark was divided into three separate parts, each concentrating on specific phenomena:

- Part A: flooding fundamentals, with captive models and simplified geometries
- Part B: transient and progressive flooding of a cruise ship
- Part C: transient and gradual flooding of a ropax ship

All participants received details about the studied geometries and test cases. In addition, some key measurement results (graphs) and some videos from the tests were shared beforehand, in order to ensure fair and equal conditions to all participants.

Water levels at sensor locations were the key quantities for comparison in Part A. For Parts B and C, the focus was more on the motions of the flooded ship, especially the development of the roll angle.

Three informal online workshops were organized between the benchmark participants who had provided simulation results. These discussions on the results enabled a better insight into the codes used by the external participants, which was essential for preparing this report, and thus complements the knowhow within the FLARE consortium.



### 1.3 Results

In total, 11 organizations provided results to some parts of the benchmark. Participants from the FLARE consortium were:

- Brookes Bell (BROO)
- DNV
- HSVA
- MARIN
- University of Strathclyde, Maritime Safety Research Center (MSRC)
- NAPA

And external participants:

- China Ship Scientific Research Center (CSSRC), China
- Korea Research Institute of Ships & Ocean Engineering (KRISO), Republic of Korea
- University of Applied Science Kiel (UAK), Germany
- University of Naples “Federico II” (UNINA), Italy
- University of Trieste (UNITS), Italy

The flooding fundamentals (Part A) confirmed that most of the codes can correctly calculate the basic flooding mechanisms, including up and down flooding, and that only one code had significant problems with these cases. Somewhat surprisingly, there was a quite notable deviation in the results for the deck flooding case (Part A4) between the Bernoulli-based simulation codes, indicating possible accumulation of numerical error in the solution of the governing equations.

For the cruise ship flooding cases (Part B), the maximum transient roll angle was predicted rather well by most of the codes, although there was a quite notable variation in the subsequent decrease of the roll until the stable heel angle was reached. In irregular beam seas with a significant wave height of 4.0 m, the same damage scenario resulted in capsizing. All participants could properly capture the capsize, but the variation in the time-to-capsize (TTC) was significant. In general, the simulated TTC was shorter than the observed for all three model test experiments. The benchmark scenarios for cruise ship flooding were extended to include an additional scenario (case B3), with a notable up-flooding and progressive flooding, since simple up-flooding cases were already found to be problematic in Part A1. Unfortunately, experimental data is not yet available for this particular case, but comparisons of the simulated water levels indicate similar results as in Part A1.

The final part of the benchmark considered a damaged ropax vessel, with a 2-compartment breach extending vertically up to the vehicle deck. For transient flooding in calm water, all codes could properly capture capsize and survival cases with different initial conditions.

### 1.4 Conclusions and recommendation

The simulation codes have developed significantly since the previous benchmark studies, organized within ITTC (International Towing Tank Conference). Most notably, with 11 organizations now participating to the FLARE benchmark, this study is much more extensive than the previous ones. This indicates a wider interest to the topic in the field, which can also be seen in that new simulation codes have been introduced.

In general, the fundamental flooding mechanisms were well captured by most of the participating codes. Also the final outcome of a flooding process, either capsize or survival, was well predicted, for both the cruise and ropax cases, but with a significant variation in the time-to-capsize. Moreover, the flooding process, especially concerning the momentum of floodwater, should be considered more carefully, and there is room for further development of the codes.

The CFD (Computational Fluid Dynamics) tools can provide valuable insight into the details of the flooding progression. However, these analyses are still computationally demanding, and thus not suitable for survivability studies, especially concerning large number of damages and complex arrangement of flooded compartments.

In order to make final conclusions on benchmark for the cruise ship model, additional model tests for the flooding scenario B3, involving also up-flooding, were considered essential. Consequently, MARIN has already planned and scheduled these tests. This new experimental data and more comprehensive analysis of the benchmark results can be included in a planned journal article, dedicated to the cruise ship flooding cases.

The following topics are considered important for future research and development of the simulation codes:

- Progressive flooding through multiple compartments, especially up-flooding, which is characteristic for grounding scenarios
- Effects of floodwater momentum on flooding progression and filling of the flooded compartments
- Drifting of the ship during flooding in beam seas
- Hydrodynamics of a flooded ship, especially roll damping
- Computational performance, which is essential when the simulation codes are used as first principle tools for survivability assessments of large passenger ships with large number of compartments

The FLARE benchmark has been a valuable study on the current capabilities and challenges of time-domain simulation of flooding progression and motions of damaged passenger ships. The results can be used to further develop the tools, and to select suitable methods for use in the other work packages of the FLARE project.

## 1.5 Recommendations for FLARE project

One of the objectives of this benchmark study was to provide guidance for the use of simulation tools for analyses of flooding and damaged ship motions within the FLARE framework in other work packages. Considering only the simulation tools that are available within the FLARE consortium, the following conclusions can be drawn:

- **CFD tools:** Suitable for providing detailed information for development and testing of simplified but more efficient tools. Due to the required extensive pre-processing and long computation times, CFD tools are practically unsuitable for survivability assessments with large numbers of damage scenarios.
- **PROTEUS:** It can be stated that in its current state, the more ship motions are governed by the external actions of waves, and when internal vertical water progression is not governing, the better the results are. In case the damaged ship motions are mainly

driven by internal water motions, e.g. for grounding damages, then the code is not capturing well the physical phenomena due to modelling simplifications. Also, transient flooding details for the ropax were not captured, although capsized cases were properly identified. Acceptable results can be expected for collision damages in calm water and in waves if there is no significant down-flooding and all up-flooding routes are modelled as vertical trunks.

- **NAPA:** Proper calculation of progressive flooding, but the simplified approach, with only dynamic roll motion, limits the applicability to moderate sea states. Capsized conditions for both the cruise and the ropax ships in waves were correctly captured, but the time-to-capsize tends to be too short.
- **HSVA-Rolls:** Suitable for simulation of at least damaged ropax vessels. The applied model with the shallow water equations seems to work for flooding of the vehicle deck and large open compartments. Suitability for complex progressive flooding cases with up/down-flooding typical to cruise ships has however not been tested.
- **XMF** by MARIN: Recently, MARIN started the implementation of a new flooding module in XMF time domain simulation environment. This library replaces the FREDYN flooding module that exists for over 25 years now, but which has certain drawbacks in application. The development includes a new solver strategy. Promising results are obtained, but the benchmark results in waves show that the progressive flooding in waves and in particular the air-entrapment functionality needs further robustness. It is expected that by the end of the FLARE project the solver is well validated and applicable for complex flooding simulations in any prescribed environment.



## 2 INTRODUCTION

Time-domain simulation of flooding progression and motions of damaged ships is already a useful tool for studying the survivability in different scenarios. These first principle tools play an essential role in the FLARE project. Proper validation of such tools against experimental data is therefore necessary. Various simulation codes have been developed over the years, based on different approaches and implementations. Although individual validation results have been published, a large benchmark with many participants is needed to obtain insight into the capabilities and limitations of the different methods available today.

Between 2001 and 2007 several international benchmark studies on damage stability of ships were carried out, mainly organized within the International Towing Tank Conference (ITTC), Papanikolaou and Spanos (2001, 2005, 2008), van Walree and Papanikolaou (2007). The results were partly promising, but also notable problems were identified.

During the past decade, new simulation methods have been introduced, such as, Dankowski (2013), Lee (2015), Acanfora and Cirillo (2016, 2017) and Braidotti and Mauro (2019, 2020). Furthermore, also application of CFD methods have been studied, e.g. Bu and Gu (2019, 2020) and Ruth et al. (2019). In many cases, also validation results have been presented, mainly using the previous ITTC benchmark material.

Most notably, flooding simulation is more frequently being used in survivability analyses for new passenger ships. Therefore, it is essential to carry out an open benchmark study on validation and analysis of the suitability and efficiency of the available time-domain simulation tools for flooding and motions of damaged ships.

Previous benchmark studies, including main results and observations, are first recalled in chapter 3. An overview of the FLARE benchmark study and participants is given in chapter 4. Details of the benchmark cases and results are presented and discussed in chapters 5, 6 and 7. Finally, main conclusions and recommendations are summarized in chapter 8.



## 3 PREVIOUS BENCHMARK STUDIES

### 3.1 ITTC Benchmark on the Capsizing of a Damaged Ro-Ro/Pass. Ship in Waves (2001)

The first international benchmark study on damage stability and simulation of capsizing of a damaged ship was carried out within the International Towing Tank Conference (ITTC) in 2001. The studied ship is the passenger/ro-ro vessel PRR01 and the case is a two-compartment damage, involving also the main vehicle deck. The results of the benchmark are described in detail in the public report by Papanikolaou and Spanos (2001) and ITTC (2002).

There were five participants in this benchmark:

- NTUA (National Technical University of Athens, Greece)
- SSRC (University of Strathclyde, UK)
- University of Osaka, Japan
- MARIN, The Netherlands
- Flensburger Schiffbau Gesellschaft, Germany

The damage and calculated righting lever curves in this damaged condition are reproduced in Figure 3.1. It is obvious that there are very notable differences in the hydrostatics of the damaged ship in calm water.

The benchmark focused on the steady state after flooding. In addition to roll decay tests in calm water, also regular and irregular waves were studied. The simulation of roll decay for an intact ship was reasonably successfully calculated by all participants. However, the simulation of roll decay in the damaged condition was less successful. Also, for the calculation of the roll response amplitude operator (RAO) the results of the participants partly differed significantly.

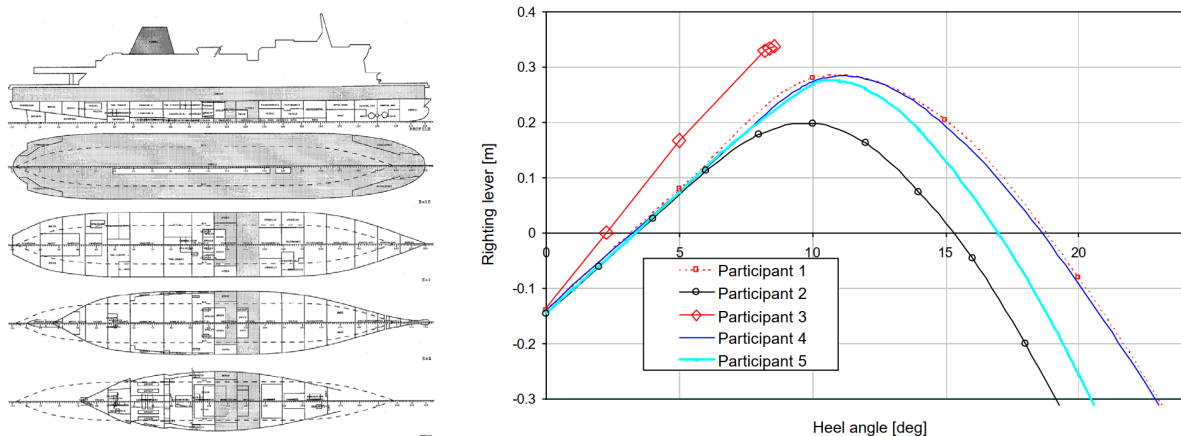


Figure 3.1 Studied damage case and comparison of righting lever curves for a damaged ship, adopted from Papanikolaou and Spanos (2001)

For the results in irregular waves, Papanikolaou and Spanos (2001) note that:

*“A visual comparison/analysis of the numerically predicted and experimentally measured time series shows a rather unsatisfactory level of agreement between the different participants and the experiments. Indeed, none of the numerical time series match satisfactorily at least in qualitative terms the experimental values where in particular the character of the experimentally measured roll response indicates a quite distinct independence of the response components induced by the wave excitation and low-frequency response due to floodwater accumulation.”*

Furthermore, Papanikolaou and Spanos (2001), conclude that:

*“it appears necessary that a more comprehensive study should be carried out in the future to investigate the relation between the employed damping models by the benchmark study participants”*

### 3.2 ITTC Benchmark on Numerical Prediction of Damage Ship Stability in Waves (2005)

Based on the recommendations from the first ITTC benchmark study on capsizing of a damaged ro-ro passenger ship in waves, a more comprehensive benchmark on numerical prediction of damage ship stability in waves was organized. Details are presented in the final report in Papanikolaou and Spanos (2005) and ITTC (2005).

There were five participants in the benchmark, partly different ones than in the previous benchmark:

- NTUA (National Technical University of Athens, Greece)
- Korea Research Institute of Ships and Ocean Engineering, KRISO
- Instituto Superior Tecnico, University of Lisbon, Portugal
- MARIN, The Netherlands
- SSRC (University of Strathclyde, UK)

The study consisted of four separate tasks, using test data from three different model tests:

- Task A: free roll motion of an intact passenger/ro-ro model PRR01
- Task B: free roll motion of PRR01 in damaged condition (same damage case as in the previous benchmark)
- Task C: free roll motion of a tanker model TNK with a large partially filled tank, no connection to the sea, presented in de Kat (2000)
- Task D: transient flooding in calm water with the passenger/ro-ro PRR02, van't Veer (2001), with flooding of an engine room compartment, including also a cross-flooding duct

Some examples of the results are shown in Figure 3.2.

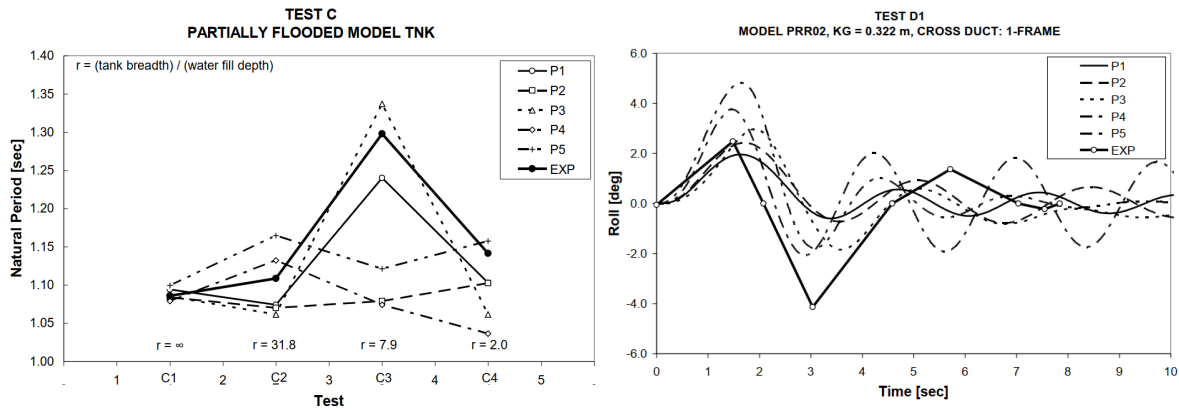


Figure 3.2 Examples of benchmark results: natural roll period for tanker with partially filled large tank (left) and comparison of roll motion in the transient flooding case with PRR02 (right), figures adopted from Papanikolaou and Spanos (2005); note that experimental data contains only a small set of points, not the full time history for PRR02 (right).

The observed deviations between the numerical methods in the damage condition were considered to result from the different approaches to the effects of floodwater on ship motions. The numerical methods assuming a horizontal waterplane in flooded compartments could not capture the floodwater dynamics properly, whereas methods considering moving water surfaces demonstrated satisfactory sensitivity with respect to the floodwater effects. Papanikolaou and Spanos (2005) also concluded that:

*“Special focus should be given on the semi-empirical weir coefficient as well as the implementation of the flooding model.”*

### 3.3 ITTC Benchmark on Time-to-Flood – Phase 1 (2007)

The next benchmark study within the ITTC focused on the calculation of progressive flooding in the compartments of the damaged ship. A box-shaped barge, with a nominal scale of 1:10, was used in this study. Details of the model and the tests have been presented in Ruponen et al. (2007). All cases were tested in calm water, and also air compression in the flooded compartments were measured.

There were five participants in this benchmark, partly different ones than in the previous benchmark:

- Helsinki University of Technology, Finland (with code NAPA)
- NTUA (National Technical University of Athens, Greece)
- MARIN, The Netherlands
- Safety at Sea, UK (with code PROTEUS)
- Maritime and Ocean Engineering Research Institute (MOERI), Republic of Korea

The results of the benchmark were presented by van Walree and Papanikolaou (2007), with anonymous codes. The model test data included experimentally evaluated discharge

coefficients for all openings in the model. However, it appeared that some of the participating codes used fixed discharge coefficient (0.6). However, the analysis of the results clearly indicates that this alone does not explain the notable differences in the predicted water levels. Some examples are shown in Figure 3.3 and Figure 3.4. Most notably, van Walree and Papanikolaou (2007) summarise that:

*“the steady state condition of all tests is reasonably well predicted by the codes. The prediction of the flooding rates and transient phenomena is less satisfactory.”*

Furthermore, they note the need to continue the benchmark with more complex internal geometries in calm water, and for seaway conditions.

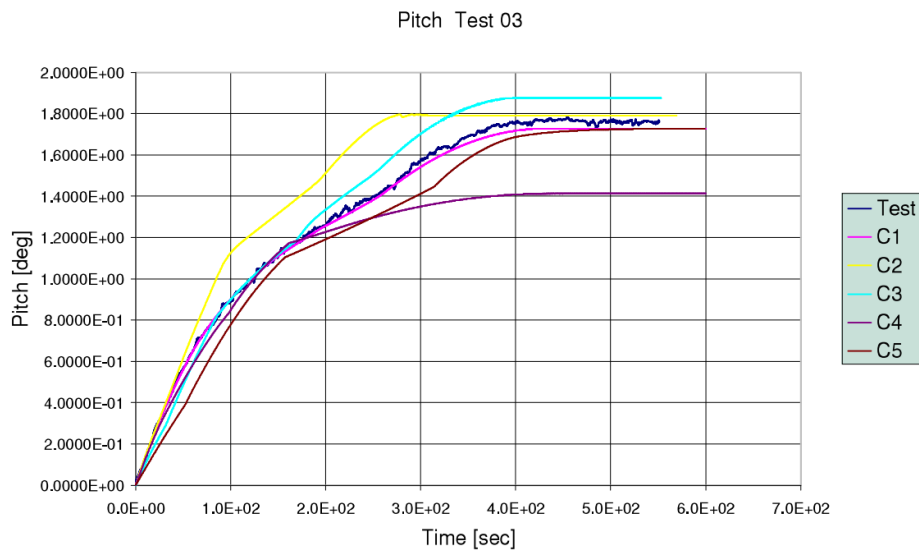


Figure 3.3 Example of experimental and numerical results for pitch/trim angle, adopted from van Walree and Papanikolaou (2007)

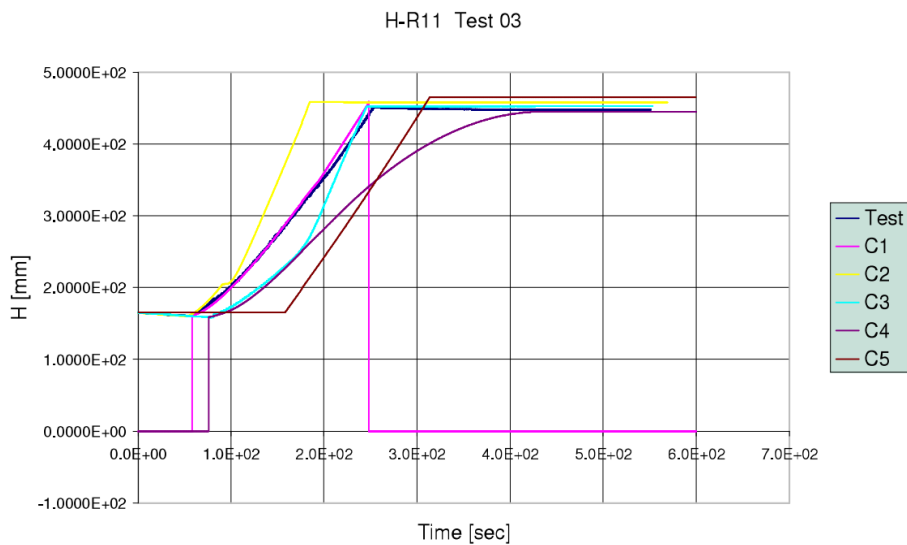


Figure 3.4 Example of experimental and numerical results for water level height in a flooded room, adopted from van Walree and Papanikolaou (2007)

### 3.4 ITTC Benchmark on Time-to-Flood – Phase 2 (2008)

The ITTC benchmark study on time-to-flood continued with a second phase with a large passenger ship design. However, this study was not a proper benchmark since no experimental data was available. Moreover, only two organizations MARIN and SSRC (University of Strathclyde) participated. The results are reported by van Walree and Carette (2008).

The two participating codes produced quite different results. An example is shown in Figure 3.5. Proper conclusions could not be drawn since experimental data was not available. However, the observed differences in the results clearly indicate the need for further validation and benchmark studies.

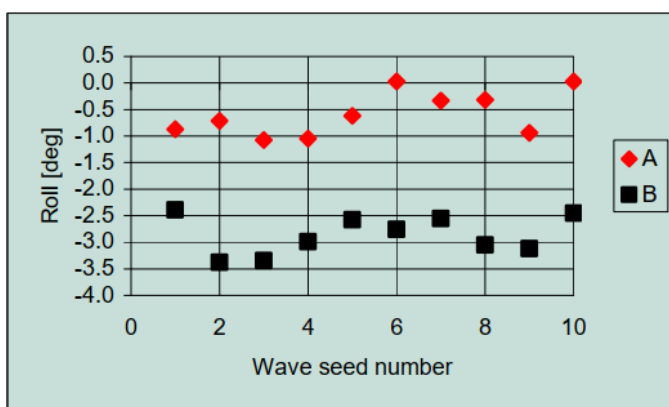


Figure 3.5 Example of mean heel angles with the two codes A and B in damage case D2 with significant wave height of 4 m, adopted van Walree and Carette (2008)

### 3.5 SAFEDOR Benchmark (2008)

An additional benchmark study was carried out within the EU FP6 project SAFEDOR. A summary was presented by Papanikolaou and Spanos (2008). Initially, there were 6 participants, but results were presented only for 4 participants:

- NTUA (National Technical University of Athens, Greece)
- SSRC (University of Strathclyde, UK)
- MARIN (The Netherlands)
- IST (Technical University of Lisbon, Portugal)

The test case is the passenger/ro-ro ferry PRR02 from the project HARDER. The model test results have been reported by van't Veer (2001). The case is the same as Task D in the second ITTC benchmark study in 2005. The damage case and some example results are presented in Figure 3.6. The results from the codes were reported anonymously in the study.

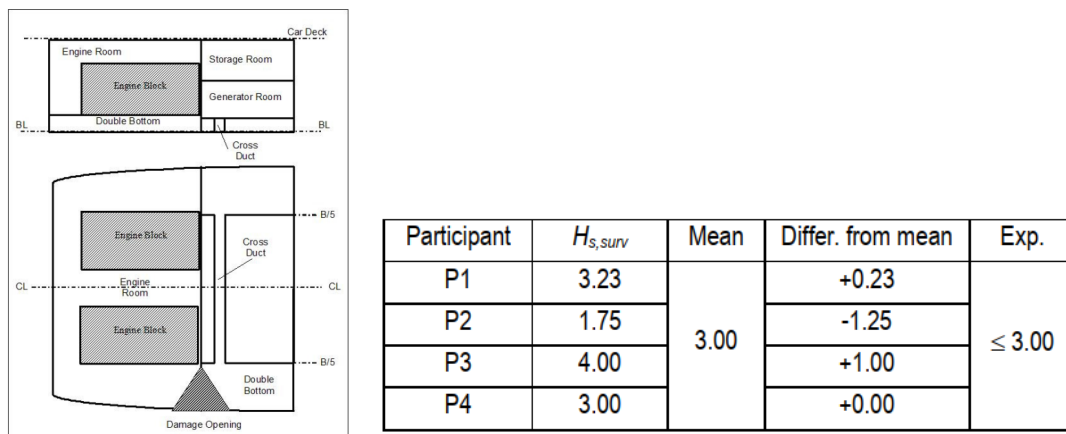


Figure 3.6 Investigated damage case in the SAFEDOR benchmark and the results for the survival boundary significant wave height

The main analysis focuses on the survival boundary, i.e. a significant wave height below which no capsizing occurred during simulations. However, Papanikolaou and Spanos (2008) point out an interesting observation:

*“While P1 and P4 seem to deliver convergent results, the detailed background analysis showed that codes simulate the test phenomena in a substantially different way; thus, it is remarkable how this difference appears subsidiary in the estimation of the survival boundary”*

This indicates that comparison of a survival boundary is not a sufficient quantity for benchmarking. Instead, the details of the simulated flooding process and damaged ship motions need to be compared.

### 3.6 Summary of recommendations

Although several model tests have been done with various different ship models, there is not enough publicly available model test data for proper benchmarking of numerical methods. Most of the previous benchmarks have used old model tests data for two passenger/ro-ro

ferries (PRR01 and PRR02) from the EU funded research projects HARDER and NEREUS. In addition, Helsinki University of Technology (currently Aalto University) in Finland, has published details and test results for progressive flooding of a box-shaped barge. These tests have been used for validation of several numerical methods during the past decade.

Even more concerning from a code validation point of view, is that there is no publicly available data for real ship geometries with extensive flooding, presenting typical characteristics of transient and progressive flooding, both in calm water and in waves.

The results of the previous benchmark studies show a notable deviation in the results, both for the dynamic roll motion of a flooded ship in waves and for progression of floodwater in relatively simple internal layout of compartments. Consequently, new benchmark studies need to also include the flooding fundamentals, such as up and down flooding and progressive flooding in a complex arrangement with a fixed floating position in calm water.

It has been over a decade since the last benchmark study, and old simulation codes have been improved and new ones have been introduced. In addition to this, the computing capacity has increased a lot, enabling detailed calculations also for large ships and larger number of damage scenarios. Therefore, one of the objectives of the Horizon 2020 project FLARE is to get an insight into the currently available simulation tools for flooding and damage stability of ships, both within the consortium and globally. Based on the previous benchmark results, it is essential to arrange an extensive study, with focus on:

- Flooding mechanisms, including breach and internal openings
- Effects of (regular) wave on flooding with a fixed floating position
- Inertia and roll damping characteristics of a flooded ship
- Flooding and damaged ship motions both in calm water and in waves, including capsized cases during both transient flooding, and progressive flooding stages
- Effects of water on the vehicle deck for a damaged ro-ro passenger vessel



## 4 FLARE BENCHMARK OVERVIEW

### 4.1 Objectives and Structure

Previous benchmarks have focused on flooding and motions of damaged ships, both in calm water and in waves. Ypma and Turner (2019) point out the importance of the coupling between flooding and ship motions in validation of flooding simulation codes. Consequently, the main objective of this new benchmark study is to obtain insight into both:

- 1) accuracy and performance of available tools in modelling typical flooding characteristics, especially for passenger ships, and
- 2) coupling of the flooding process and damaged ship dynamics in both calm water and in waves.

In addition, to flooding tests in both calm water and in waves, also fundamental flooding mechanisms in a controlled environment need to be included. Therefore, the benchmark study consists of three separate parts, each with different test cases:

- Benchmark Part A: Flooding fundamentals
  - A1: up-flooding
  - A2: down-flooding
  - A3: cross-flooding in regular waves
  - A4: extensive flooding on a deck of a cruise ship
- Benchmark Part B: Cruise ship flooding
  - B1: transient flooding in calm water
  - B2: transient and progressive flooding in waves
  - B3: progressive flooding in calm water
- Benchmark Part C: Ropax ship flooding
  - C1: transient flooding in calm water
  - C2: transient flooding in waves
  - C3: gradual flooding and capsize in waves

The participants had the opportunity to choose which parts of the benchmark they wanted to contribute to, based on the assumptions and limitations of the applied codes. In order to enable a more detailed analysis of the results, Part A was recommended for everyone.

### 4.2 Schedule

In addition to the FLARE project partners, also other experts outside the consortium were invited to this benchmark study. An early invitation was sent to selected flooding and damage stability experts in December 2019, and the structure of the benchmark was released in May 2020. Details about the benchmark cases, including geometry, were later shared to the confirmed participants. The timeline of the benchmark is presented in Table 4.1. Model tests were carried out at MARIN and HSVA during the spring and summer 2020. The COVID-19 situation, and consequent remote working, unfortunately had an adverse effect on the original schedule. In addition, some further model tests were required, and therefore the deadline of the benchmark had to be extended.

Table 4.1 Benchmark timeline

<b>12/2019</b>	Early invitation to potential external participants
<b>05/2020</b>	Invitations, benchmark structure released with details on Part A
<b>07/2020</b>	Part A details and videos distributed & geometry of Part B released
<b>10/2020</b>	Initial results on Part A received and updated material on Parts B & C distributed
<b>19.11.2020</b>	Online workshop between participants on preliminary results of Part A
<b>12/2020</b>	Comparison of hydrostatics, test cases for Part C distributed
<b>1/2021</b>	Preliminary results for Part C and clarifications to the geometry in Part B
<b>26.3.2021</b>	Online workshop on preliminary results of Part C (ropax)
<b>13.4.2021</b>	Online workshop on preliminary results of Parts B (cruise ship)

### 4.3 Material

Model tests for the fundamental flooding cases and cruise ship were conducted by MARIN and tests with the ropax vessel by HSVA. The experiments formed the FLARE WP4.2 and the relevant experimental results<sup>1</sup> were shared beforehand to all confirmed participants, in order to enable fair and equal benchmarking conditions to all. In general, the following data was provided:

- 3D geometry (Rhino 3dm and/or Autodesk dwg files)
- Hull form geometry in IGES format (Parts B & C)
- 2D drawings in dxf/dwg format
- Locations of level sensors, coordinate convention, etc.
- Overview of measurements, containing measured water levels (Part A) and roll angle (Parts B & C) in graphical format
- Videos on tests for Parts A and B

Hydrostatic and volumetric data were collected and checked beforehand, in order to find out possible modelling errors before conducting the calculations. The benchmark instructions were frequently updated.

---

<sup>1</sup> Graphs of measured data and videos

## 4.4 Participants

In total 11 organizations contributed to this benchmark study. Most of the codes are in-house tools, developed at a university or a research institute, with NAPA and the CFD software being the exceptions. The participants for each of the benchmark parts and tests are summarized in Table 4.2.

Table 4.2 Summary of benchmark participants

Organization	Code	Type	Flooding fundamentals				Cruise ship			Ropax ship		
			A1	A2	A3	A4	B1	B2	B3	C1	C2	C3
BROO	PROTEUS	in-house	✓	✓	✓	✓	–	–	–	✓	✓	✓
CSSRC	wDamstab	in-house	✓	✓	✓	✓	✓	✓	✓	–	–	–
CSSRC	StarCCM+	commercial	–	✓	✓	✓	–	–	–	–	–	–
DNV	OpenFOAM	commercial	–	✓	✓	✓	–	–	✓	–	–	–
HSVA	HSVA-ROLLS	in-house	–	–	–	✓	–	–	–	✓	✓	✓
KRISO	SMTP	in-house	✓	✓	✓	✓	✓	✓	✓	✓	✓	✓
MARIN	XMF	in-house	✓	✓	✓	✓	✓	✓	✓	✓	✓	✓
MARIN	ComFLOW	in-house	✓	✓	✓	✓	–	–	–	–	–	–
MSRC	PROTEUS	in-house	✓	✓	✓	✓	✓	✓	✓	✓	✓	✓
NAPA	NAPA	commercial	✓	✓	✓	✓	✓	✓	✓	✓	✓	–
UAK	E4 flooding	in-house	✓	✓	✓	✓	–	–	–	–	–	–
UNITS	LDAE	in-house	✓	✓	–	✓	✓	–	✓	–	–	–
UNINA	FloodW	in-house	✓	✓	✓	–	–	–	–	✓	✓	–

A short description of each participating code is given below, including some key references for more thorough presentation of the applied methods. These descriptions were collected from the correspondents of each participating organization.

BROO & MSRC	In-house code <b>PROTEUS</b> owned by Safety at Sea Ltd, a subsidiary of BROO. Originally developed at University of Strathclyde (MSRC). Flooding rates are calculated applying Bernoulli's equation with a hard-coded discharge coefficient of 0.6. Floodwater motions are modelled as a pendulum (Free-Mass in Potential Surface). Resolution of a multi-body multi-degrees of freedom system, with 6-DOF for ship motion and 3-DOF per each flooded compartment. Regular and irregular waves. Froude-Krylov and restoring forces integrated up to the instantaneous wave elevation. Radiation and diffraction are derived from 2D strip theory. Hydrodynamic coefficients vary with the attitude of the ship during the flooding process (heave, heel and trim). Details presented in Jasionowski (2001).
CSSRC-CFD	Commercial CFD software <b>Star-CCM+</b> is used, with volume of fluid (VOF) approach for floodwater. Six degrees of freedom ship motions can be considered. Both regular and irregular waves can be considered by instantaneous integral of pressure along the wet surface. Details of the method are presented in Bu and Gu (2019, 2020).
CSSRC-Meth1	In-house code <b>wDamstab</b> . Bernoulli for flooding rates with horizontal surface for floodwater. Four degrees of freedom (Sway-heave-roll-pitch) can be considered. Ship motion is calculated based on the potential flow theory (STF). regular waves, Froude-Krylov and hydrostatic forces can be calculated based on the integration of pressure along instantaneous wet surface. Described in Bu et al. (2018, 2020), in Chinese.

DNV	<b>OpenFOAM</b> CFD toolbox is used. The air and water flow is resolved by a finite volumes formulation with overset mesh for vessel motions to solve the Reynolds-Averaged Navier-Stokes (RANS) equations. For the cross-flooding in waves case, i.e. A3, the StarCCM+ software was used, due to time constraints. For details about using CFD in flooding analyses, see Ruth et al. (2019).
HSVA	In-house version code the Rolls code, <b>HSVA-Rolls</b> . The ship roll motion and surge are solved with ordinary differential equations using nonlinear hydrostatics in waves (NAPA based) + linear strip theory for wave excitation and for RAOs (response amplitude operators) of other four Degrees of Freedom (DOF); altogether 2 non-linear DOF + 4 linear DOF solved in time domain. Flooding rates are calculated with Bernoulli, using empirical discharge coefficients. Floodwater is treated either with a pendulum model, or with shallow-water-equations (SWE).
KRISO	In-house code <b>SMTP</b> . Flooding rates calculated with Bernoulli, using empirical discharge coefficients. Floodwater has either horizontal surface or pendulum model appropriate at each compartment. The program provides several kinds of types for compartments and openings, and their numbers are unlimited. Ship motions are calculated by 6-DOF non-linear equations in time-domain, the hydrodynamic forces are calculated by strip method. Details presented in Lee (2015).
MARIN	The Extensible Modelling Framework (XMF) is a software toolkit on which all MARIN's fast-time and real-time simulation software is based applying Newtonian dynamics, of which Fredyn and ANySim are known examples. XMF is recently extended with a flooding module library (XHL) based on Bernoulli's equation with empirical discharge coefficients, using generic 3D defined floodable objects. A graph-solver technique is utilized to capture the complexity of entrapped air in compartments and for hydrostatic pressure-corrections from fully flooded compartments.
MARIN – CFD	The CFD code <b>ComFLOW</b> is a Cartesian (cut cell) grid-based Volume of Fluid (VOF) CFD solver, using a staggered finite-volume discretization of the Navier-Stokes equations. Geometrically reconstruction of the free surface interface. Automatic grid refinement by means of surface and object tracking criterion and explicitly integrating the free surface in time using a variable time step. Details are given by Veldman et al. (2014) and Bandringa et al. (2020).
NAPA	The commercial software <b>NAPA</b> is used. The flow rates are calculated from Bernoulli's equation, with user-defined discharge coefficients for each opening. Horizontal free surface assumed in all flooded rooms. Pressure-correction algorithm applied to solve the governing equations (continuity and Bernoulli). Ship motions are either fully quasi-static (heel, trim & draft) or with a dynamic roll motion. Effect of waves (regular or irregular) on flooding can be considered. Details are presented in Ruponen (2007, 2014).

UAK	In-house code <b>E4 Flooding Method</b> , with flooding calculated by using Bernoulli's equation with horizontal surface and flooding path modelled as directed graphs. Ship motions either 3-DOF quasi-static or 6-DOF dynamic, with support for regular waves and other effects e.g. interaction with cargo and seabed, Dankowski and Dilger (2013), conditional openings and leakage, Dankowski et al. (2014) and cargo shift. Details of the simulation method are presented in Dankowski (2013) and Dankowski and Krüger (2015).
UNINA	In-house tool <b>FloodW</b> , coded in Matlab-Simulink. Flooding rates are calculated based on Bernoulli's equation with empirical discharge coefficients. Floodwater is treated as a non-horizontal flat surface, in agreement with the pendulum model. Regular and irregular wave effects are modelled, accounting for all pertinent nonlinearities. Details are presented in Acanfora and Cirillo (2016, 2017) and Acanfora et al. (2019).
UNITS	In-house code <b>LDAE</b> . The flooding process is modelled using a DAE system based on the Bernoulli equation, which is linearized and solved analytically. A flat horizontal free surface is assumed for the sea and waterplanes inside flooded rooms. An adaptive integration time step, based on floodwater level derivatives, is adopted. The model does not include dynamic ship motions. Only quasi-steady change of heel, trim and sinkage is considered. Details in Braidotti and Mauro (2019, 2020).



## 5 FLARE BENCHMARK A – FLOODING FUNDAMENTALS

### 5.1 Overview

The first part of the FLARE benchmark study aims at analysis of the accuracy and performance of the flooding simulation tools for various typical flooding mechanisms. Simplified geometries and flooding scenarios are used in captive model tests, so that the floating position of the model is fixed.

The flooding fundamentals part consists of the following individual test cases:

- A1: up-flooding
- A2: down-flooding
- A3: cross-flooding in regular waves
- A4: extensive flooding on a deck of a cruise ship

### 5.2 Discharge Coefficients

Many simulation codes use a hydraulic model, based on Bernoulli's theorem, for calculation of the flow rates through the openings. This approach is efficient, when compared to CFD tools, but it requires semi-empirical discharge coefficients, to model the flow losses. For full-scale simulations, the so-called industry standard value 0.6 has proven to be reasonably accurate, Ruponen et al. (2010). Since frictional losses are proportional to the Reynolds number, a somewhat larger discharge coefficient is characteristic for model-scale openings, Idel'chik (1960). This has also been observed in the previous experimental studies, e.g. Katayama and Ikeda (2005), and Ruponen et al. (2007). Consequently, all participants using Bernoulli's theorem in their codes, were recommended to use discharge coefficients given in Table 5.1. The values were obtained from analysis of various dedicated tests carried out by MARIN.

Table 5.1 Recommended discharge coefficients

Part	Opening	C <sub>d</sub>	Explanation
A1, A2, A3	80 mm × 80 mm	0.65	Average from dedicated tests by MARIN
A1	80 mm × 40 mm	0.65	Same as for the inflow openings
A2	40 mm × 40 mm	0.70	Average from dedicated tests by MARIN
A3	Cross-duct 120 mm × 60 mm	0.65	Assumed, based on results for the 80 mm × 80 mm opening
A4	Narrow openings (width < 30 mm)	0.73	Based on test by MARIN with an opening size of 17 mm × 34 mm
A4	Wide openings (width ≥ 30 mm)	0.70	Based on test by MARIN with an opening size of 47 mm × 34 mm
A4	Breach	0.65	Same as for the inflow openings in A1, A2 & A3

It should be noted that the software PROTEUS, used by both BROO and MSRC, has a hard coded discharge coefficient of 0.6, and therefore, it was necessary to compensate this by adjusting other opening characteristics, in order to achieve the same effect on flooding progression. BROO modelled the effect by considering the openings as leaking doors with a large leakage area ratio, while MSRC modified the opening areas.

## 5.3 Case A1 – Up-Flooding

### 5.3.1 Description

Calculation of flooding progression through a compartment that is filled-up with water is known to be challenging for simulation codes, since the effective hydrostatic pressure is higher than the pressure at the top of the filled-up compartment. Therefore, the first benchmark case focuses on up-flooding with an extremely simple geometry. The model has two sub-compartments that are separated by a deck with a hole in the middle. There is a breach hole in the side of the lower compartment, as shown in Figure 5.1. The test condition is:

- Atmospheric pressure, both rooms vented so that full ventilation can be assumed
- Constant draft of 400 mm
- Fixed floating position at even keel (zero heel and trim)
- Inflow opening to lower compartment: 80 mm × 80 mm
- Opening in the tween deck: 80 mm × 40 mm

The main dimensions are presented in Figure 5.2.

When the lower room is filled up, also the ventilation pipe is flooded. The inner diameter of the pipe is 50 mm. Therefore, some participants also modelled the pipe as an extension to the room, typically in a simplified way. Comparison of the calculated water volumes at equilibrium with different codes is presented in Figure 5.3. There is some small variation, but it can be concluded that the geometry of the compartment has most likely been correctly defined by all participants.

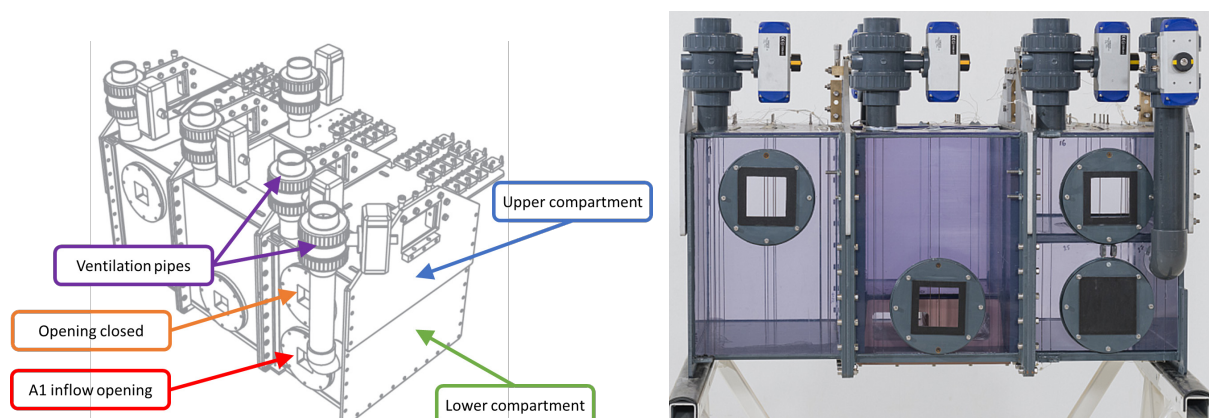


Figure 5.1 Benchmark case A1 up-flooding (left) and photo of the test box (right, courtesy of MARIN)

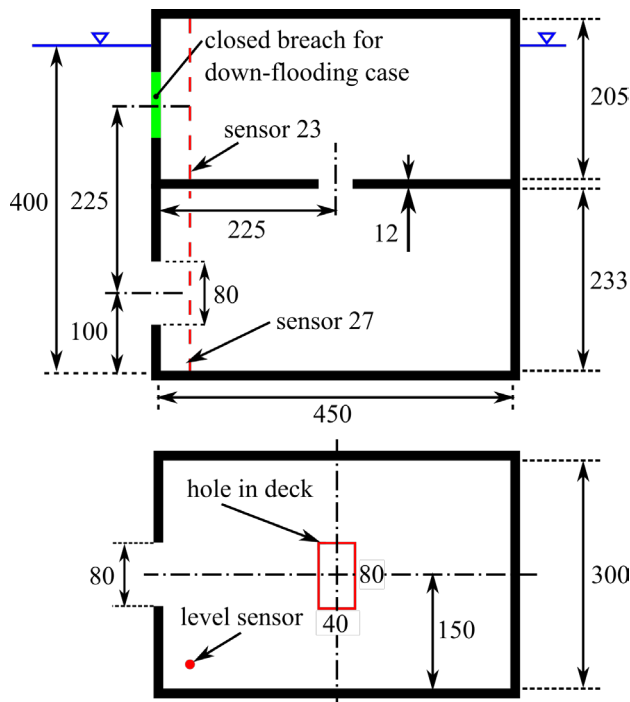


Figure 5.2 Sketch of the box arrangement used for up-flooding case A1

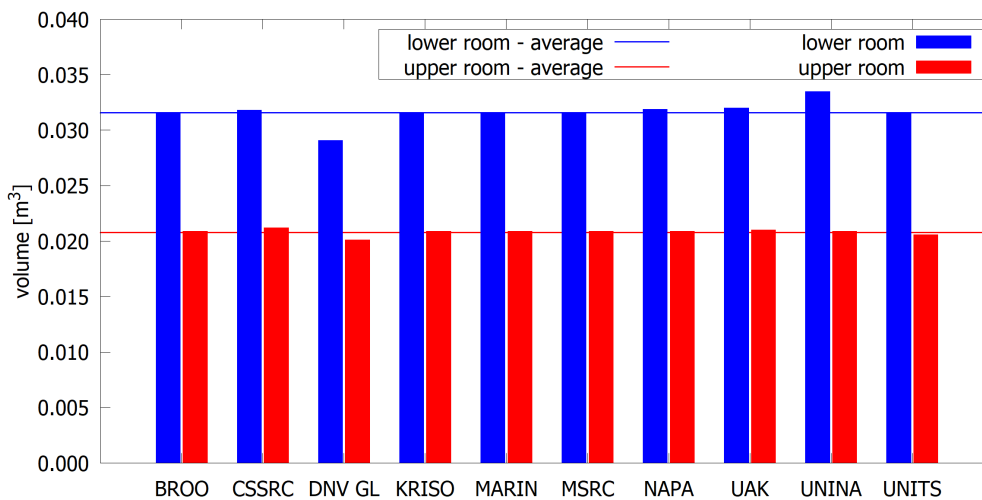


Figure 5.3 comparison of volumes of floodwater at equilibrium (for both A1 and A2)

### 5.3.2 Results

Most codes can predict the flooding progression rather well, and hence each code is compared separately against the measured water levels in Figure 5.4. In general, the rise of the water level in the lower compartment during the first 3.5 s is slightly underestimated. The only exception is the code PROTEUS, used by both BROO and MSRC, predicting a slightly slower flooding to the lower compartment than the other codes that were also based on Bernoulli's method. According to code level analysis by MSRC, this is caused by a built-in ramp function that slows down the initial flooding from the sea in the beginning of a simulation. However, the

PROTEUS code has problems in calculating up-flooding through the filled-up lower compartment. Based on analysis by MSRC, this is a problem in the core level implementation, and can only be overcome by artificial changes to the geometry to avoid up-flooding through a completely filled-up room.

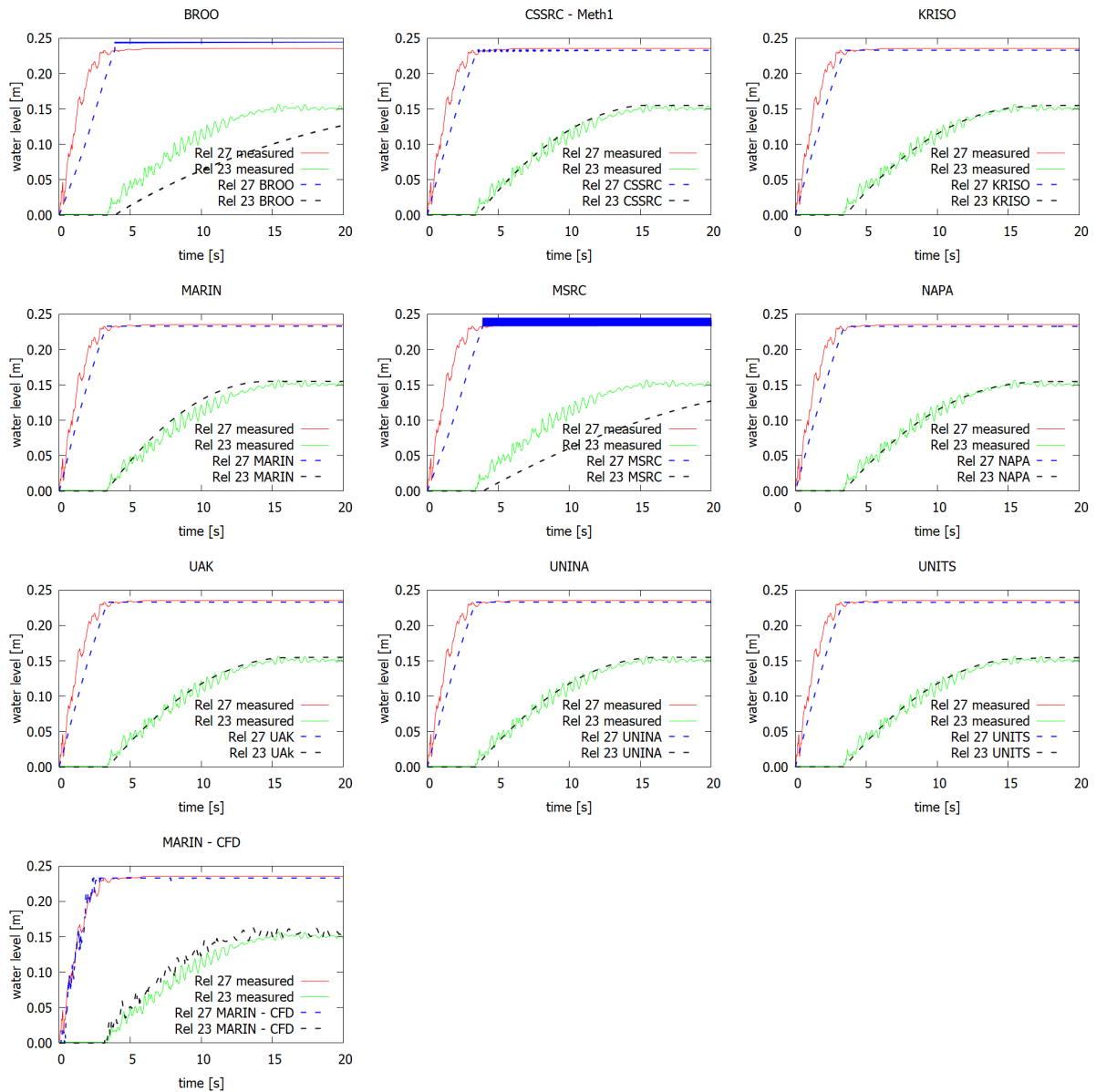


Figure 5.4 Comparison of water levels in the Part A1 (up-flooding)

Due to unfortunate circumstances, only MARIN provided CFD results for this case. A snapshot from the ComFLOW simulation is shown in Figure 5.5, clearly visualizing that the water surface in the lower compartment does not remain horizontal, as assumed with the simplified simulation methods. However, this does not seem to have a notable effect on the flooding progression from a more generic perspective.

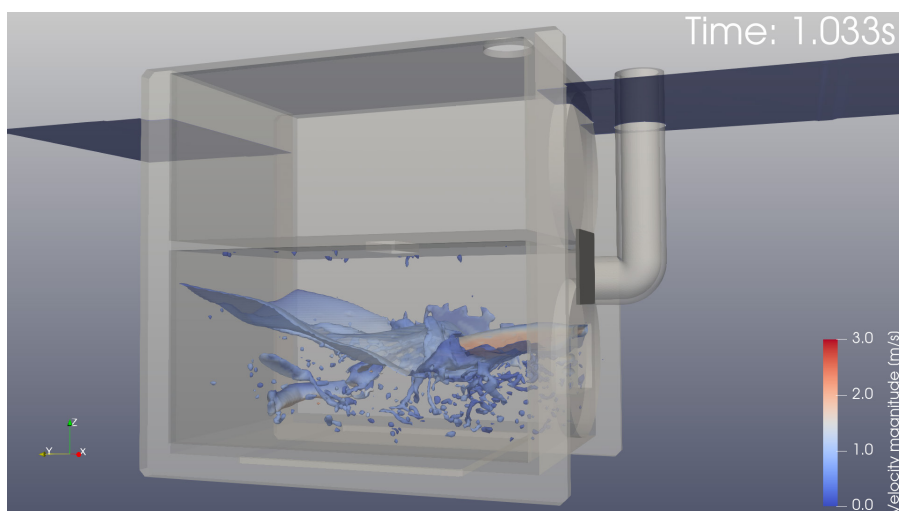


Figure 5.5 Snapshot on initial flooding progression in case A1 from ComFLOW simulation by MARIN

## 5.4 Case A2 – Down-Flooding

### 5.4.1 Description

Similar to up-flooding, also down-flooding is a fundamental flooding process that is very typical, especially in case of extensive progressive flooding in passenger ships. Therefore, the second case in the benchmark focuses on simulation of this simple flooding mechanism. The compartment geometry is the same as in Case A1, but the breach opening is now located in the upper compartment, and the hole in the deck is smaller. The test condition is:

- Both rooms are vented, the test was done in atmospheric air pressure, but full ventilation can be assumed in the simulations
- Constant draft of 400 mm
- Fixed floating position at even keel (zero heel and trim)
- Inflow opening to upper compartment 80 mm × 80 mm
- Opening in the tween deck: 40 mm × 40 mm

The down-flooding case has also been calculated with CFD tools by CSSRC, DNV and MARIN. A short comparison of the applied methods and modelling is presented in Table 5.2. Normally “no-slip”, i.e. wall condition is used for decks and bulkheads. Since in the physical model the plexiglass surfaces are much smoother than the steel structures in a full-scale ship, CSSRC decided to study separately also the “slip” condition, i.e. a perfectly smooth surface, considering only the normal pressure without tangential force.

Table 5.2 Comparison of CFD methods used in down-flooding case (Part A2)

	CSSRC – CFD	DNV	MARIN – CFD
<b>Software</b>	Star-CCM+	OpenFOAM	ComFLOW
<b>Grid size (number of cells)</b>	2 370 000	232 000	1 140 000 ... 1 610 000
<b>Boundary condition</b>	Slip & no-slip separately	Wall	No-slip
<b>Turbulence model</b>	Realizable k-ε two layer	Laminar flow	Laminar flow
<b>Time step</b>	1.0 ms	10 ms	0.064...1.44 ms

### 5.4.2 Results

Most codes accurately predict the increase of the water level in the upper compartment. In general, the down-flooding rate is slightly under-estimated, Figure 5.6. The small increase in the water level in the upper compartment, when the lower compartment is filled-up, is also captured. All simulation codes with a hydraulic Bernoulli-based flooding model provide good results, except the PROTEUS code, used by BROO and MSRC. This code can predict the flooding of the upper compartment, but the down-flooding rate is seriously underestimated. Similar problems are not encountered with the other Bernoulli-based simulation codes. According to the code analysis by MSRC, this results from a ramp function for down-flooding openings that unrealistically reduces the flow rate.

The down-flooding case was calculated with CFD tools by CSSRC, DNV and MARIN. Moreover, CSSRC used two different boundary conditions. With the no-slip condition there is a strange slowing down of the down-flooding rate after about 12 s, whereas with the slip boundary condition the level in the upper compartment decreases slowly. The ComFLOW simulations by MARIN match well with the measurements. Moreover, the OpenFOAM simulation by DNV provides very accurate results, although a much coarser computational grid is applied. However, in general the differences between measurements and CFD results are of the same magnitude as with the much simpler and computationally significantly much more efficient hydraulic flooding models.

Some captures of the flooding process from the OpenFOAM simulation by DNV are presented in Figure 5.7, showing that the down-flooding jet is not perpendicular. Examples of detailed results by CSSRC with different boundary conditions are shown in Figure 5.8.

With the “slip” condition the start of down-flooding is delayed, and in general the “no-slip” condition results match better with the measurements, although it seems that after about 13 s the flooding is slowed down. In this respect, the less detailed and faster CFD analysis by DNV provides much more reasonable results that are also fully in line with the Bernoulli-based codes. A snapshot on the down-flooding from the ComFLOW simulation by MARIN is presented in Figure 5.9, showing very similar characteristics as with the other CFD tools.

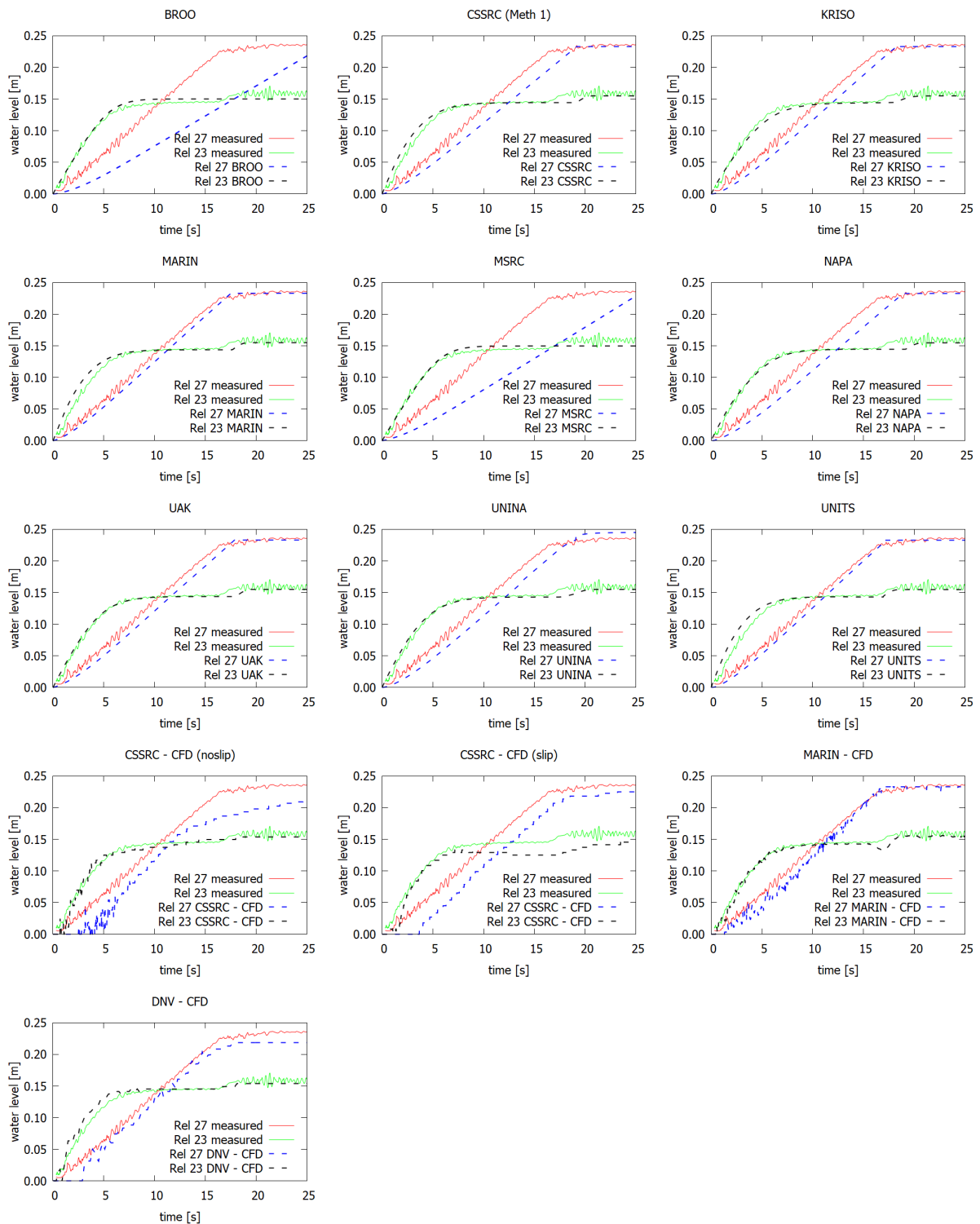


Figure 5.6 Comparison of water levels in Part A2 (down-flooding)

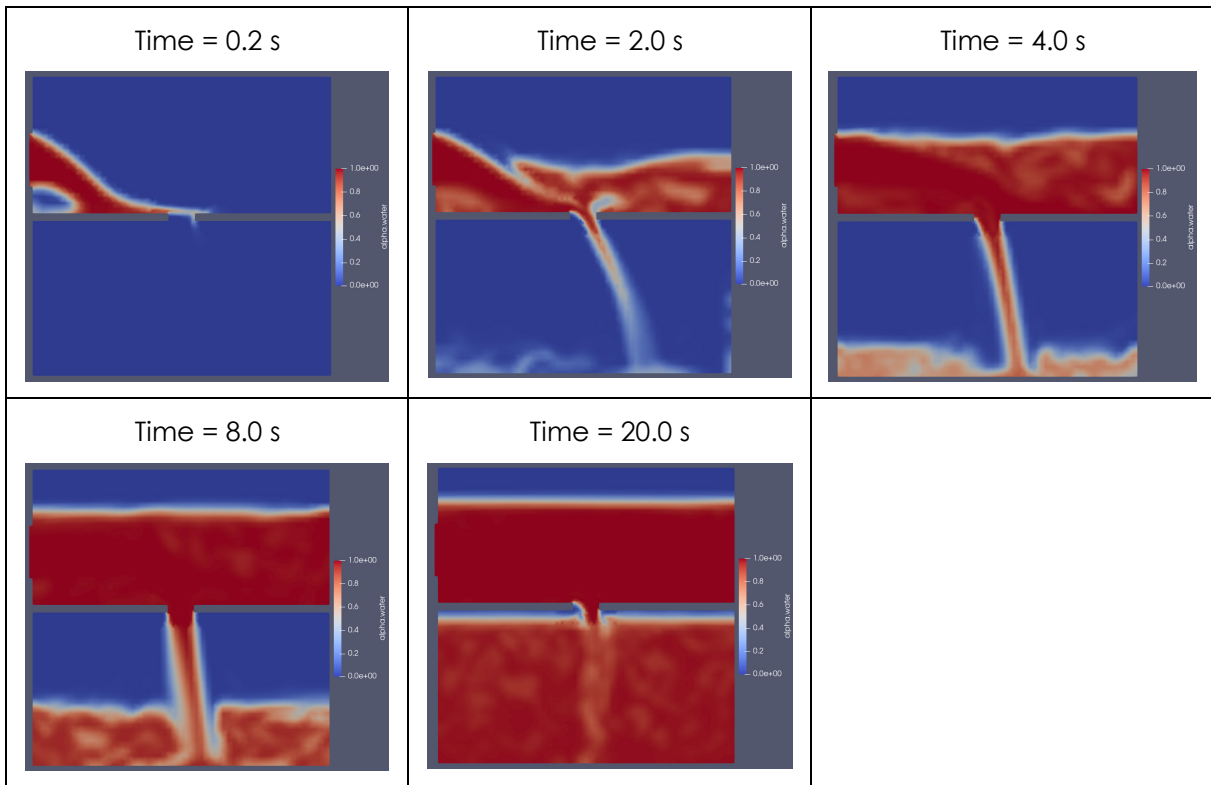


Figure 5.7 Flooding progression from OpenFOAM calculations for down-flooding case by DNV, quantity alpha presenting the portion of water in the grid cells

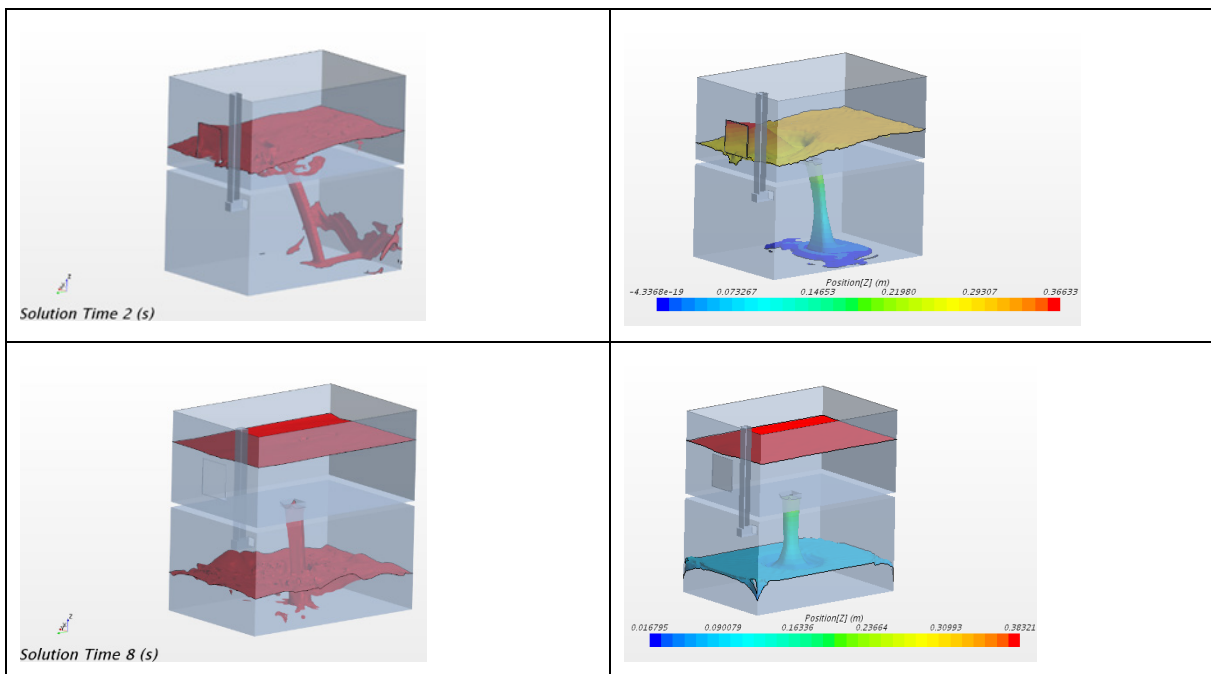


Figure 5.8 Snapshot of flooding progression in the down-flooding case at 2 s and 8 s from the CFD results by CSSRC using "no-slip" (left) and "slip" (right) boundary condition

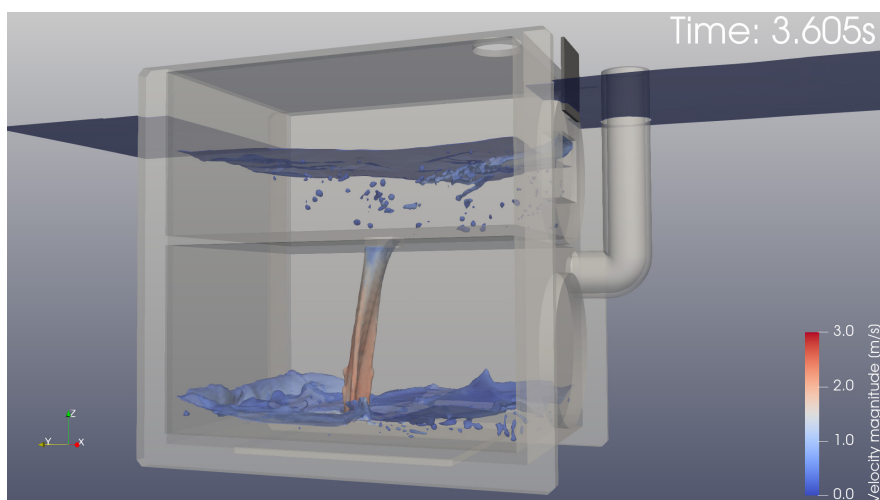


Figure 5.9 Snapshot of down-flooding from ComFLOW simulation by MARIN

## 5.5 Case A3 – Effect of Waves on Cross-Flooding

### 5.5.1 Description

Waves can have a notable effect on the flooding process, and therefore, a simple cross-flooding arrangement was studied in regular waves, Figure 5.10. The arrangement contained two box-shaped rooms, connected by a cross-duct with a size of 120 mm × 60 mm and length of 250 mm. Model tests were done in atmospheric air pressure and both rooms were properly vented, so that air compression effects were considered negligible. The floating position of the model was fixed with a draft of 325 mm (at calm water level) at even keel (zero heel and trim). The breach hole (80 mm × 80 mm), facing the waves, was initially open and both rooms are flooded up to the external calm water level in the beginning of the test. Regular (sinusoidal) waves were used with an amplitude  $a_w = 70\text{mm}$  and period of  $T_w = 2.5\text{s}$ . The dimensions of the arrangement are presented in Figure 5.11.

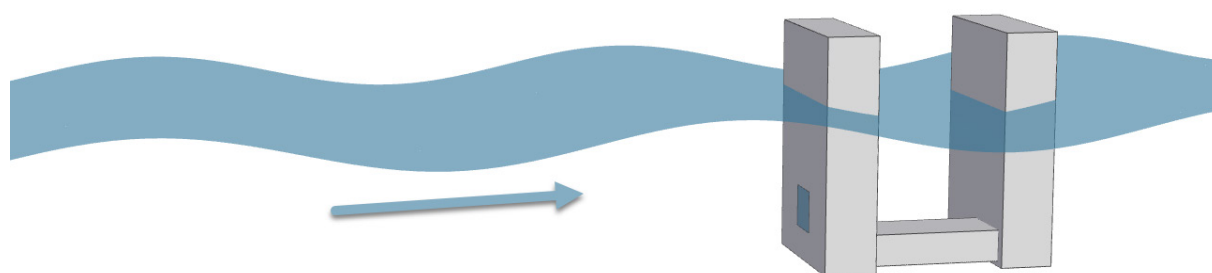


Figure 5.10 Illustration of cross-flooding case in waves (shorter waves used to for visualization); the arrow points the direction of the waves

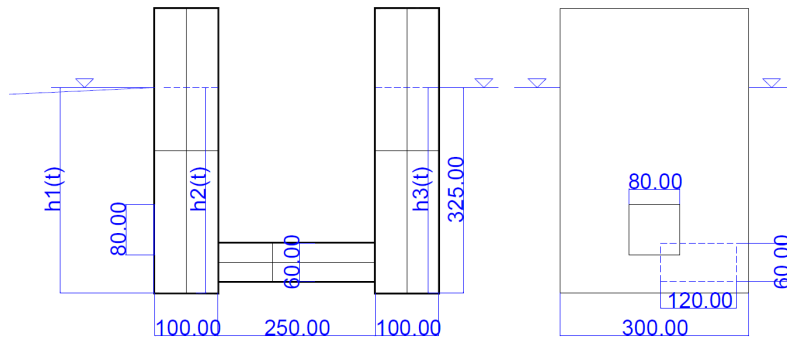


Figure 5.11 Key dimensions of the cross-flooding case (A3), courtesy of UNINA

The external water level at the breach is:

$$h_1(t) = d + a_w \sin(\omega t)$$

where  $d = 325\text{mm}$  is the calm water draft of the model and  $\omega$  is the circular frequency of the wave.

Participants were requested to provide simulation results for water level for the breach side, at REL\_14 i.e.  $h_2(t)$ , and for the intact side, at REL\_15 i.e.  $h_3(t)$ .

### 5.5.2 Results

With the given wave condition, i.e.  $T_w = 2.5\text{s}$ , the system is in resonance, resulting in a phenomenon where the water level amplitude for the intact side (REL 15) is larger than for the breached side (REL 14). This was not originally intended. The resonance condition with regular waves is not very relevant for simulation of realistic ship flooding cases, where possible waves are always irregular.

The time histories of water elevation on both sides are presented in Figure 5.12. Furthermore, MSRC provided results with two different modelling principles, first considering the duct as a separate room (official results) and secondly by using a simplified approach with only two compartments, connected by an opening. The results for both approaches are shown in Figure 5.13.

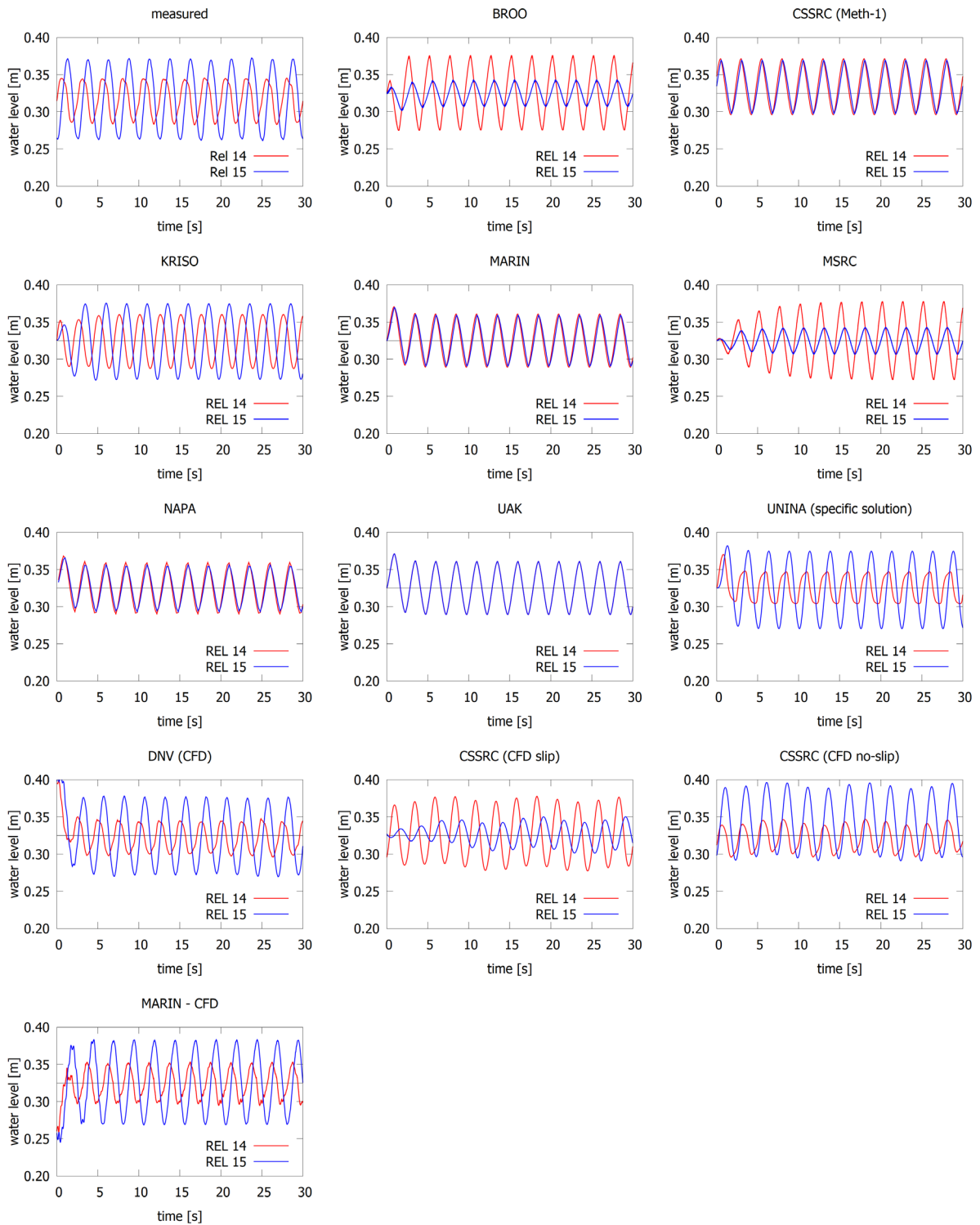


Figure 5.12 Water elevation histories in the cross-flooding case A3 at sensors REL 14 in the breached side and REL 15 in the intact side of the U-void

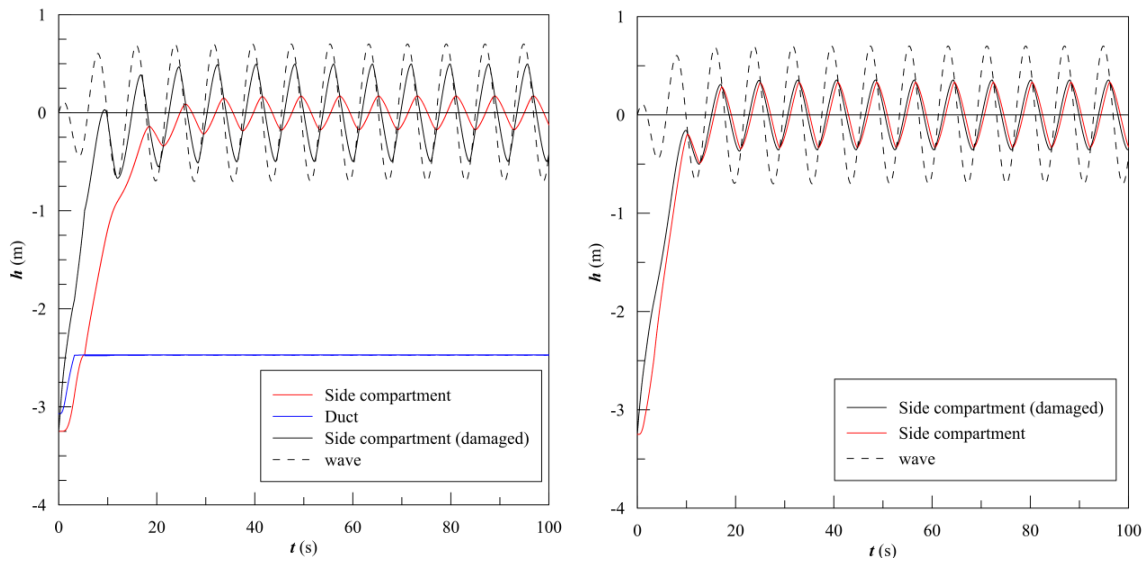


Figure 5.13 PROTEUS results by MSRC for the cross-flooding in waves (A3) with two different modelling principles: on the left the duct is a separate room and on the right only two compartments are considered

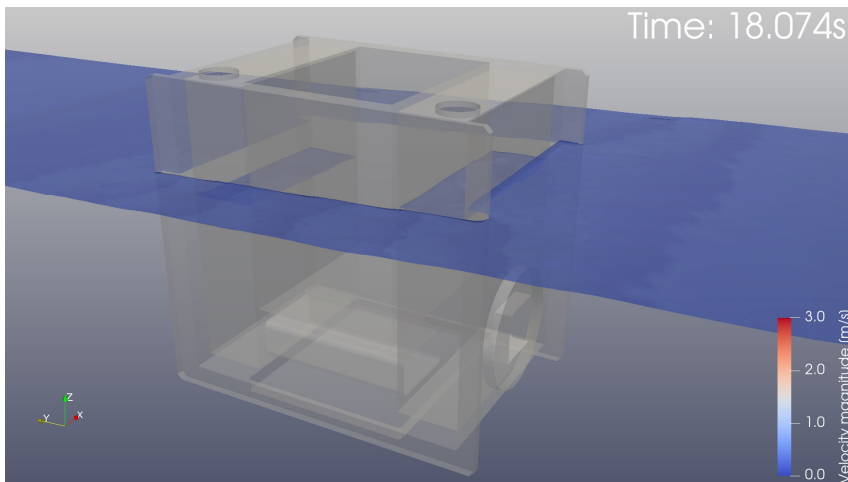


Figure 5.14 Snapshot of ComFLOW simulation results by MARIN for the case A3

Table 5.3 Comparison of CFD methods used for the cross-flooding in waves case (Part A3)

	CSSRC – CFD	DNV	MARIN – CFD
<b>Software</b>	Star-CCM+	Star-CCM+	ComFLOW
<b>Grid size (number of cells)</b>	3 230 000	93 000	624 000 ... 1 140 000
<b>Boundary condition</b>	Slip & no-slip separately	No-slip	No-slip
<b>Turbulence model</b>	Realizable k-ε two layer	Laminar flow	Laminar flow
<b>Time step</b>	1.0 ms	25 ms	0.128...5.77 ms

Based on the results for cross-flooding in regular waves, the following observations are made:

- Many participants, CSSRC (Meth1), MARIN, NAPA and UAK, predict almost equal water levels on both sides of the U-shaped compartment. This is due to the applied Bernoulli method for the calculation of the water flow through the relatively large openings.
- The PROTEUS code, used by both BROO and MSRC, results in a notable phase shift, and significantly smaller water level amplitudes in the intact side. However, if the cross-duct is not modelled as a separate room, the results are more consistent with the other participants codes using hydraulic models, Figure 5.13. Therefore, this may be a result of the incorrect calculation for the flow through a filled-up room (see results for the benchmark Part A1).
- The code by KRISO captures correctly that water level amplitudes in the damaged side is smaller than in the intact side. The main reason is the newly implemented “vertical column model” in the code, that also considers the dynamic pressure component due to the vertical average velocity in the water column.
- The code by UNINA provided a specific numerical solution for this oscillating flow in U-tube problem, and the results match fairly well with measurements, however, the amplitude in the breached side is underestimated.
- The CFD solutions used by DNV (Star-CCM+ for this case) and MARIN (ComFLOW) correctly capture the resonance phenomenon and the larger amplitudes in the intact side of the tank. The Star-CCM+ solution used by DNV slightly underestimated the amplitude in the damaged side, while the ComFLOW simulation used by MARIN provides a better estimate.
- CSSRC used Star-CCM+ with two different boundary conditions in their CFD analyses. The “slip” condition seems to be unsuitable for this problem, indicating that the surface friction is not negligible. On the other hand, the “no-slip” condition captures the larger water level amplitude in the intact side. In general, the results are neither qualitatively nor quantitatively comparable to the calculations by DNV and MARIN. This may result

from the scale effects, and that the approach with a turbulence model could be more suitable for full-scale analyses.

In general, conventional Bernoulli-based flooding simulation tools are not capable to solve this kind of a resonance condition in a U-shaped compartment. In fact, this proved to be a very complex case also for CFD codes. However, the new improved code of KRISO seems to be very promising. Finally, it should also be noted that these results are not providing much insight into the applicability of the codes on more realistic flooding scenarios in irregular waves, which are studied in the Parts B and C of the benchmark.

## 5.6 Case A4 – Progressive Flooding on Deck

### 5.6.1 Description

Progressive flooding in a complex arrangement of rooms and openings is very characteristic for passenger ships. The studied case is part of the bulkhead deck of a large cruise ship, consisting of 20 individual compartments, bounded by bulkheads and connected through 33 internal openings, representing open doors. The scale of the model is 1:60, and the model is kept captive with an external water level 30 mm above the deck level. All compartments were open on top to ensure full ventilation. The arrangement is illustrated in Figure 5.15. The inlet room that connects the deck to the sea was initially dry, and some participants also modelled this room, whereas others considered only the flooding of the deck. The thickness of the bulkheads is 4 mm, and participants were advised to consider this in their modelling. The breach is in the side of one compartment, and it is opened instantly in the beginning of the test, causing the flooding of the deck.

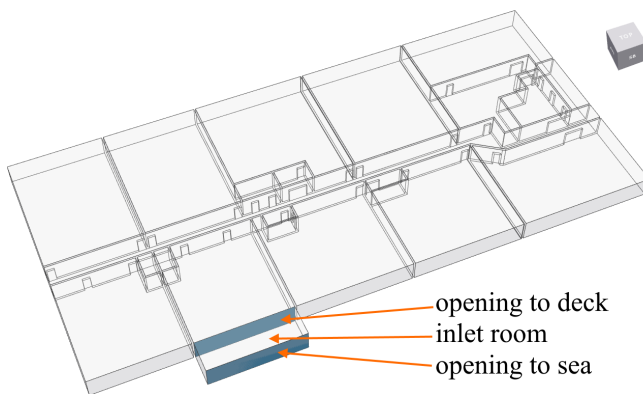


Figure 5.15 Deck arrangement for benchmark Part A4.

With the simulation methods that are using hydraulic model, the long corridor needs to be divided into smaller parts that are connected by large openings. This modelling practice was introduced by Santos et al. (2002) for capturing transient asymmetric flooding of symmetric machinery areas, and it enables more accurate calculation of the flooding progression along the corridor, especially in the test condition with fixed zero trim. Initially, modelling instructions were not provided, and each participant modelled the corridor according to their best practices, see Figure 5.16.

In general, the following two different approaches were applied:

- General division, based on partial bulkheads and/or assumed location of open doors along the corridor; constant discharge coefficient for all “virtual” openings
- Case specific definition, based on the location of the breach (MSRC & UNITS also applied different effective  $C_d$  values for different “virtual” openings). In the case of MSRC this was obtained by adjusting the opening areas.

With CFD and SWE (Shallow Water Equations) methods, applied by CSSRC, DNV, MARIN and HSVA, the compartments were discretized into a calculation grid.

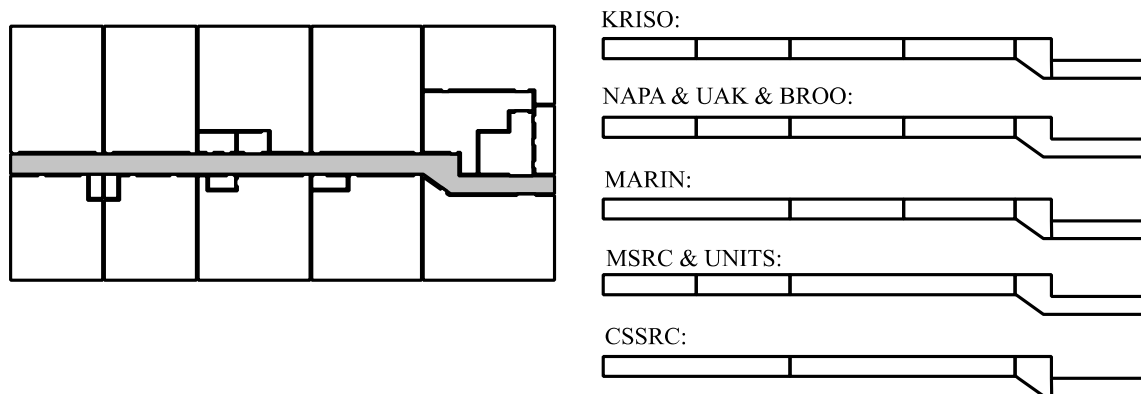


Figure 5.16 Initial modelling of the long corridor in the deck flooding case A4, illustrating the variety in the different approaches

During an online workshop, where initial results were presented and discussed, it was decided that in order to ensure fair and equal benchmarking, it is essential that the corridor is modelled in a unified way with the same discharge coefficients. Since these openings are not restricting the flow along the corridor, a discharge coefficient value of 1.0 was selected, Figure 5.17. After this decision Chantiers de l'Atlantique provided an initial general arrangement drawing for the sample ship, showing that this part of the corridor would likely have quite many double leaf fire doors, Figure 5.18, and therefore, the adopted unified modelling would correspond well with typical modelling practices for such corridor arrangement.

The total volume of floodwater in full scale at equilibrium is presented in Figure 5.19. The variation is quite small, and likely caused by simplifications in modelling the bulkhead thicknesses. As a summary, it is believed that the modelling accuracy is reasonably good, and notable differences in the simulation results cannot be explained by modelling mistakes.

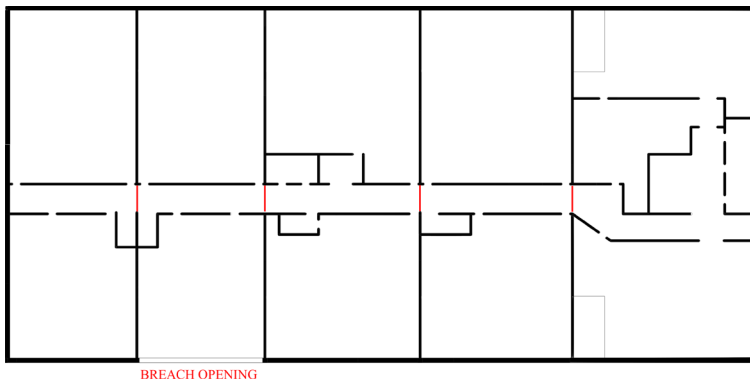


Figure 5.17 Unified modelling instructions for the corridor with division by large openings (red lines) at the locations of the partial transverse bulkheads, each with  $C_d = 1.0$ .



Figure 5.18 Initial general arrangement of the deck section, with planned double leaf doors in the service corridor (Courtesy of Chantiers de l'Atlantique)

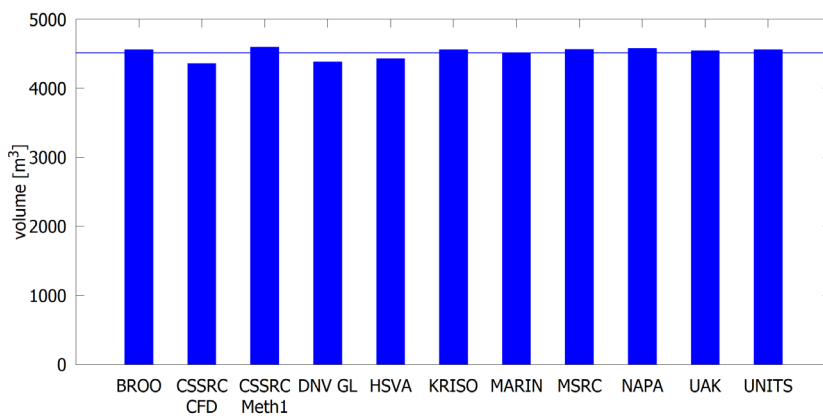


Figure 5.19 Comparison of total volume of water (in full scale) at equilibrium; the blue line marks the average

Both CSSRC and DNV calculated the case with CFD tools, using Star-CCM+ and OpenFOAM, respectively. In both cases volume of fluid (VOF) method was applied, and model scale was used. CSSRC used a very detailed mesh and short time step, whereas DNV aimed at using as coarse grid as possible to obtain maximum computational performance. Moreover, a laminar flow was assumed. A comparison of the parameters is presented in Table 5.4.

Table 5.4 Comparison of CFD methods used in deck flooding case (Part A4)

	CSSRC	DNV	MARIN
<b>Software</b>	Star-CCM+	OpenFOAM	ComFLOW
<b>Grid size (number of cells)</b>	1 080 000	165 000	505 186 ... 1 196 604
<b>Boundary condition</b>	Slip & no-slip separately	Wall	No-slip
<b>Turbulence model</b>	Realizable k-ε two layer	Laminar flow	Laminar flow
<b>Time step</b>	1 ms	10 ms	0.08 ... 2.6 ms

HSVA used shallow water equations (SWE) model for the calculation of flooding in the rooms. A grid of 38 × 78 cells was applied, and the long corridor was considered as a single room. Bernoulli's equation, with the recommended discharge coefficients, was used for calculation of the flow rate in the openings, with the recommended discharge coefficients.

### 5.6.2 Results

Measured water levels at sensors are used for detailed assessment of flooding progression on the deck. The selected sensors at different areas of the deck layout are presented in Figure 5.20.

In the model test water flooded rapidly along the corridor and through large openings to the rooms on both ends of the deck (sensors 3 and 27). Flooding to the rooms in the middle (sensor 16) is initially slower, Figure 5.21.

Comparison of water levels at the selected sensors are presented in Figure 5.22 – Figure 5.29. The locations of the sensors are shown in Figure 5.20. The breached room is flooded rapidly, and the water level temporarily exceeds the external sea level, Figure 5.22. This behaviour is captured by the CFD and SWE methods, used by CSSRC, DNV and HSVA. However, there is a quite notable difference in the amplitude, period and dampening of the water elevation. On the other hand, the methods based on a hydraulic model predict only the filling up of the room to the external sea level.

At sensor REL 21 that is in a room on the other side of the corridor, opposite to the breached room, all methods capture the development of the water elevation rather well, Figure 5.23. In general, the Bernoulli-based codes predict a slightly faster initial flooding, whereas the CFD by CSSRC and the SWE code by HSVA predict a slower flooding. Consequently, the deviation in the results is quite notable, but the shapes of the simulated water elevation curves match quite well with the measurements.

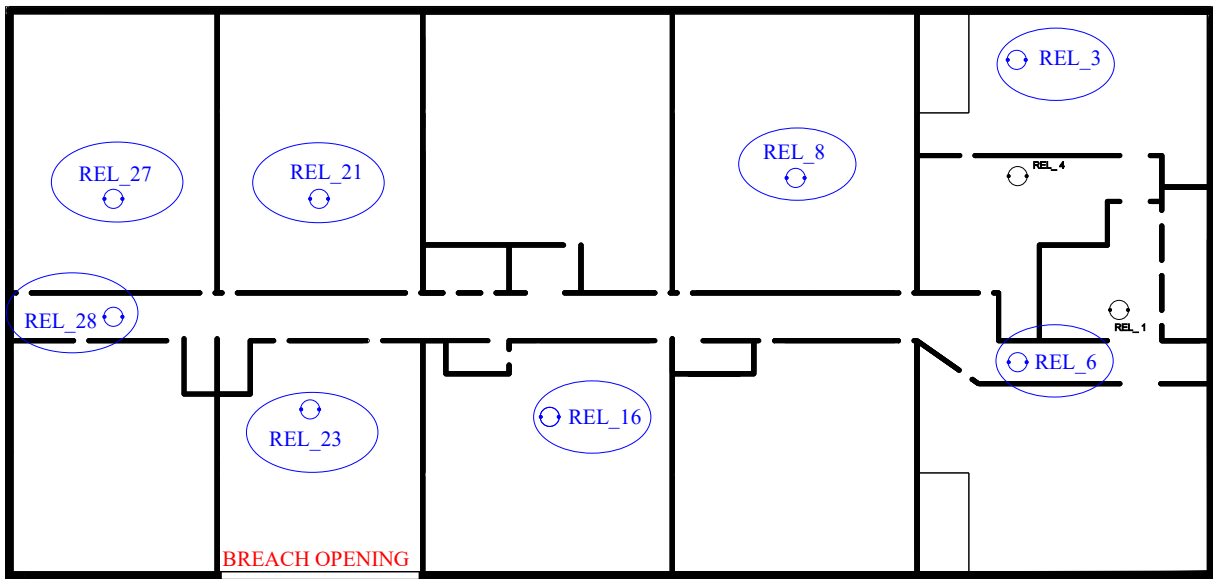


Figure 5.20 Locations of selected water level sensors for comparing simulation results with the measurements

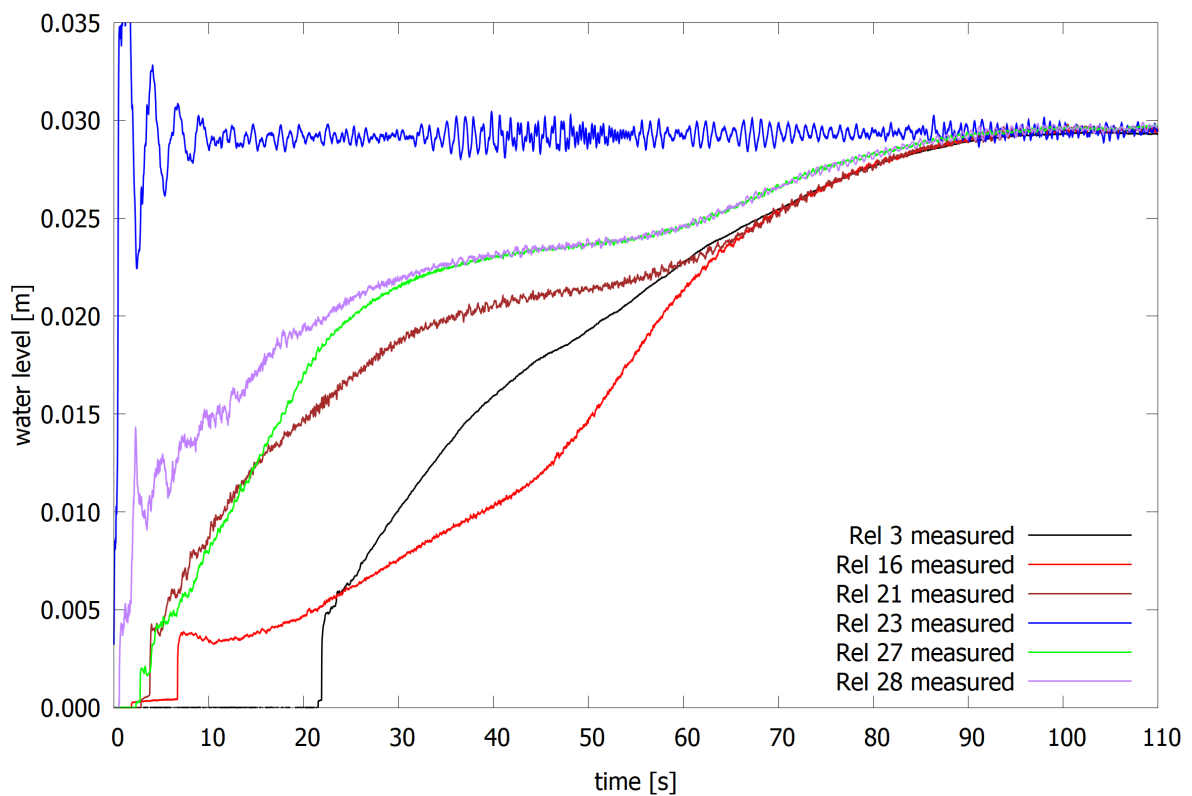


Figure 5.21 Measured water levels for selected sensors in the deck flooding case

The floodwater progresses rapidly along the long corridor, and therefore the water elevation at sensors REL 16 and REL 8 are very interesting. At REL 16, the flooding is initially slow, but after about 45 s the water level starts to increase more rapidly. CFD tools by CSSRC, DNV and MARIN, as well as the SWE simulation by HSVA capture this rather well, Figure 5.24. This behaviour is even more pronounced at sensor REL 8, Figure 5.25, where the flooding of the room from the corridor is notably delayed, which is properly predicted only by CFD codes and the code used by KRISO. In general, the Bernoulli-based codes predict a much faster flooding of these compartments, and despite of the unified modelling principles, the scatter of the results is very wide. The code used by KRISO provides very good results, likely due to the newly implemented “corridor room model” that considers the momentum of the flow along the corridor. The details of this new feature have not yet been published by KRISO.

Water elevation at the aft end of the corridor, sensor REL 28, is predicted rather well by the simulation codes, Figure 5.26. However, the fluctuations in the beginning of the flooding are captured only by the CFD and SWE methods (CSSRC, DNV, MARIN CFD and HSVA). Also flooding of the room at the aft end of the corridor on port side, REL 27, Figure 5.27, is predicted well, Figure 5.27. Only the SWE method by HSVA results in a much slower flooding process than measured.

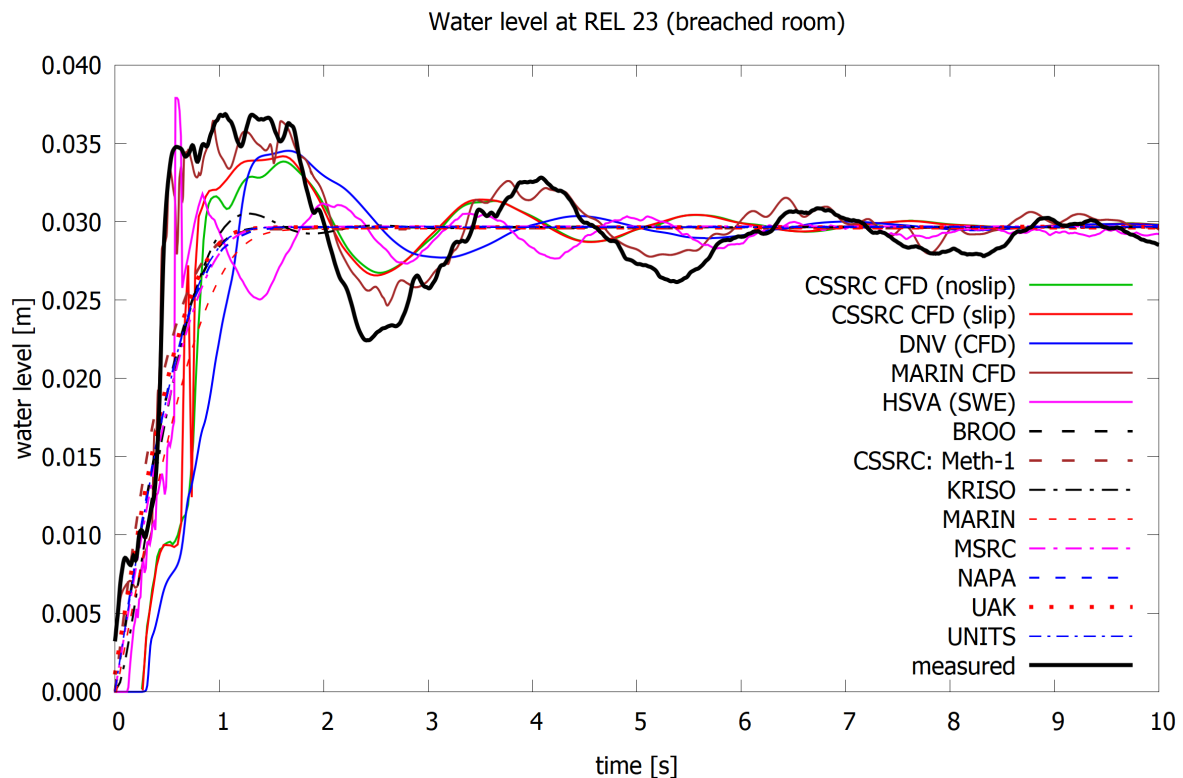


Figure 5.22 Comparison of water level at sensor REL 23 that is located in the breached room

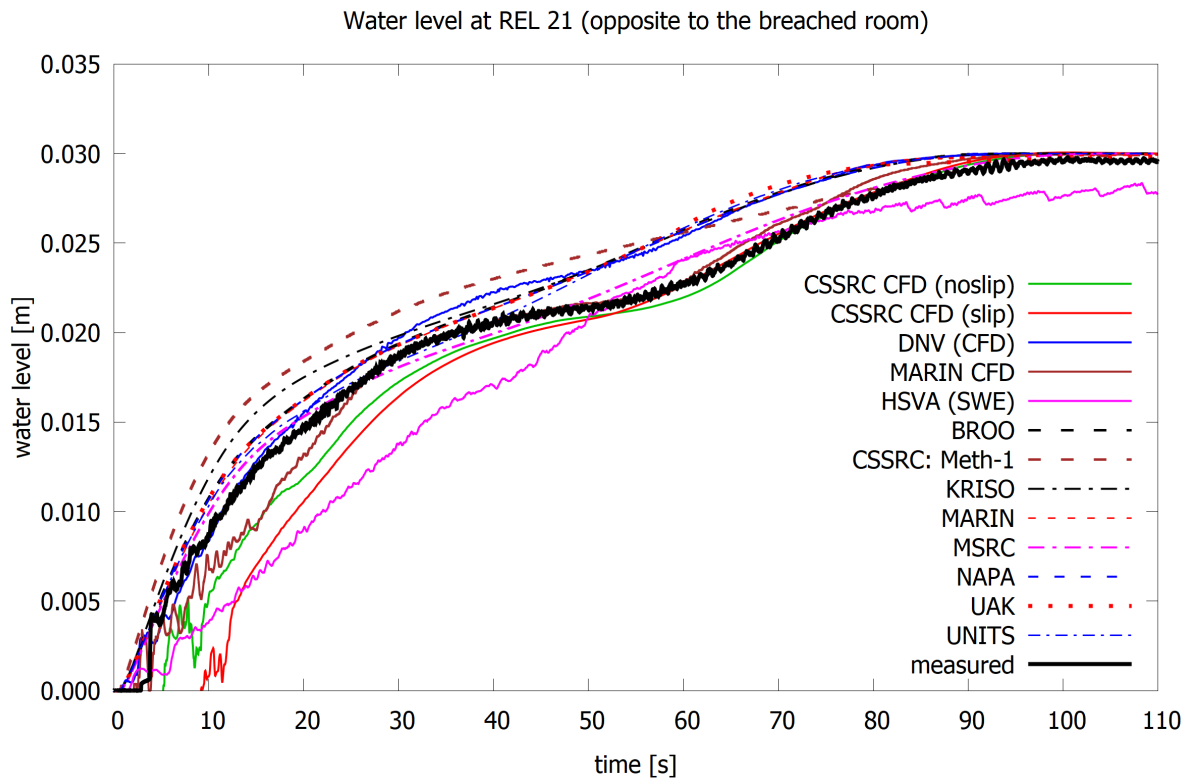


Figure 5.23 Comparison of water level at sensor REL 21 in a room that is opposite to the breached room

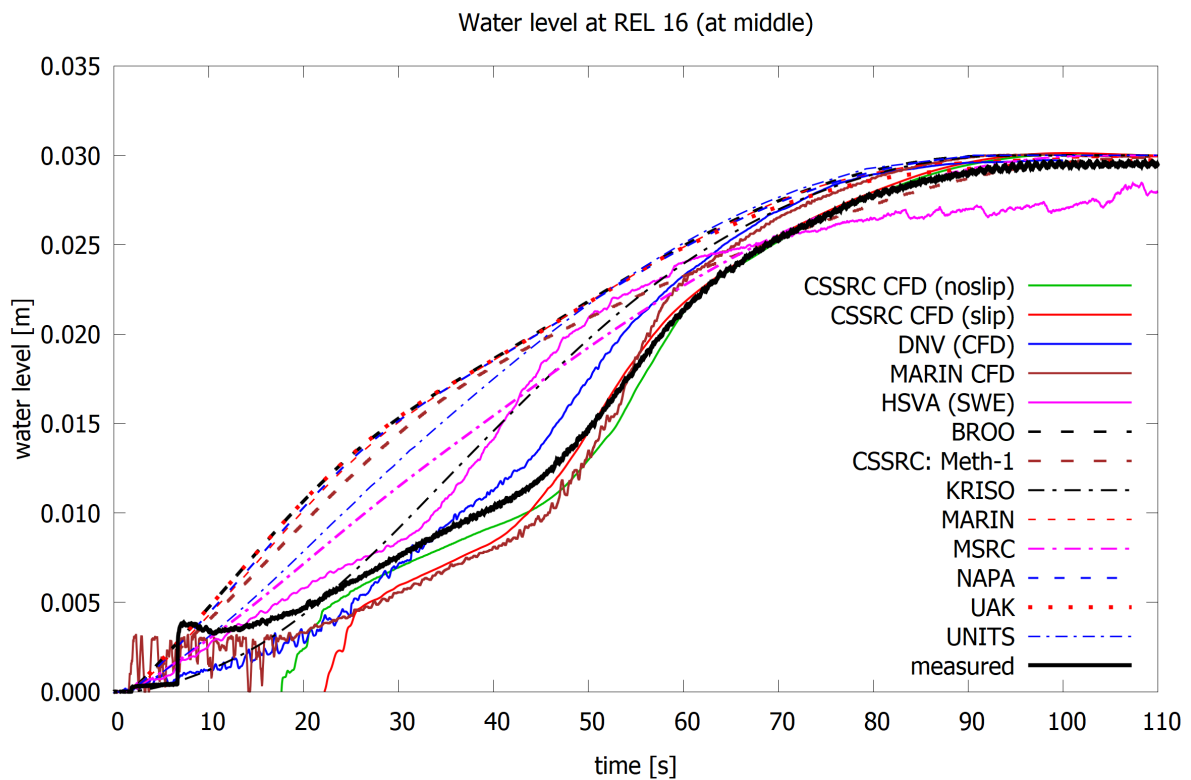


Figure 5.24 Comparison of water level at sensor REL 16 that is located in a room at the middle of the deck

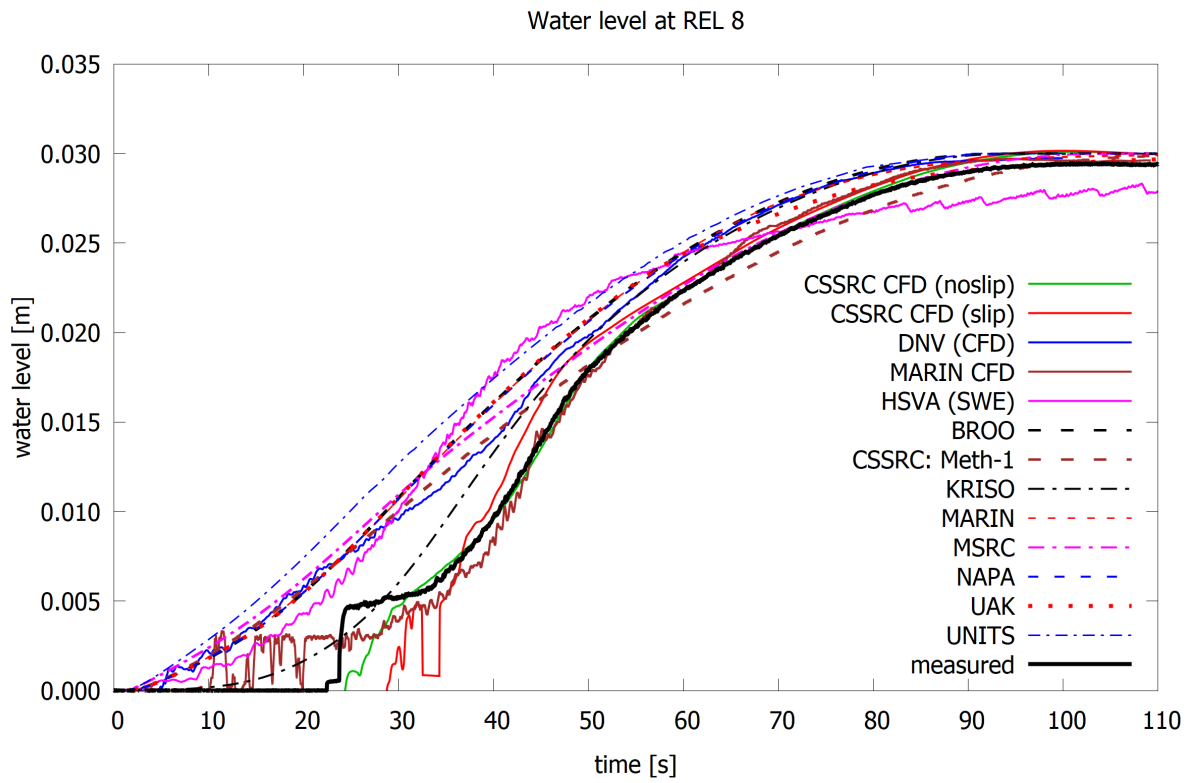


Figure 5.25 Comparison of water level at sensor REL 8 that is located in a room at the middle of the deck

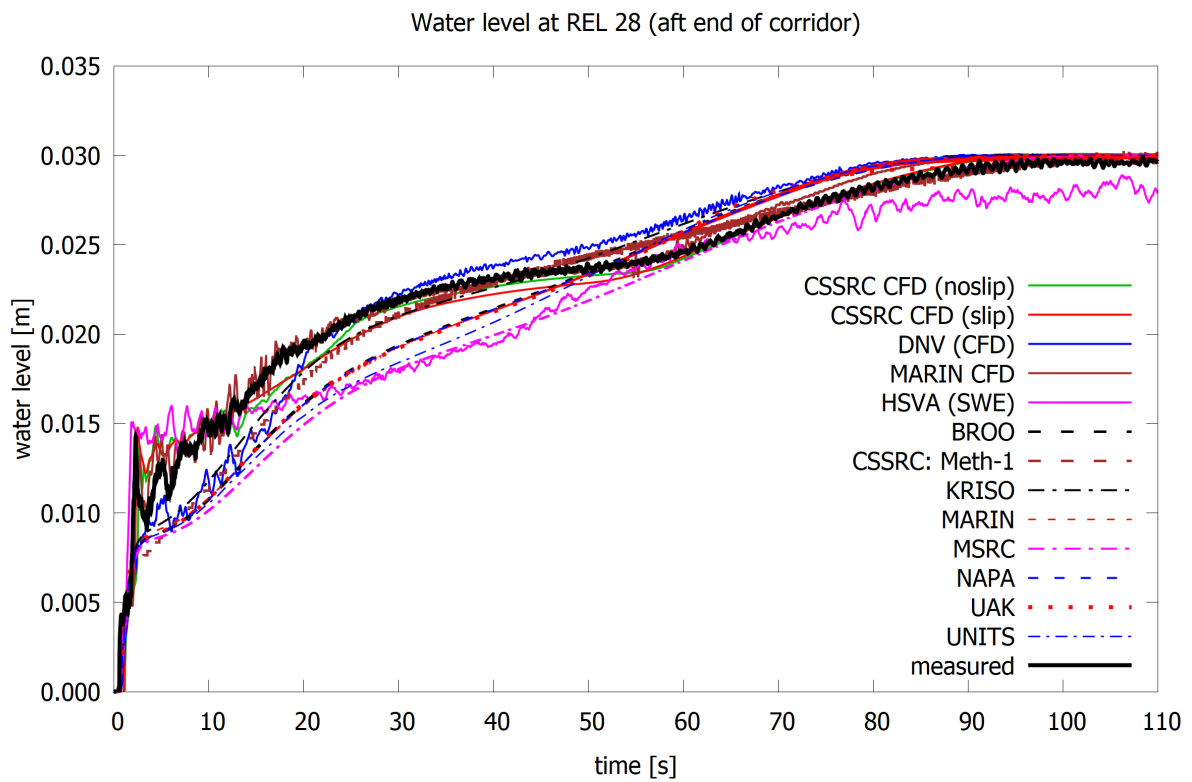


Figure 5.26 Comparison of water level at sensor REL 28 that is located in the aft end of the corridor

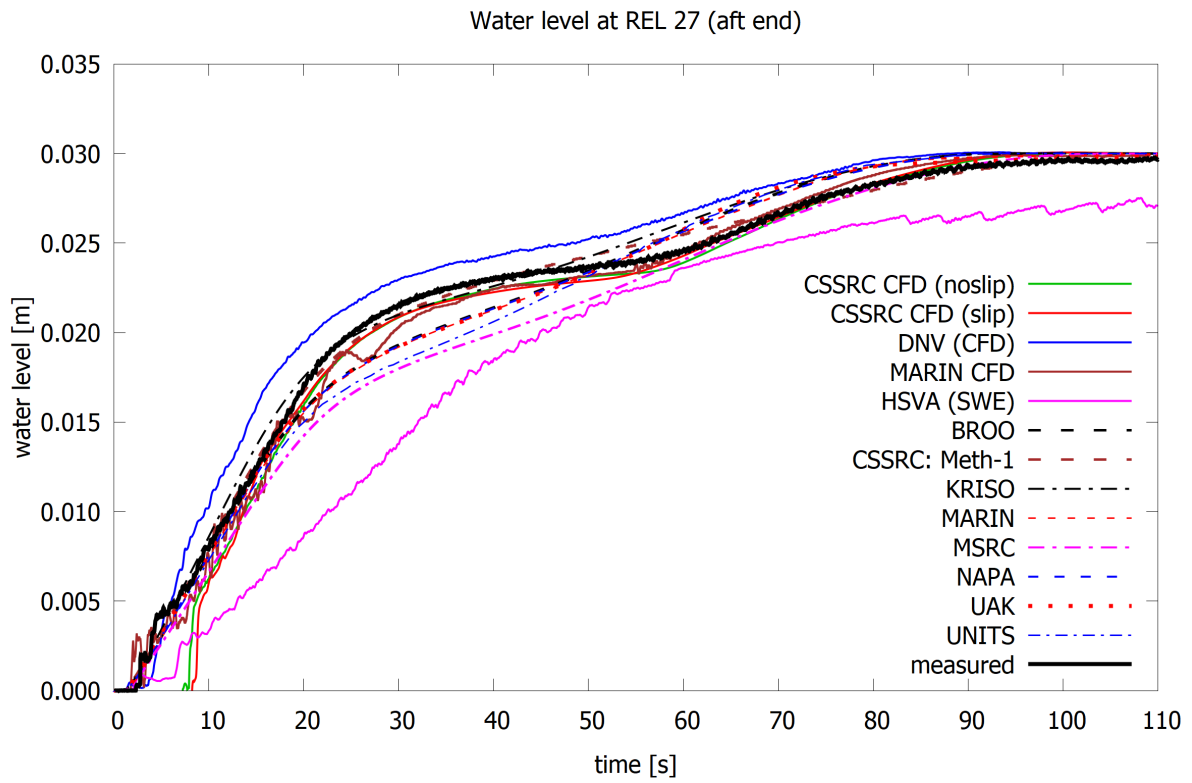


Figure 5.27 Comparison of water level at sensor REL 27 that is located in a room in the aft end of the deck

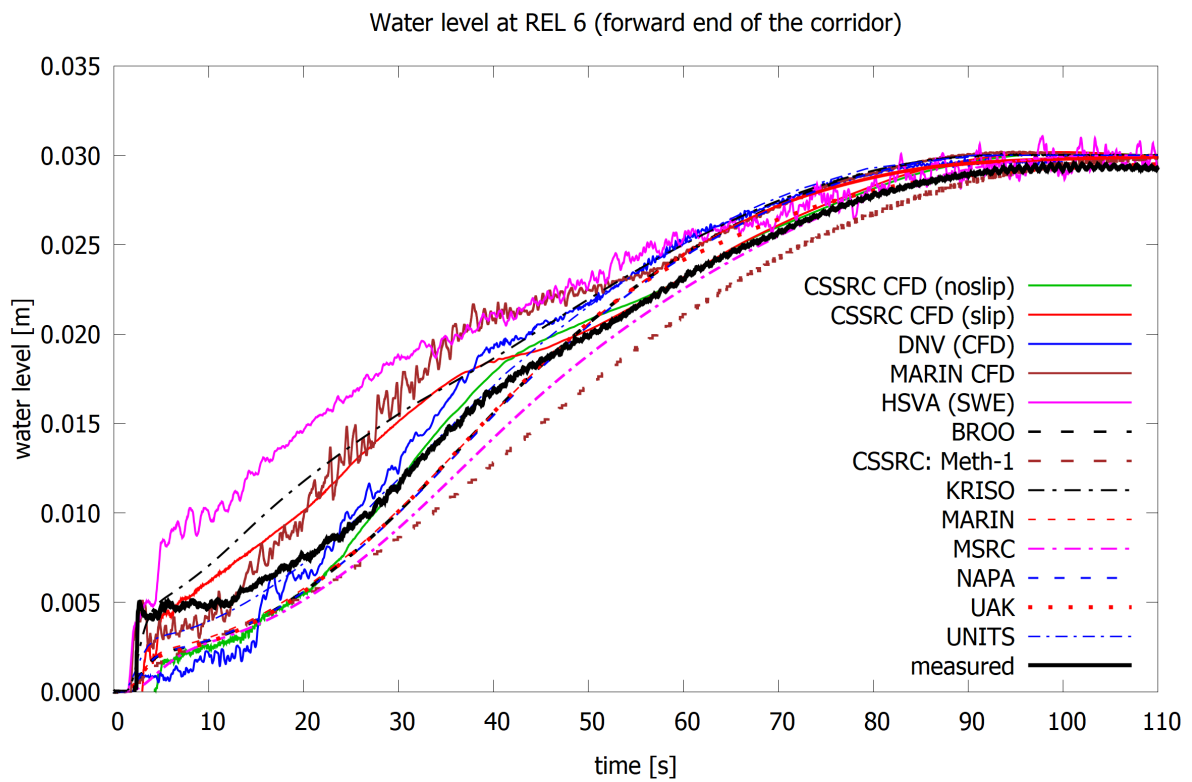


Figure 5.28 Comparison of water level at sensor REL 6 that is located in the forward end of the corridor

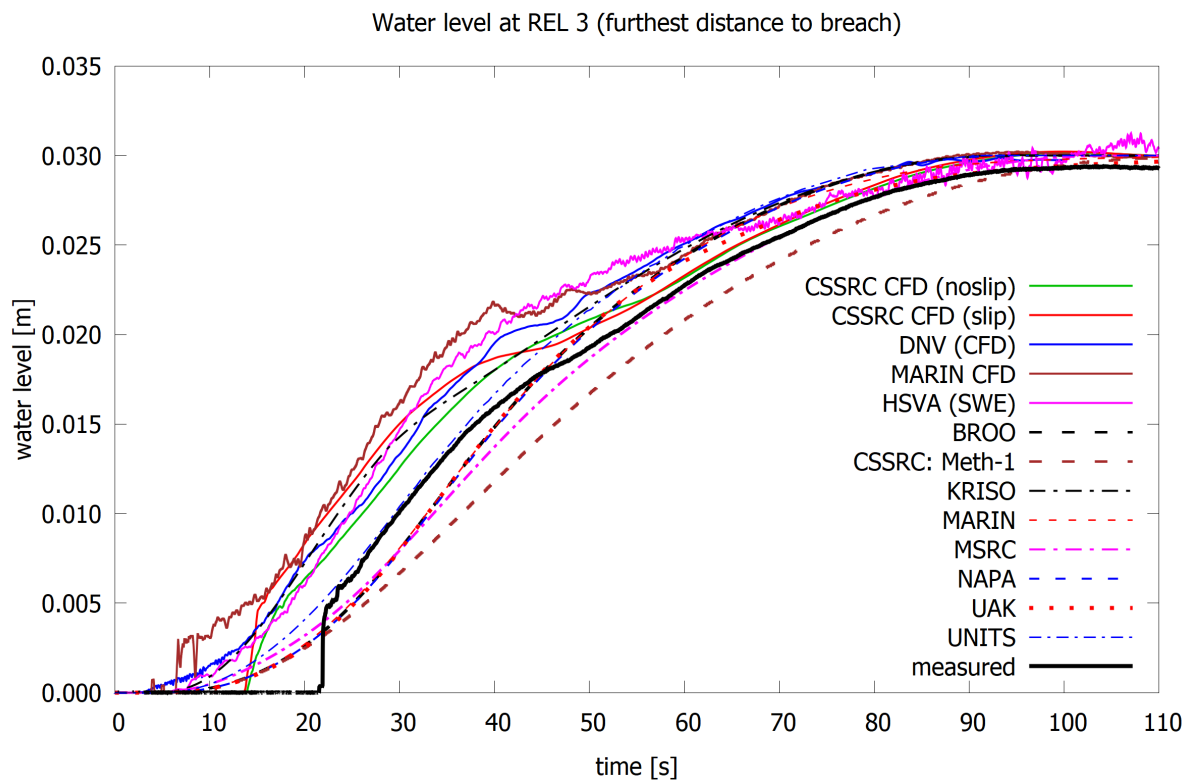


Figure 5.29 Comparison of water level at sensor REL 3 that is located far from the breach opening

When water level reaches about 15 or 20 mm, the numerical simulation results match better with the measurements, and the actual time-to-flood is captured very well. It is worth noticing that the scale of the model (1:60) is smaller than the minimum scale (1:40), as recommended in ITTC (2017). However, the model basin restrictions did not allow a larger scale for testing such a large cruise ship, and using part of the actual cruise ship arrangement for both Part A and Part B (cruise ship flooding) was considered as an advantage.

Due to the small scale of the model, the surface tension had a notable effect in the flooding process with small water levels. This is clearly visible in the video capture in Figure 5.30. In general, this behaviour cannot be captured by the applied simulation methods. However, the CFD methods, used by CSSRC, DNV and MARIN provide rather good results also for the early stages of flooding of the compartments, whereas the Bernoulli-based simulation methods predict more uniform progressive flooding to all rooms.

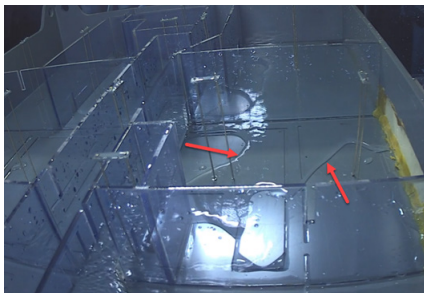


Figure 5.30 Surface tension effects during the beginning of flooding of a compartment are clearly visible in the video capture from the experiment.

The CFD simulations by CSSRC, DNV and MARIN predicted well the water levels in different compartments. Visualisation of flooding progression at selected time steps are presented in Figure 5.31 (MARIN), Figure 5.32 (CSSRC) and Figure 5.33 (DNV). The results demonstrate the rapid flooding along the corridor and that the side rooms in the middle of the deck arrangement are flooded later than the rooms in both ends.

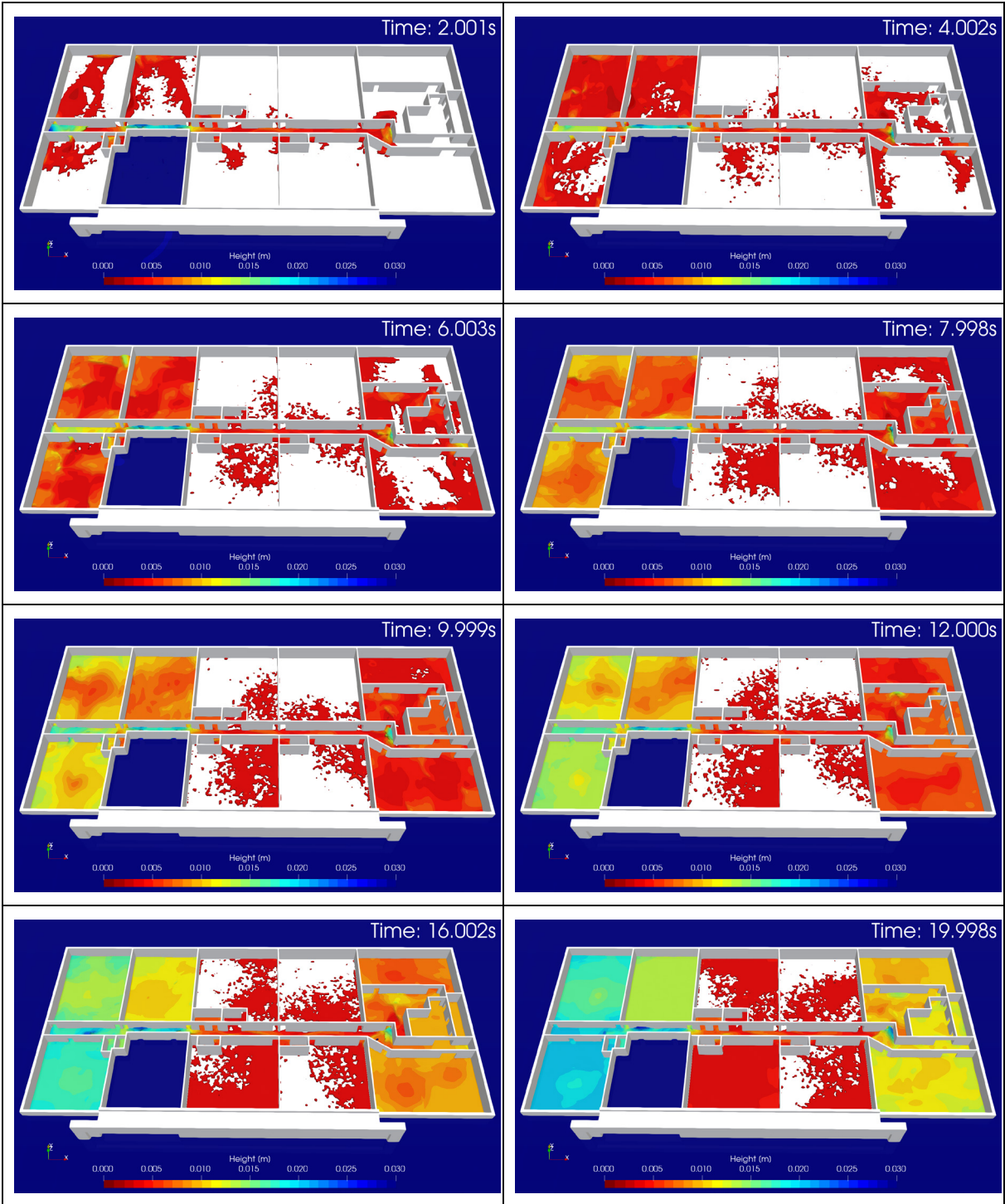


Figure 5.31 Visualization of the deck flooding from the ComFLOW CFD simulation by MARIN

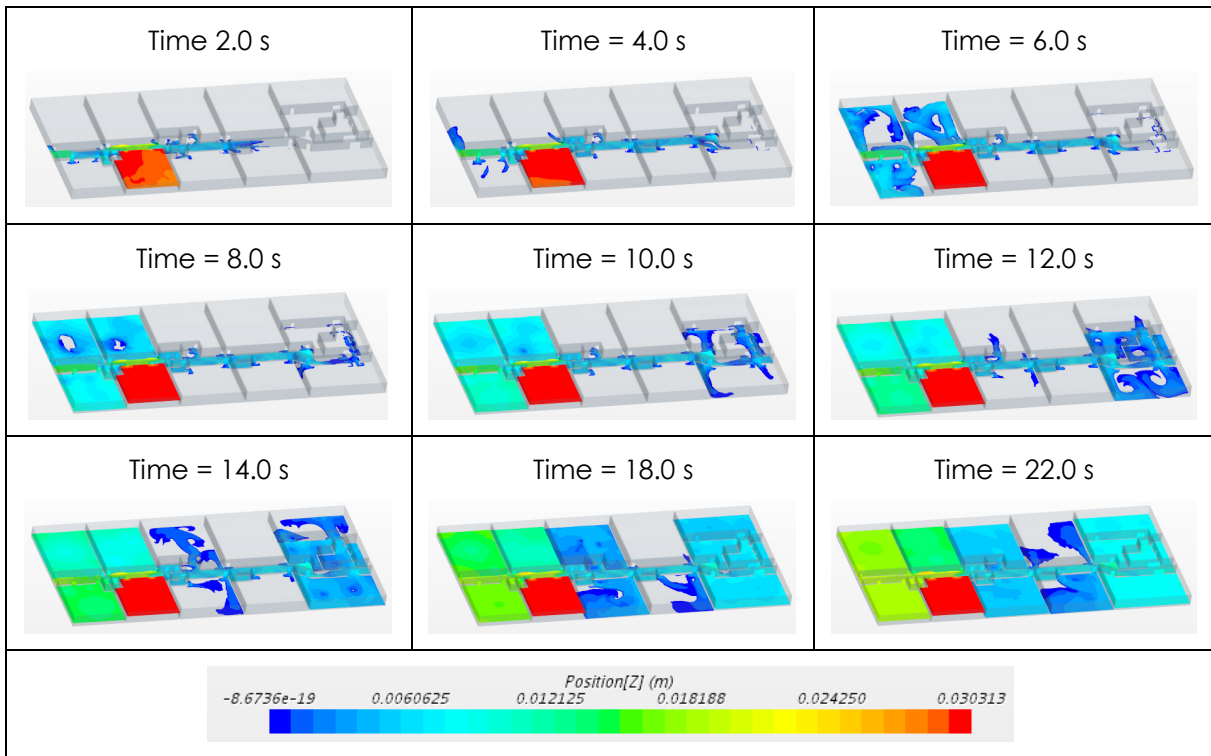


Figure 5.32 Visualization of the deck flooding from CSSRC CFD simulation with Star-CCM+ using no-slip boundary condition

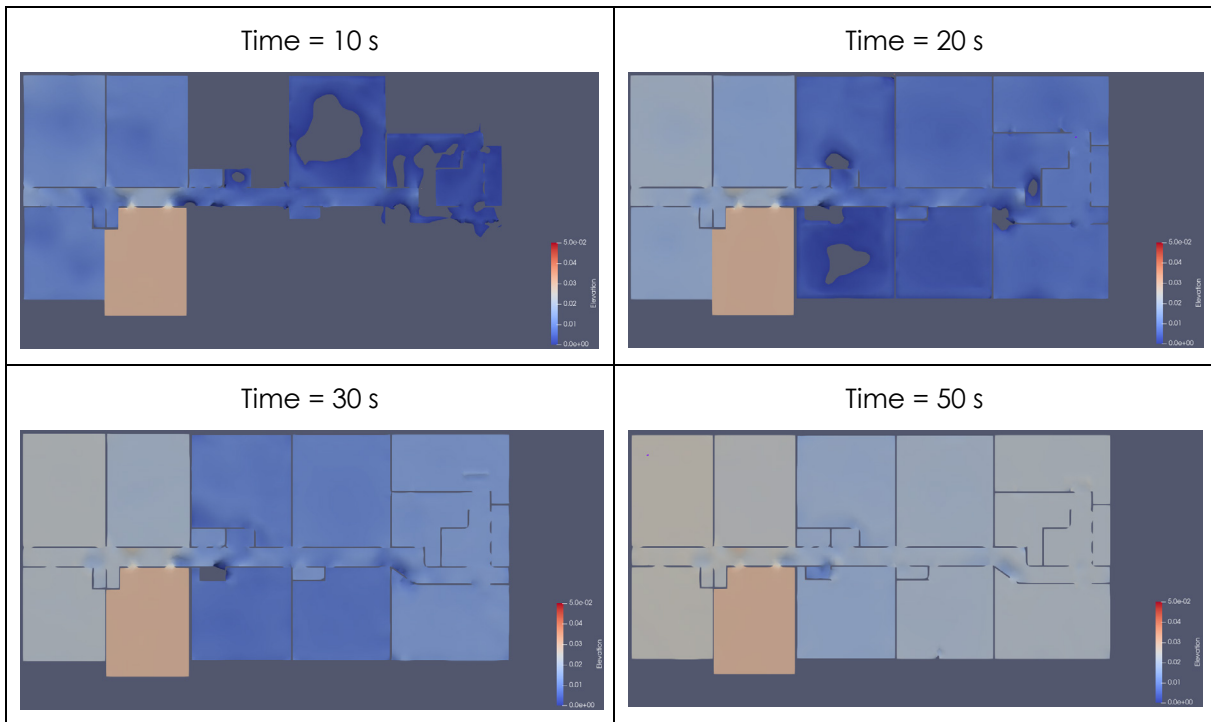


Figure 5.33 Water elevation on the deck flooding after 10, 20, 30 and 50 s from the OpenFOAM calculation by DNV, view from top

### 5.6.3 Computational performance

In order to obtain some insight into the required computational resources for flooding simulations, each participant was asked to provide:

- Computation time for the case
- Short description of applied hardware

The quantity used in comparison is relative computation time:

$$t_{rel} = \frac{t_{comp}}{t_{sim}}$$

where  $t_{comp}$  is the reported computation time and  $t_{sim}$  is the maximum full-scale simulation time. CFD tools were used in model scale, and the provided results have been converted to full scale.

The results are presented in Figure 5.34 on a logarithmic scale. It should be noted that some participants reported CPU time, whereas most presented a wall clock time. A short summary of the reported information is given in Table 5.5. Obviously, the applied time step affects also the computational performance of the code. The participants could freely select a suitable time stepping in the simulations since the applied time integration method and implementation of the code may set restrictions.

Different codes also use different methods and algorithms, for calculation of volumes within the simulation process, and these also affect the total performance. For example, UNITS has reported that about 50% of the total computation time is spent in these auxiliary calculations with pressure integration techniques.

Only the CFD calculations were slower than the simulated time, i.e.  $t_{rel} > 1$ . With most of the Bernoulli-based methods the computations were significantly faster. However, the variation in the relative computation time is quite large, and it cannot be explained solely by the applied hardware. For the CFD tools the applied hardware and parallel computing can have a significant effect on the required computation time, yet in any case these will be notably slower than real time.

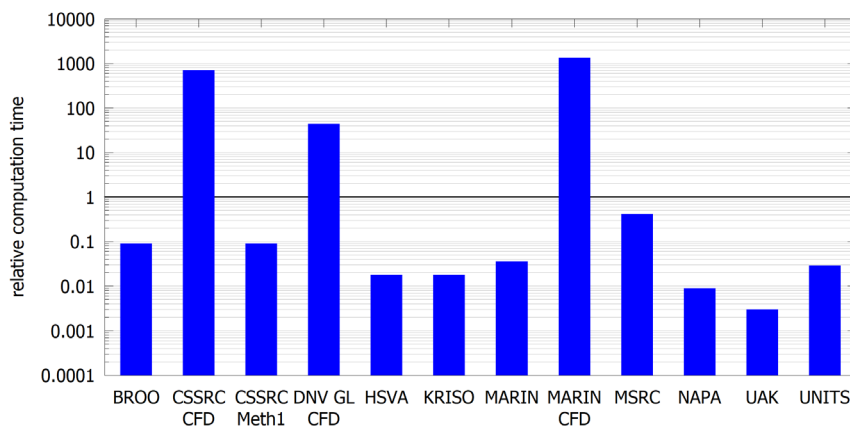


Figure 5.34 Reported relative computation time for deck flooding case A4

Table 5.5 Summary of deck flooding case simulations and applied hardware

code	time step [s]	scale	time	hardware
BROO	0.020	full	clock	Intel i5 8th gen
CSSRC-CFD	0.001	model	clock	20 cores
CSSRC-Meth1	0.032		clock	Intel i7 3rd gen
DNV GL	0.010	model	clock	16 cores on an old cluster Intel Xeon CPU E5-2690 0 @ 2.90Hz
HSVA	0.100	full	CPU	Intel Xeon (Linux)
KRISO	0.010	model	clock	Intel i7 4th gen
MARIN	0.050	full	clock	Intel Core i7-8850H CPU @ 2.60GHz, 6 Core(s)
MARIN CFD	$8 \cdot 10^{-5}$ - 0.026	model	clock	Parallel computation with 24 cores
MSRC	0.020	full	clock	Intel i7 8th gen
NAPA	1.000	full	clock	Intel i7 8th gen
UAK	0.200	full	CPU	Intel i7 10th gen
UNITS	0.035 - 11.298	full	clock	Intel i7 4th gen

## 6 FLARE BENCHMARK B – CRUISE SHIP FLOODING

### 6.1 Model Geometry

Cruise ships are characterized by complex arrangement of compartments, with several non-watertight decks and bulkheads in the watertight compartments. The FLARE sample ship 3, provided by Chantiers de l'Atlantique, was selected as a representative design for the benchmark.

The flooding model tests were conducted at MARIN in the scale 1:60. The internal arrangement is simplified yet representative of the real arrangement. The profile of the ship, a photo of the model and the main dimensions in full and model scale are presented below in Figure 6.1, Figure 6.2 and Table 6.1, respectively.

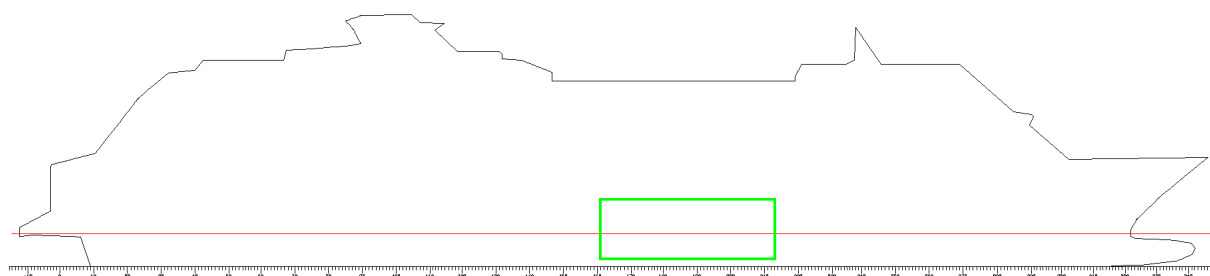


Figure 6.1 Profile picture of the cruise ship, with the damage location illustrated with the green rectangular



Figure 6.2 Cruise ship model (courtesy of MARIN)

Table 6.1 Main dimensions of the studied ship in full-scale and model scale (1:60)

	<b>Full scale</b>	<b>Model scale</b>
Length over all	About 300 m	About 5.0 m
Length between perpendiculars	270.00 m	4.5 m
Breadth	35.20 m	0.587 m
Subdivision draught	8.20 m	0.137 m
Height of bulkhead deck	11.00 m	0.183 m
Gross tonnage	95 900	-

Three separate cases were studied:

- B1: transient flooding in calm water
- B2: transient flooding in beam seas
- B3: smaller breach resulting in up-flooding in calm water

The examined damage is a large (3 compartment) breach on the starboard side, forward from amidships, Figure 6.3. In the cases B1 and B2 the breach extends vertically over 6 decks from the double bottom. In the model tests the breach was opened instantly, resulting in an extreme transient flooding condition. In the case B3 the breach is vertically limited to the lowest two decks.



Figure 6.3 Breach opening in the SB side of the model (courtesy of MARIN), note that on decks 3 and 4 the breach length is smaller in the aft end

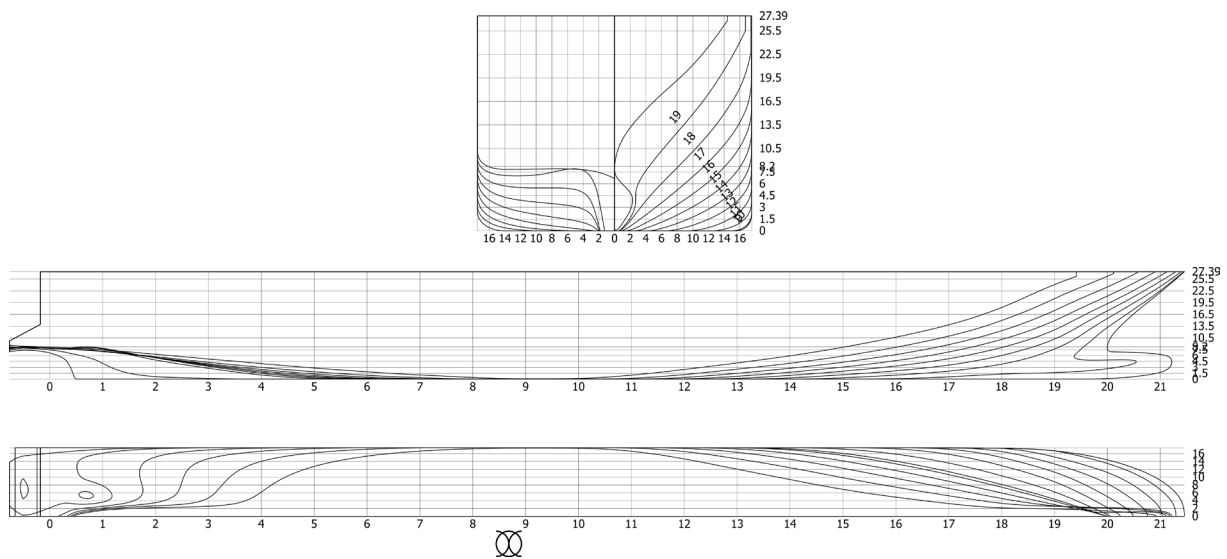


Figure 6.4 Lines drawing of the studied cruise ship

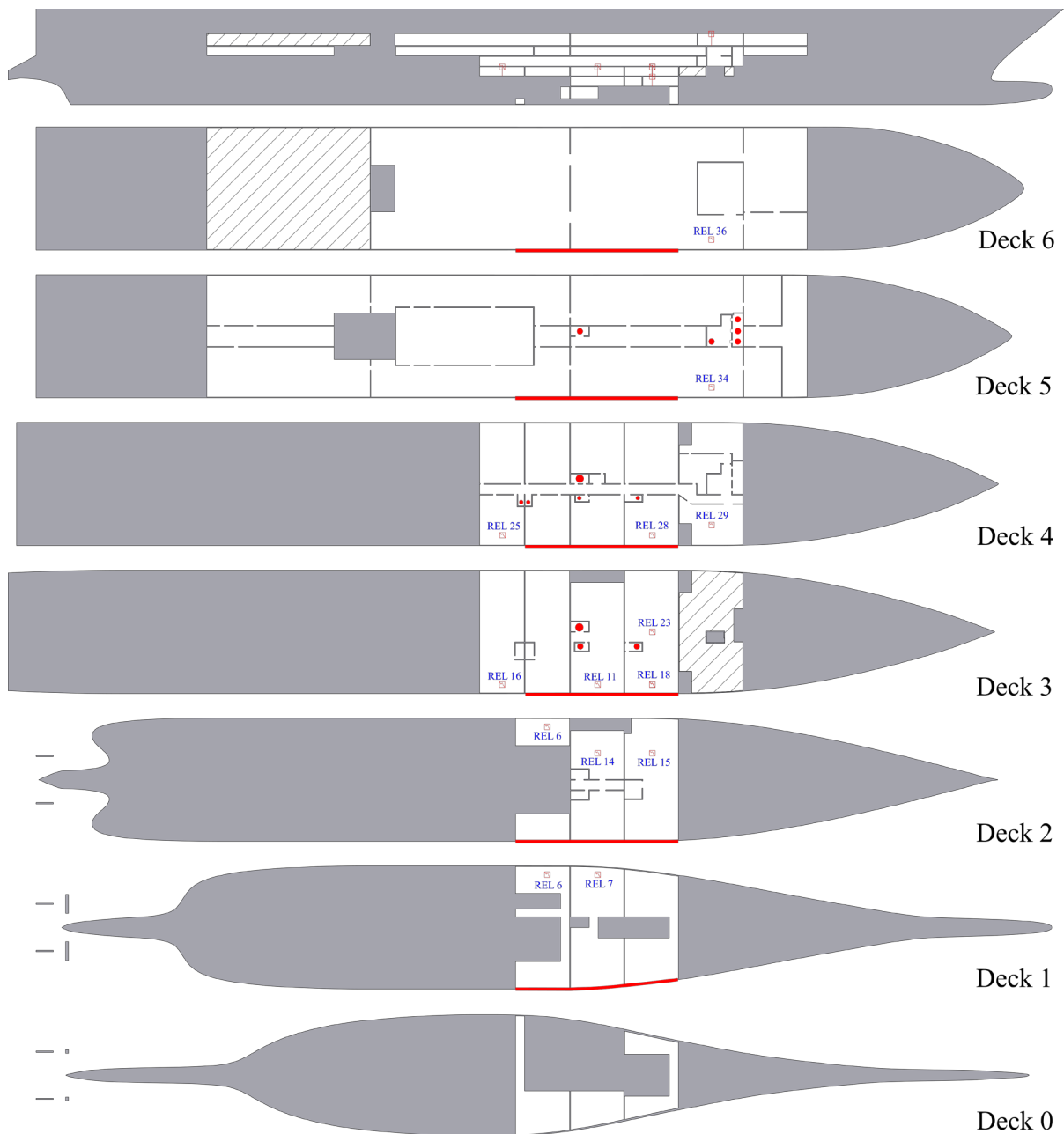


Figure 6.5 Floodable compartments; the hatched rooms were filled with foam and thus not floodable, and the red squares mark the selected water level sensors, filled red circles denote holes in the deck and thick red lines mark the breach locations (in cases B1 and B2)

The compartments were ventilated through pipes on the intact side of the ship. In the benchmark study simulations, all compartments could be assumed as fully ventilated.

A lines drawing of the cruise ship is presented in Figure 6.4 and the floodable compartments, including the selected water level sensors are shown in Figure 6.5.

With Bernoulli-based simulation methods it is essential to divide the large rooms on decks 0 and 1 into smaller ones, connected by openings, in order to properly capture the transient asymmetric flooding of such large compartments. Participants used slightly different approaches, as shown in Figure 6.6. For CFD tools such artificial modelling technique is not

needed. MARIN also modelled the air pipes on the intact side of the ship and KRISO approximated the air vents based on the submitted material. With the other Bernoulli-based codes a full ventilation of compartments was assumed.

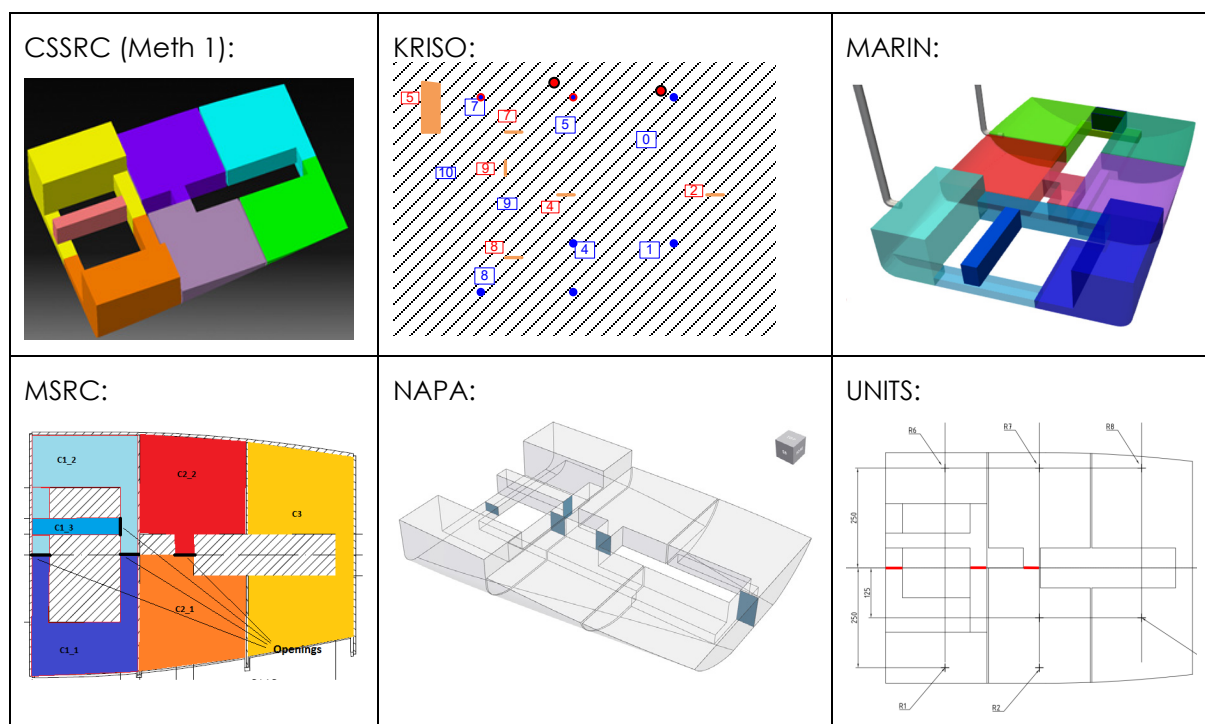


Figure 6.6 Modelling the compartments on the lower decks with different simulation codes

## 6.2 Comparison of Hydrostatics

The geometry of the potentially flooded internal compartments was shared to all participants in both 3D model (Rhino model in 3dm format) and conventional 2D drawings in dxf and dwg formats. The hull surface was provided in both IGES-format and conventional offset tables, prepared with NAPA software.

The volumes of the modelled intact displacement, buoyant hull and floodable compartments are presented in numerical format in Table 6.2. The differences are considered very small, but due to the complex arrangement of the compartments and different modelling principles, it was not possible to conduct detailed comparisons for individual rooms or openings.

Table 6.2 Comparison of volumes and centroids of different numerical models of the cruise ship

ID	Hull up to T = 20.4 m				Hull up to T = 8.2 m				Compartments			
	Vhull	Xhull	Yhull	Zhull	Vdisp	Xdisp	Ydisp	Zdisp	Vrooms	Xrooms	Yrooms	Zrooms
	m <sup>3</sup>	m	m	m	m <sup>3</sup>	m	m	m	m <sup>3</sup>	m	m	m
CSSRC	161555	126.111	0.000	11.287	51218	127.926	0.000	4.612	47947	149.695	-0.167	13.451
KRISO	161831	126.379	0.000	11.267	51356	127.920	0.000	4.591	48059	149.726	-0.169	13.434
MARIN	164300	124.346	0.000	11.337	51476	127.943	0.000	4.591	47689	149.675	-0.126	13.511
MSRC	162007	126.226	0.000	11.263	51548	127.801	0.000	4.591	48110	149.800	-0.172	13.418
NAPA	165638	126.089	0.000	11.176	53748	127.325	0.000	4.513	48005	149.641	-0.172	13.437
UNITS	162003	126.166	0.000	11.272	51477	127.813	0.000	4.596	47993	149.703	-0.171	13.443

The same initial condition, as listed in Table 6.3, is used for all three benchmark cases. It should be noted that the GM value is low, resulting in an extreme transient roll angle that the ship barely survives without capsizing. This may be very sensitive to small inaccuracies in the geometrical model or roll damping characteristics. Therefore, the participants were instructed to adjust the GM, if necessary, to ensure survival with correct stable heel angle in calm water.

Table 6.3 Initial condition of the cruise ship model (values in full-scale) as provided by MARIN

Draft	8.20 m
Trim	0.00 m
Initial metacentric height $GM_0$	2.36 m
Natural roll period	19.91 s

The provided initial  $GM_0$  is based on an inclining test of the model. In simulation tools the primary input is typically vertical center of gravity,  $KG$ , evaluated from the definition of the metacentric height:

$$GM_0 = KB_0 + \frac{I_T}{\nabla} - KG$$

Where  $KB_0$  is vertical center of buoyancy,  $I_T$  is transverse surface moment of inertia of the waterplane, and  $\nabla$  is volume of displacement.

Due to the hull form of the studied cruise ship,  $I_T$  changes rapidly when the ship is heeled, and the conventional analysis of an inclining test is therefore not very accurate.

Another source of inaccuracy is the applied discretization and integration methods in the numerical codes, especially related to calculation of the surface inertia moment. The simplified modelling of the appendages may also affect the vertical center of buoyancy.

Results for the studied damage scenarios are considered sensitive to the intact stability, and consequently, many participants finetuned the  $KG$  value to ensure that the steady heel angle after flooding (in benchmark case B1) matched the measured angle.

The main observations from the comparison of the hydrostatics and intact condition are:

- The static righting lever (GZ) curve for the intact ship and corresponding trim angle with different codes are presented in Figure 6.7. At larger heel angles, the differences are notable, and this needs to be considered when evaluating simulation results with large transient roll angles. On the other hand, for smaller heel angles the GZ values are consistent.
- The actual applied  $KG$  values are listed in Table 6.4. The values used are within a range of 0.14 m, corresponding to about 2 mm in model scale.
- Hydrostatic results for the hull and floodable compartments are listed in Table 6.2, indicating that participants had modelled the hull form with very similar results for the vertical centre of buoyancy. However, modelling of the appendages and different methods for calculating integrals may result in small variation in the actual vertical centre of gravity in the intact condition.

As a summary, differences in the righting lever values of the intact ship at large angles of heel may have some effect on the simulation results, especially during the transient flooding stage of the case B1.

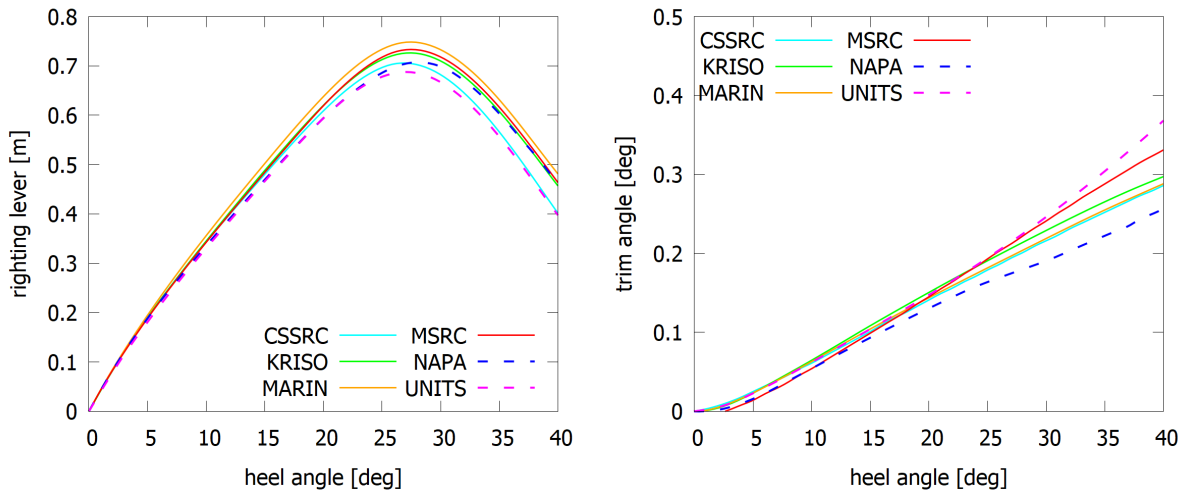


Figure 6.7 Righting lever (GZ) curves and related trim angle curves for the intact cruise ship

Table 6.4 Comparison of actual vertical center of gravity used by the participants

Participant	KG [m]
CSSRC	17.58
KRISO	17.50
MSRC	17.50
MARIN	17.45
NAPA	17.45
UNITS	17.59

### 6.3 Roll Decay for Intact Ship

Especially during the transient flooding stage, modelling of the roll damping can have a significant effect on results for roll motion. The cruise ship model was equipped with the following appendages:

- rudders
- propellers
- propeller shafts with supports
- bilge keels (outside the floodable compartment section)

as shown in Figure 6.8. Detailed geometry of these appendages was provided by MARIN. The displacement of the appendages is small, and therefore, some participants chose to use a bare hull for hydrostatics. However, the appendages have a significant effect on the roll damping characteristics.





Figure 6.8 Appendages of the cruise ship model (photo courtesy of MARIN)

A roll decay test was performed at MARIN for the intact model in the initial condition for the flooding tests. Based on analysis of the test results, logarithmic decrement  $\lambda = p + q\phi$  (in which  $\phi$  is the roll angle) was evaluated, resulting in  $p = 0.1082$  and  $q = 0.0285$  1/deg. Natural roll period of the intact ship was measured to be 19.91 s (full-scale).

Measurement data on the roll decay test, as well as detailed geometry of the appendages, was distributed to the participants beforehand to enable finetuning of various input parameters. Consequently, a simulation of the roll decay test was also requested, and the comparison is presented in Figure 6.9. The damping of the roll motion is fairly well captured by all codes, but there are still some notable differences.

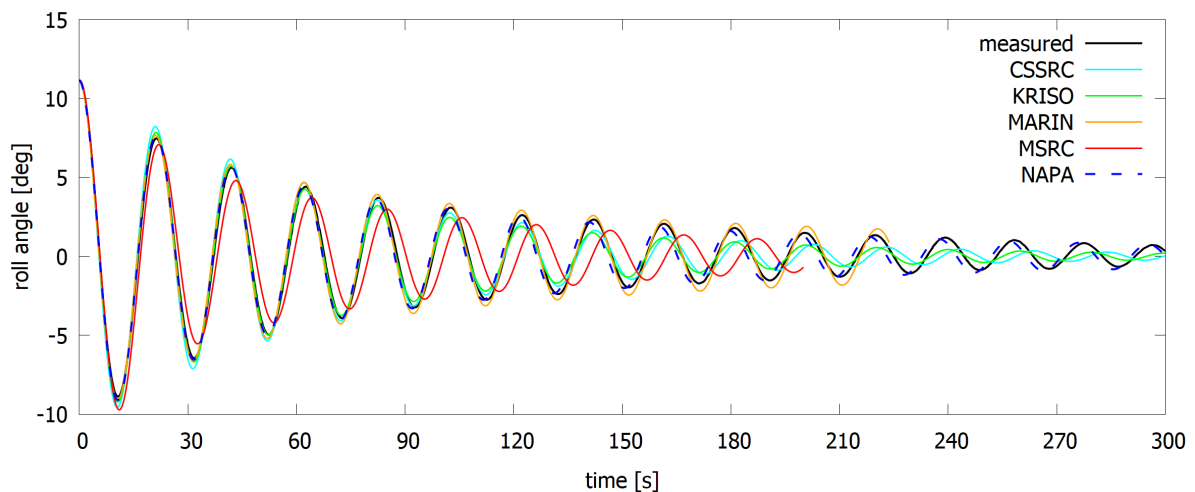


Figure 6.9 Measured and simulated roll decay

It should be noted that the code SMTP, used by KRISO, does not use roll damping input. Instead, the roll damping is considered to consist of the wave making damping calculated by potential theory, the skin friction of the hull, and eddy making damping of the bilge keel. The skin friction and eddy making damping are calculated by an empirical formula.

## 6.4 Case B1 – Transient Flooding in Calm Water

### 6.4.1 Description

The examined damage is a large (3 compartment) breach on the starboard side, forward from amidships. Vertically the breach extends over 6 decks from the double bottom. In the model tests the breach was opened instantly, resulting in an extreme transient flooding condition. In all tests, soft mooring was used.

The compartments are all ventilated through pipes on the intact side of the ship. Therefore, in the benchmark study simulations, all compartments can be assumed as fully ventilated. This subject is discussed in detail in section 6.7.

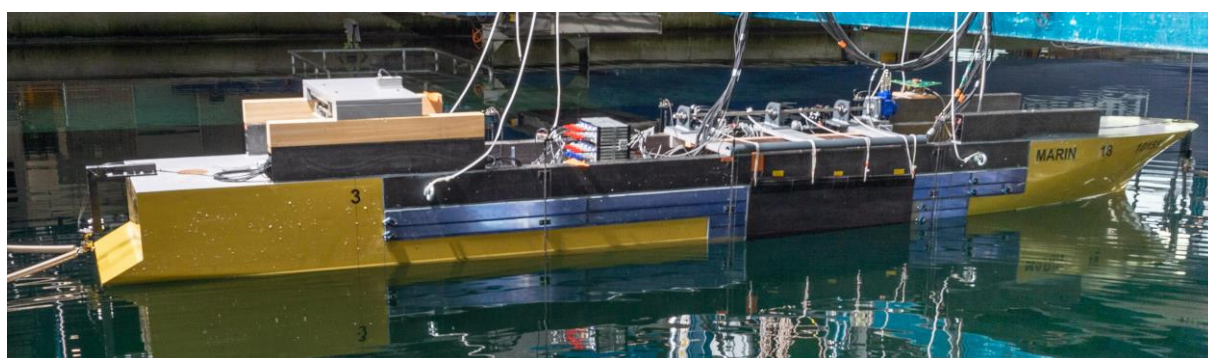


Figure 6.10 Floating model with the breach opening closed (courtesy of MARIN)

### 6.4.2 Results

The key quantities for comparison are the maximum roll angle and the time-to-flood (TTF). It should be noted that in this case, there is neither up-flooding nor down-flooding due to the large vertical extension of the breach, and in practice, floodwater propagates simultaneously on all immersed deck levels. During the large transient roll, also the upper decks are temporarily flooded.

The measured and simulated development of roll angle is presented in Figure 6.11. The maximum measured transient roll angle is  $30.7^\circ$ , and it was reached about 17.4 s (full scale) after the breach was initiated. After about 90 s a steady heel angle of about  $7^\circ$  is achieved. There is also some variation in the final steady state heel angle. However, since the maximum difference to the measured value is about  $0.5^\circ$ , it may be concluded that the initial condition and geometry of the flooded compartments have been modelled sufficiently accurately by all participants.

Sensitivity of the simulation results to the applied intact  $KG$ , as well as some modelling principles for the cross-flooding on Decks 0 and 1, are discussed in detail in Annex B: Sensitivity Analyses for Cruise Ship Flooding Cases on page 108.

There is some variation in the maximum simulated transient roll angle, and in general this is slightly underestimated. The smaller second peak is also captured by the codes with dynamic motions. NAPA uses a simplified method, combining dynamic roll motion and quasi-static trim and sinkage, but still captures the maximum transient roll rather well, although the equalizing

of roll is not properly predicted. UNITS simulation is based on purely quasi-static ship motions, and yet providing rather good results for a very dynamic flooding scenario.

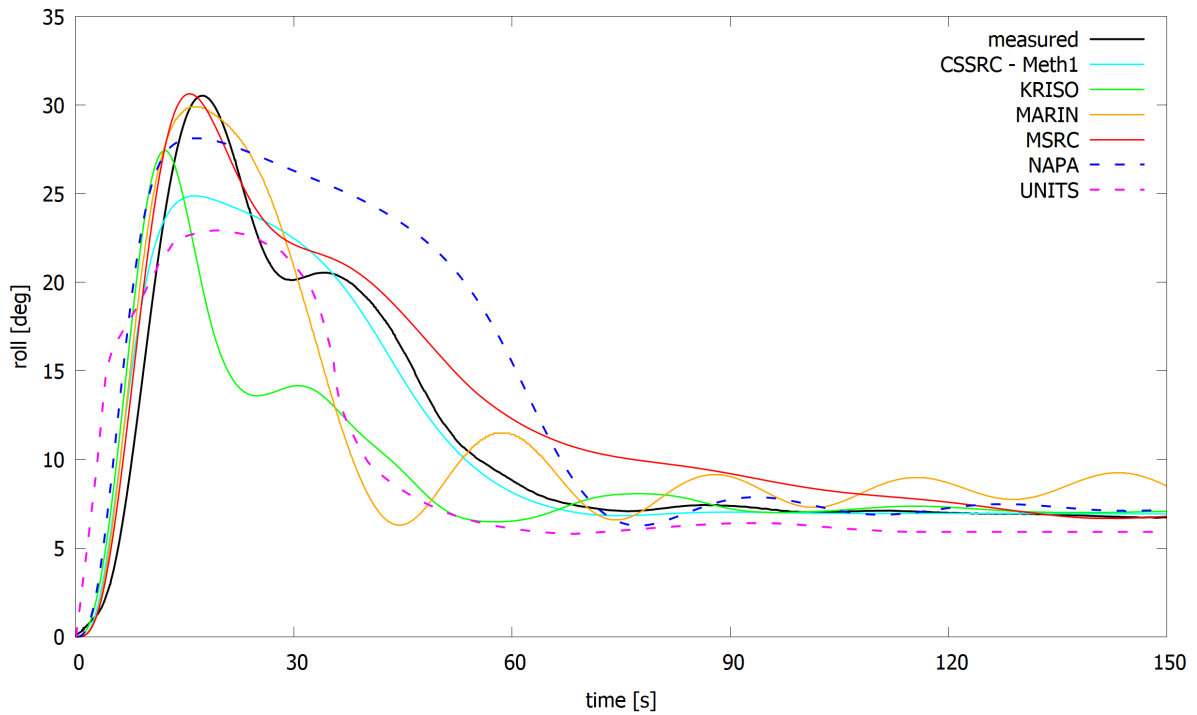


Figure 6.11 Measured and simulated roll motion for the transient flooding in calm water case B1

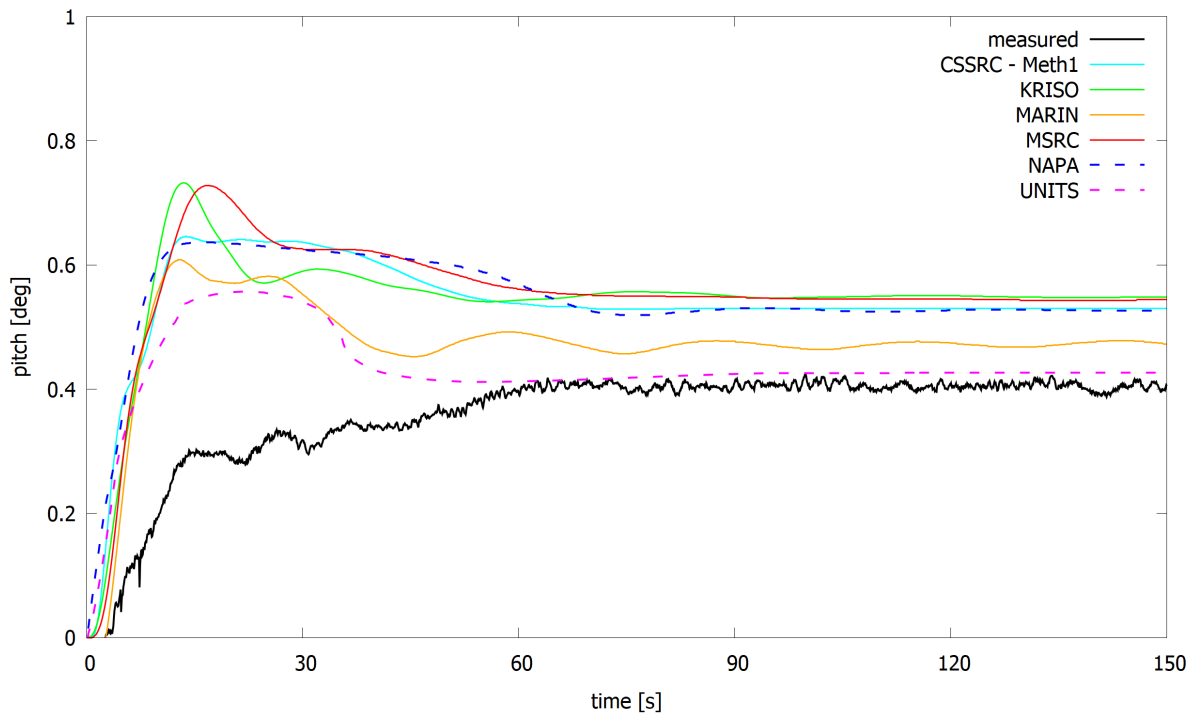


Figure 6.12 Measured and simulated pitch motion for the transient flooding in calm water case B1

The comparison of pitch, i.e. trim, angle is shown in Figure 6.12. All codes result in slightly larger pitch angle than measured, with UNITS having the best match. The maximum difference is about  $0.15^\circ$ , which is a rather small angle, but still has a notable effect on the draft values at bow and stern.

Comparisons of water levels are presented in Figure 6.13 – Figure 6.16. The locations of the selected water level sensors are shown in Figure 6.5.

The effect of transient large roll angle can be seen in temporary increase in the water level at sensor REL 6 in the intact side of the large void space (Deck 0 – Deck 2) in the aftmost damaged compartment. The sensor is briefly dried up due to the large transient roll towards the damage. After that, flooding continues and the whole room is filled up with water, Figure 6.13. The general behaviour is captured quite well, but there is significant variation in the height and time of the first peak in the water level. KRISO predicts a too rapid filling of the void space, whereas in the simulation by MSRC the filling is notably delayed. MARIN does not capture the peak in water level during transient roll motion, likely due to overestimated counter air pressure. The air pressure also explains why the whole sensor is not immersed within 150 s.

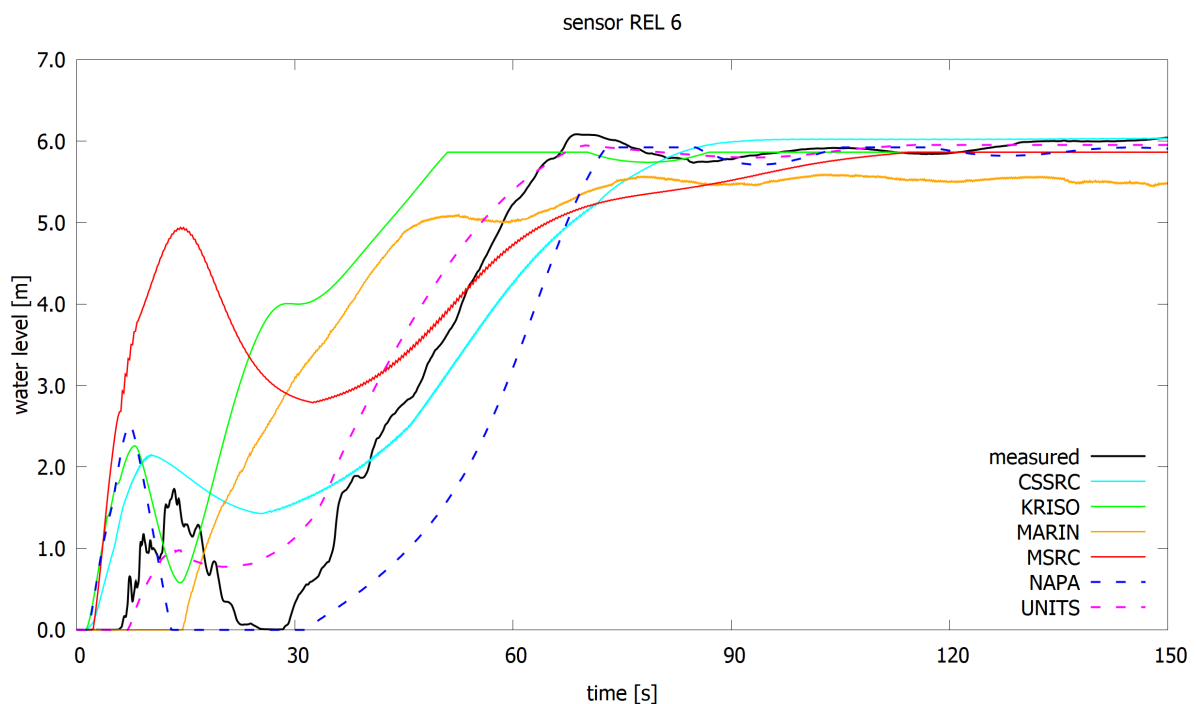


Figure 6.13 Measured and simulated water level in case B1 at sensor REL 6, in the intact side of the aftmost void space deck 0

The sensor REL 14 is located on deck 3 on the intact side. There are two longitudinal bulkheads with openings, separating the sensor from the breached room. Also here a small initial water level peak is measured, Figure 6.14, and proper flooding is started at about 25 s after the breach was opened. MARIN significantly overestimates the flooding rate at this location. Also KRISO predicts too fast flooding. NAPA and CSSRC predict the filling of the room rather accurately, while with both UNITS and MSRC simulations the flooding rate slows down after a while.

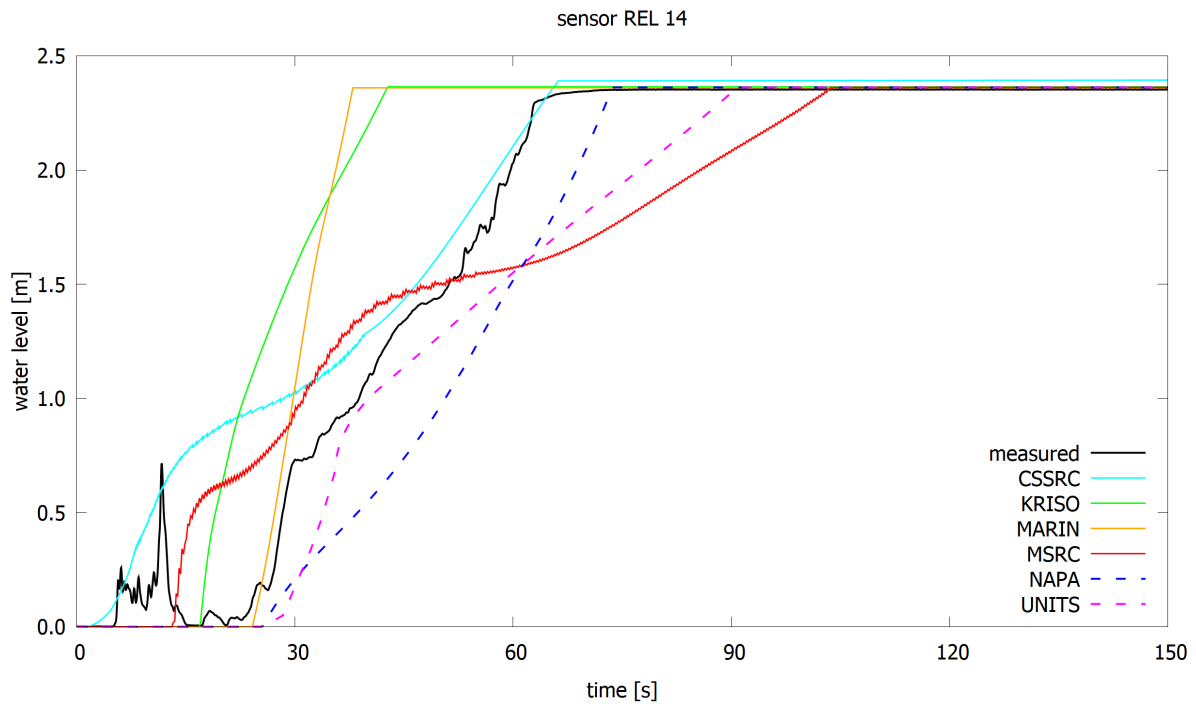


Figure 6.14 Measured and simulated water level in case B1 at sensor REL 14, in the intact side on deck 2

Another sensor of special interest is REL 28, located on the damaged side of the deck 4. The entire sensor is temporarily immersed during the large transient roll motion, Figure 6.15. All codes predict well the fast immersion of the sensor, but there is significant variation in the time when the water level starts to decrease. Only in the simulation by CSSRC the full sensor is not immersed, although the roll angle is larger than with UNITS results, where the whole sensor REL 28 is immersed. Similar behaviour is also observed at sensor REL 34 on deck 5, Figure 6.16. For both sensors REL 28 and REL 34, there is a quite notable variation in the final water level height. This corresponds to the observed variation in the pitch angle of the ship, as presented in Figure 6.12.

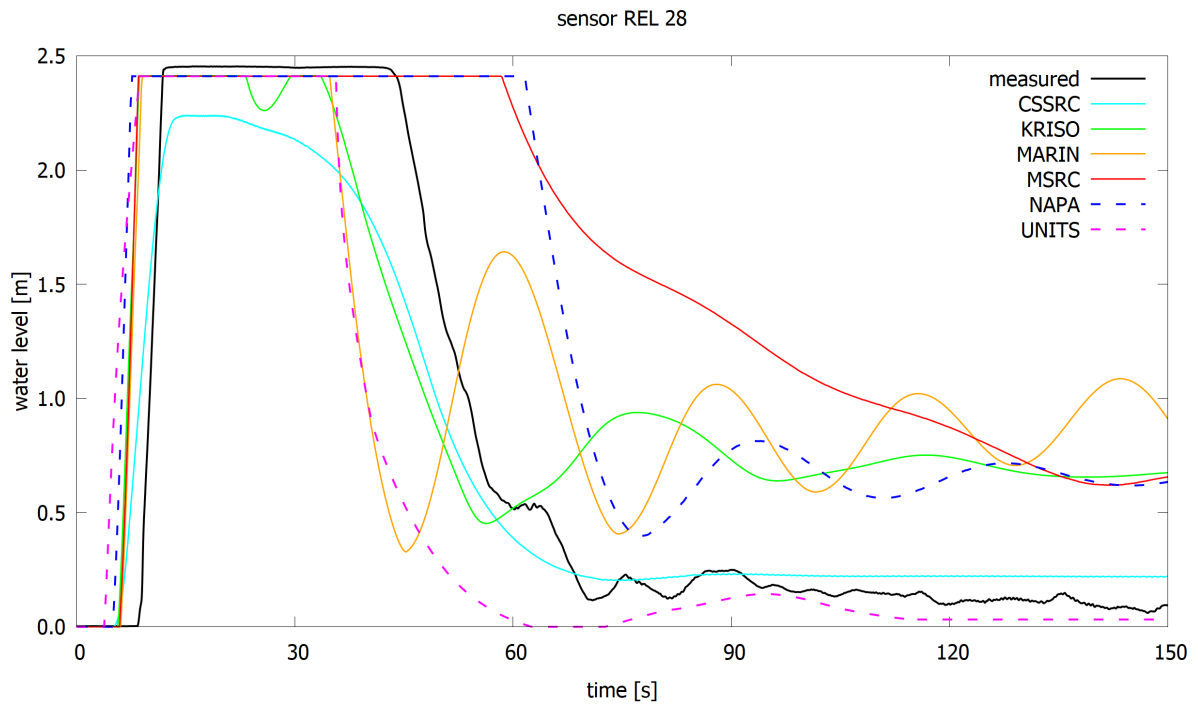


Figure 6.15 Measured and simulated water level in case B1 at sensor REL 28, in the damaged side on deck 4

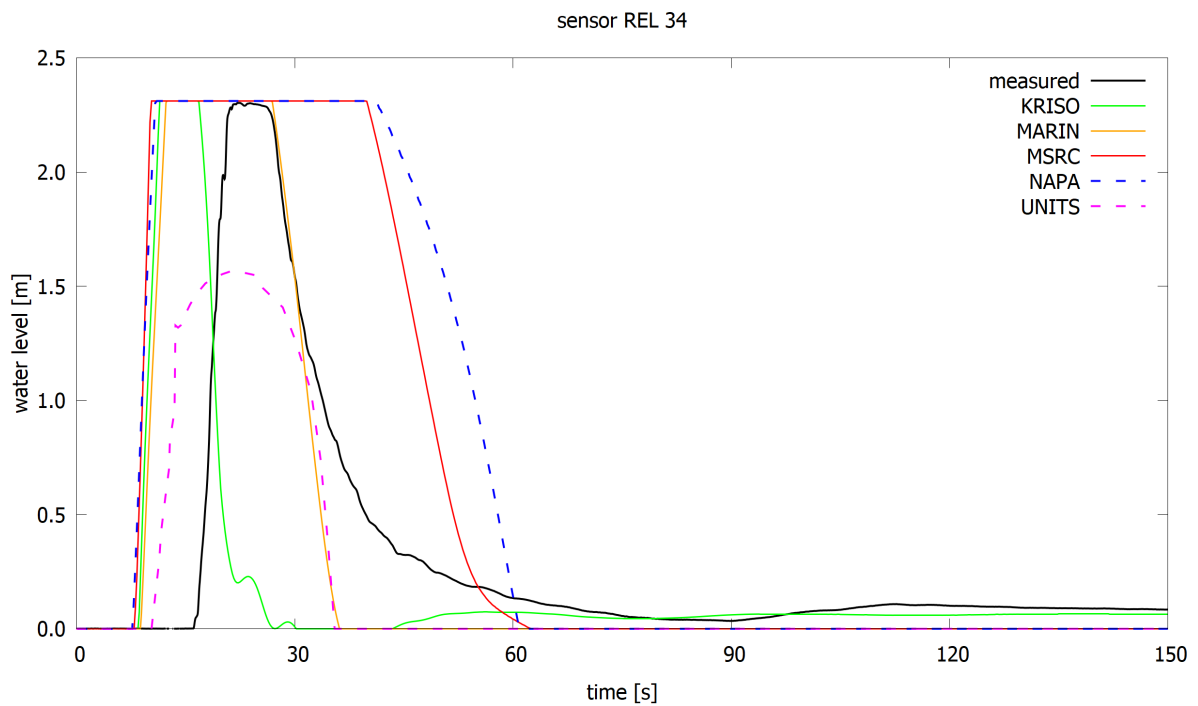


Figure 6.16 Measured and simulated water level in case B1 at sensor REL 34, in the damaged side on deck 5

A summary of observations from the comparison of simulation results:

- CSSRC Meth1 predicts the qualitative behaviour of the ship well, although the initial transient roll angle is slightly underestimated.
- KRISO simulation captures the shape of the roll motion graph, including the second peak. However, the maximum transient roll angle is slightly underestimated.
- MARIN simulation captures the transient roll angle very well, and only the second peak is notably smaller and occurs later than measured.
- PROTEUS simulation by MSRC captures the development of roll angle well. However, the foremost breached compartment with cross-flooding had to be modelled as a single flooded room in order to avoid capsize in this case.
- NAPA simulation is based on a simplified 1-DOF dynamic roll motion, yet the maximum transient roll angle is only slightly underestimated. However, the second peak is not captured, and the equalizing cross-flooding seems to be slower than in the experiment.
- UNITS simulation uses fully quasi-static ship motions, and therefore the transient roll angle is much smaller than measured. Otherwise, the flooding progression is captured well. Also UNITS modelled the foremost breached compartment as a single room without cross-flooding.

## 6.5 Case B2 – Transient and Progressive Flooding in Waves

### 6.5.1 Description

In this test the model is softly moored in irregular beam seas with the damage facing the waves, Figure 6.17. The breach and intact conditions are the same as in case B1 for the transient flooding in calm water.

The measured undisturbed wave history was also provided as input, and participants were advised to use this instead of a random wave realization of the sea state. Obviously, not all codes had the possibility of using a given wave train as input, and alternatively 10 realizations of the same sea state were simulated.

The measured roll angle is presented in Figure 6.18, along with measurements for two other realizations of the same sea state. In all three tests the roll during the transient flooding is almost identical. In general, the flooding process does not depend significantly on individual waves, but the time-to-capsize can vary significantly. The measurements from the 1<sup>st</sup> wave realization are used for detailed comparison against the simulation results.



Figure 6.17 Cruise ship model in irregular beam seas (courtesy of MARIN)

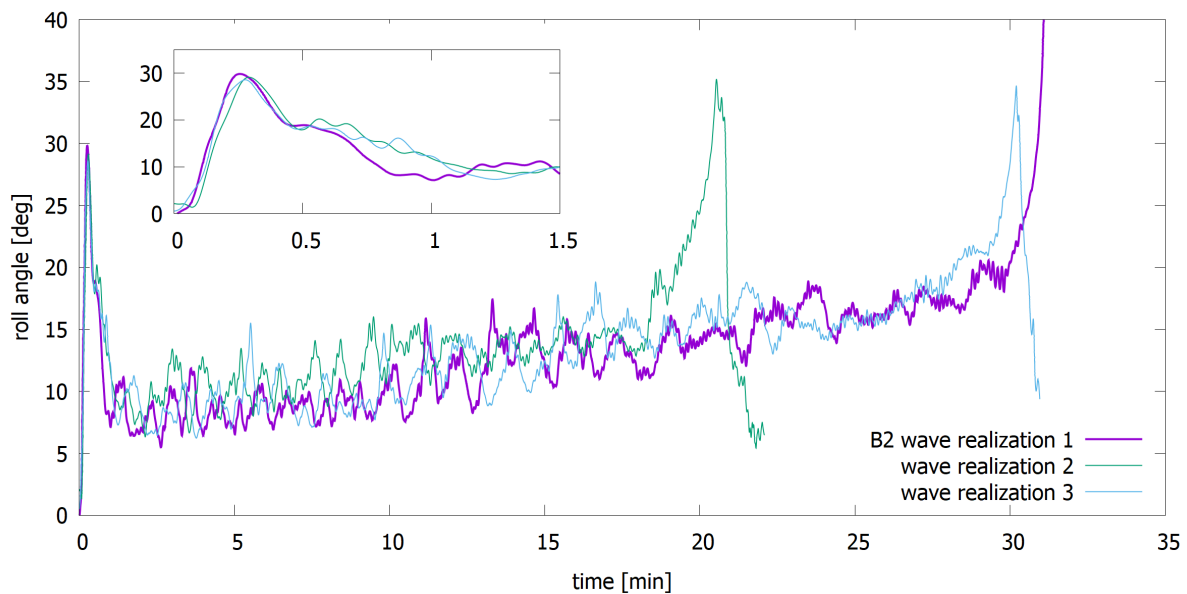


Figure 6.18 Measured roll angle in test case B2 and with two other wave realizations of the same sea state

## 6.5.2 Results

Time histories for the roll angle are presented in Figure 6.19. As in the calm water case B1, the simulation codes slightly underestimate the maximum transient roll angle. In the experiment, the roll angle is rapidly decreased to around  $10^\circ$ , which is then gradually increased over a longer period of time, until enough water has accumulated on the decks and the ship capsizes after about 36 min. The MSRC simulation predicts a slower decrease in the roll angle after the initial transient stage.

NAPA simulation results in a too short time-to-capsize, about 12 min. This likely results from the assumption of quasi-static pitch and heave motions, and subsequent faster accumulation of water on the upper decks. In the MSRC simulation the roll angle is eventually decreased, and the subsequent slow development of the roll angle until capsizing is well predicted. The simulation by KRISO captures the whole process well. CSSRC (Meth1) slightly underestimates the transient roll angle, but the following roll development is rather well predicted and TTC is only slightly underestimated.

As in case B1, MARIN considered also air compression. Moreover, the soft mooring lines, restricting the drifting were included in the numerical model. The simulation overestimates the transient roll by about  $5^\circ$ . The roll angle also increases more rapidly than measured during the transient flooding, and consequently, TTC is also too short. However, the main flooding characteristics are captured.

It should be noted that CSSRC and KRISO used random wave realizations, and the “best match” case, out of 20 repetitions, has been selected for comparisons. Due to the high frequency limit of the wave generator at the scale 1:60, a peak-enhancement factor  $\gamma = 7.0$  was used in the wave spectrum for the experiments. Some participants had applied the standard factor  $\gamma = 3.3$  of JONSWAP wave spectrum. According to analysis of MARIN, the measured significant wave height was 4.07 m and peak period 7.85 s.

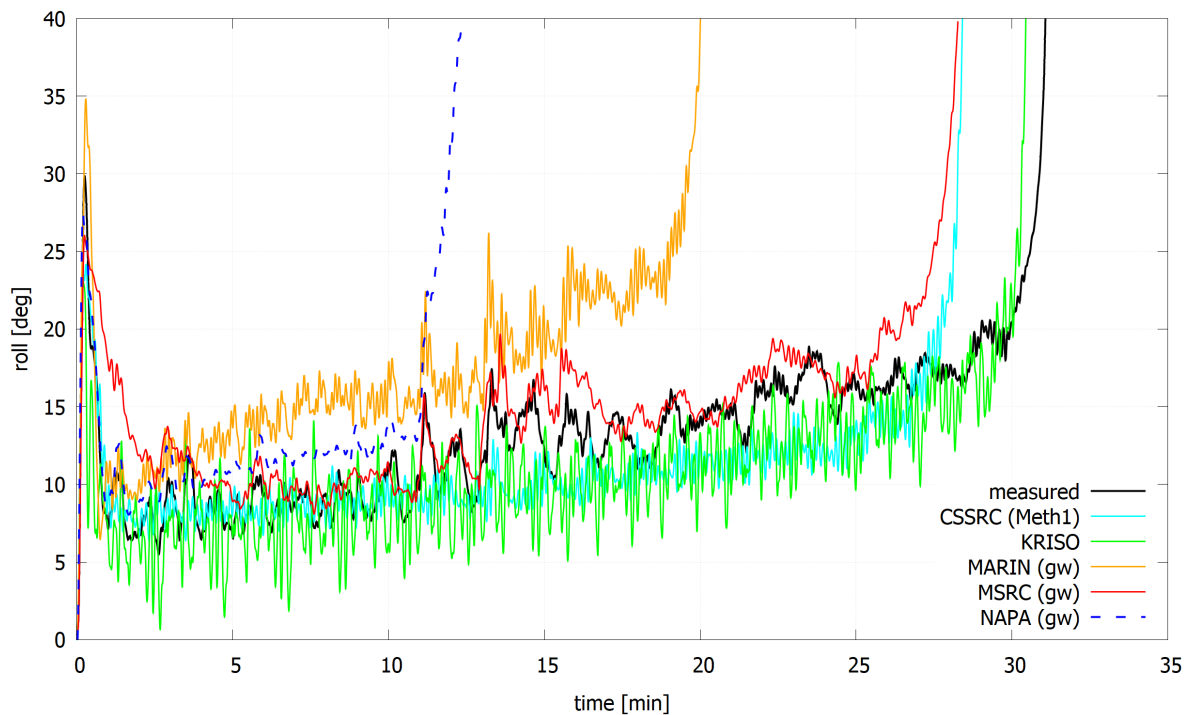


Figure 6.19 Roll angle in transient flooding and capsizing in waves case B2. Codes marked with (gw) used the given wave train, while for others the random realization of the given sea state with the best match has been selected

The maximum transient roll angle and time-to-capsize are listed in Table 6.5 and the main observations from results with different simulation codes are presented below:

- CSSRC provided results for 20 different wave realizations. In three cases the ship capsized during the transient flooding, and for the others the TTC varied between 9 min and 28 min. In the best match case, the transient roll angle is only marginally underestimated.
- KRISO also performed simulations with 20 different wave realizations. In one of them the ship capsizes during the transient stage, whereas in the other cases the TTC is between 26 min and 31 min, corresponding well with the experimental results. In general, the roll motion during the flooding process has a larger amplitude than in the experiments.
- MARIN simulation with the given wave train overestimates the transient roll angle, and progressive flooding in the given wave train is faster than measured, resulting in TTC of about 20 min.
- MSRC captured the TTC very accurately when using the given measured wave train. Also the transient roll angle was only about 4° smaller than measured, although the decay of the transient roll was delayed.
- NAPA also used the measured wave train, and the applied simulation is based on dynamic roll motion and wave pumping effect. The transient roll angle is predicted surprisingly accurately, only 2.4° less than measured. However, apparently due to the assumption of quasi-static heave and pitch motions, water accumulates on the upper decks more rapidly than in the model tests, and consequently, the transient roll is not equalized as much as in the experiments. Eventually, this causes a too short TTC.

Table 6.5 Summary of results for flooding in waves, Part B2

ID	trans. Roll	TTC	wave input
	deg	min	
measured	29.8	31.1	-
CSSRC (Meth1)	24.2	28.4	best match from 20 random wave seeds
KRISO	23.1	30.4	best match from 20 random wave seeds
MARIN	34.8	20.0	given wave
MSRC	26.0	28.3	given wave
NAPA	27.4	12.4	given wave

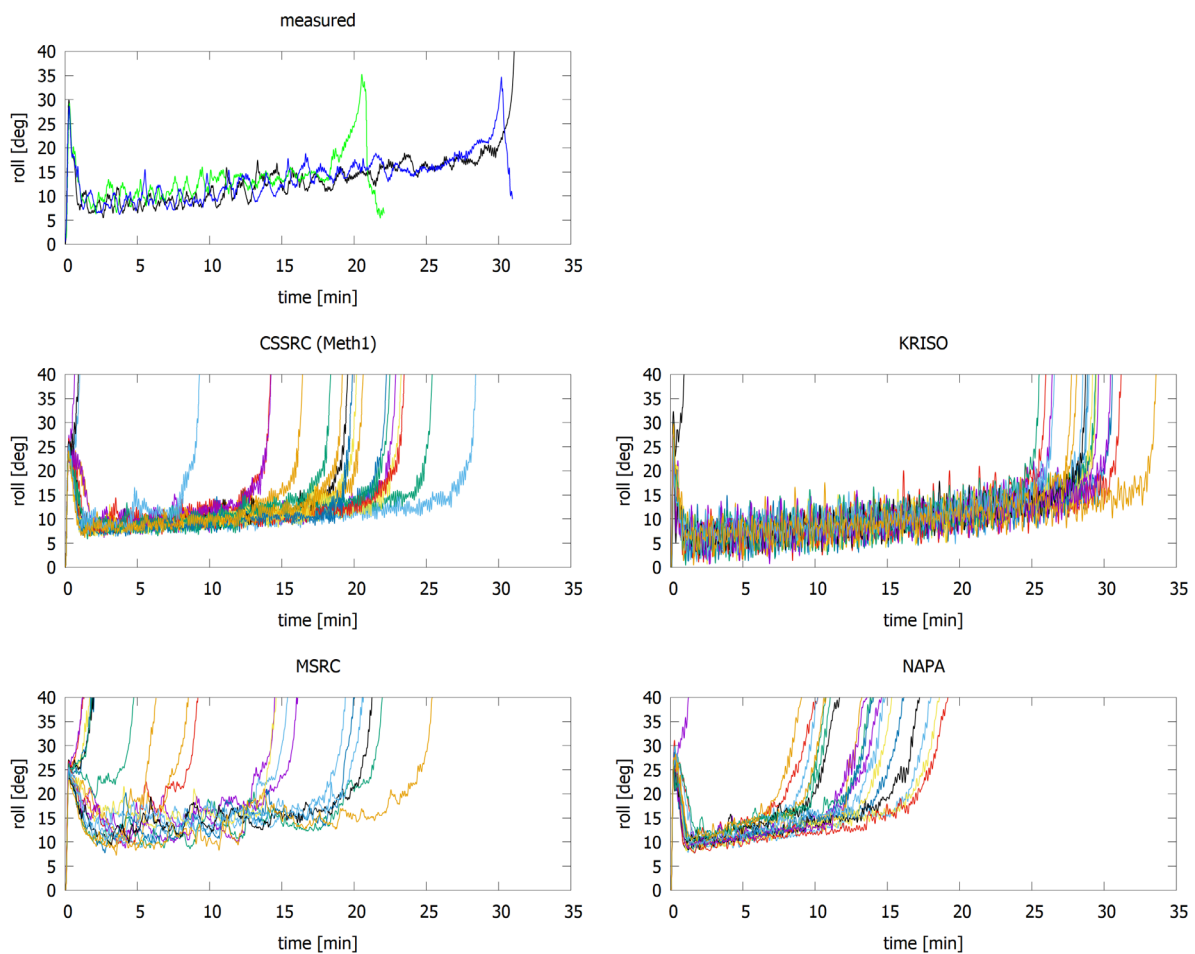


Figure 6.20 Simulation results for roll angle with random realizations of the given sea state for case B2

Since some participants provided results for different realizations of the studied sea state, i.e.  $H_s = 4.0$  m and  $T_p = 8.0$  s, instead of using the given measured wave train. Consequently, also MSRC and NAPA provided simulation results for 20 random wave realizations. the stochastic nature of the capsizing is evident, Figure 6.20. In the three model tests for the same state, the TTC was always longer than 20 min, but in the various simulations, also capsizes during the

transient flooding stage were observed. Cumulative distributions of TTC are presented in Figure 6.21. KRISO results are very close to the measurements, while others predict significantly shorter TTC. For KRISO and NAPA simulations only one out of 20 cases resulted in capsize during the transient flooding stage, while CSSRC (Meth-1) predicts a 15% and MSRC a 30% probability of a rapid capsize within the first two minutes. The results from MARIN are preliminary, and proper observations and conclusions cannot be made based on this.

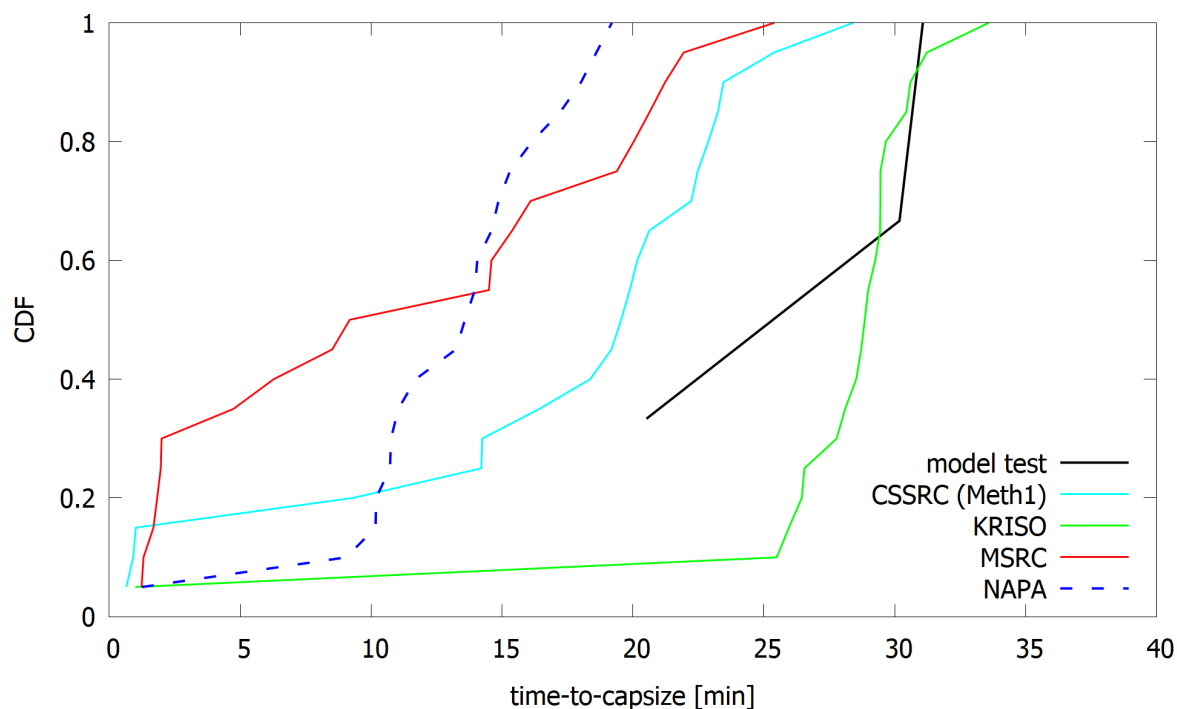


Figure 6.21 Cumulative distribution of time-to-capsize (TTC) for the case B2

The capsize in waves is caused by progressive flooding to the upper decks. The main routes of flooding progression are visualized in Figure 6.22. On deck 4 water flows along the service corridor and accumulates in the rooms with the sensors REL 25 and REL 29. Furthermore, through a “staircase” from the corridor, there is down-flooding to a room aft from the breached compartments, which is detected by the level sensor REL 16. High waves also pump water to the decks 5 and 6, causing slow accumulation of water forward of the breached rooms.

Comparisons of the water levels in the progressively flooded rooms indicates that different codes actually predict a somewhat different flooding and capsize mechanisms, as described below.

In the forward part of deck 4, at sensor REL 29, the predicted flooding progression is very similar, albeit with different flooding rates, Figure 6.23. MARIN and NAPA predict very similar results, albeit too fast flooding. MSRC and KRISO results have a better match with the measurement. On the other hand, in the aft part of the deck 4 at sensor REL 25 flooding starts after about 12 min, Figure 6.24. MSRC predicts a strange peak of water level in the beginning, but the later progress is rather well captured. KRISO predicts nearly linearly increasing water level with

flooding of the room already about 1 min after damage. In NAPA simulation the volume of floodwater in this room remains so small that the sensor remains dry due to the heel angle throughout the flooding process.

On deck 6, the sensor REL 36 is temporarily immersed due to the large transient roll angle, Figure 6.25. This is flowed by several peaks, caused by high waves, and eventually more water is accumulated on the deck and the ship capsizes. MSRC used the measured wave train as input and can accurately also predict the peaks in the water level at sensor REL 36. On the other hand, in the KRISO simulation only small water levels are observed until the final capsizes event.

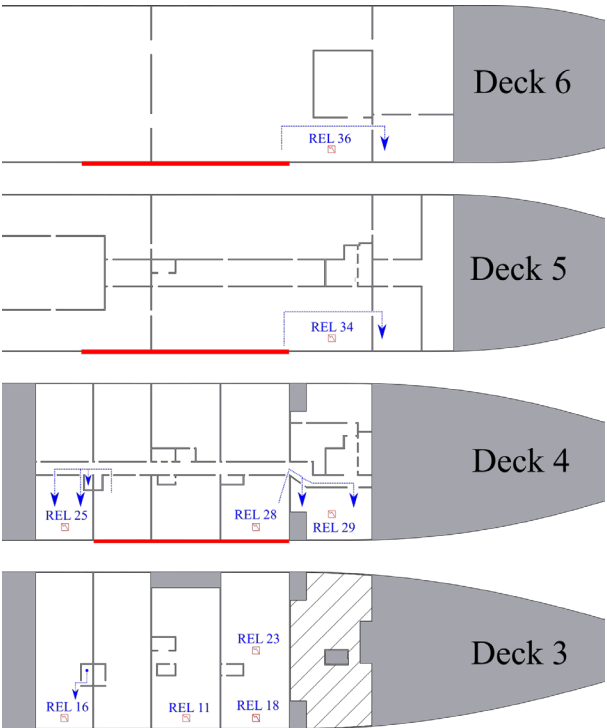


Figure 6.22 Identified routes of flooding progression in case B2



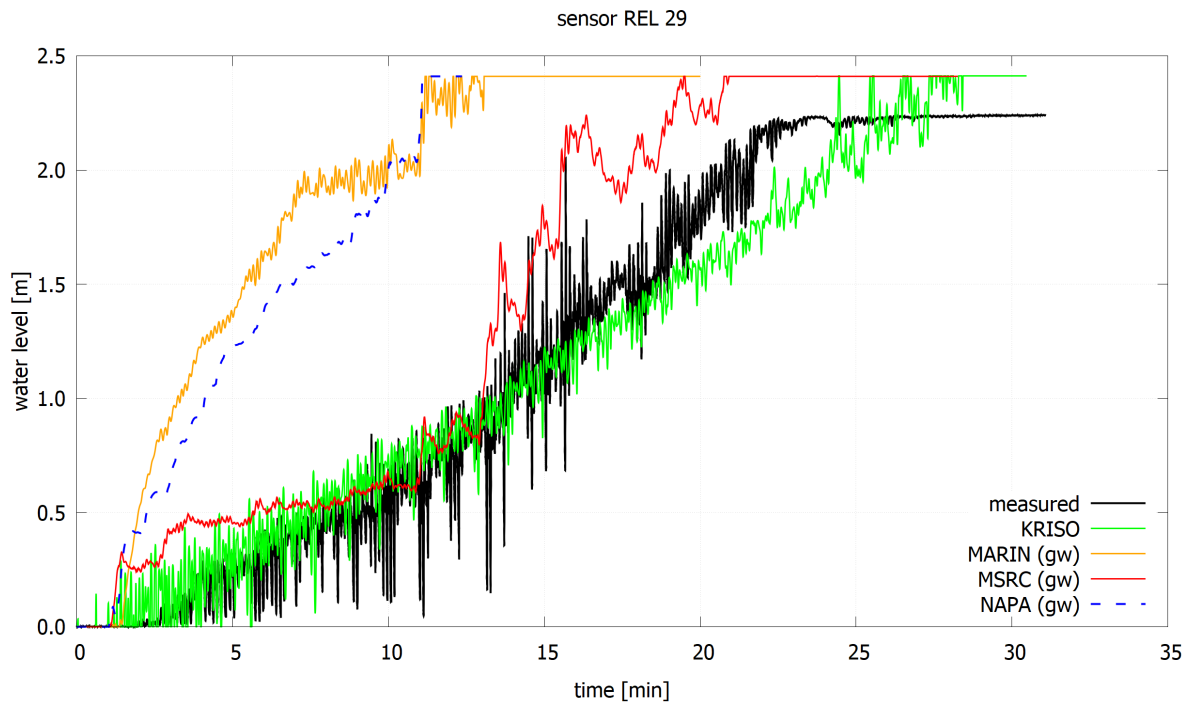


Figure 6.23 Comparison of water levels at sensor REL 29, indicating progressive flooding on the forward part of deck 4

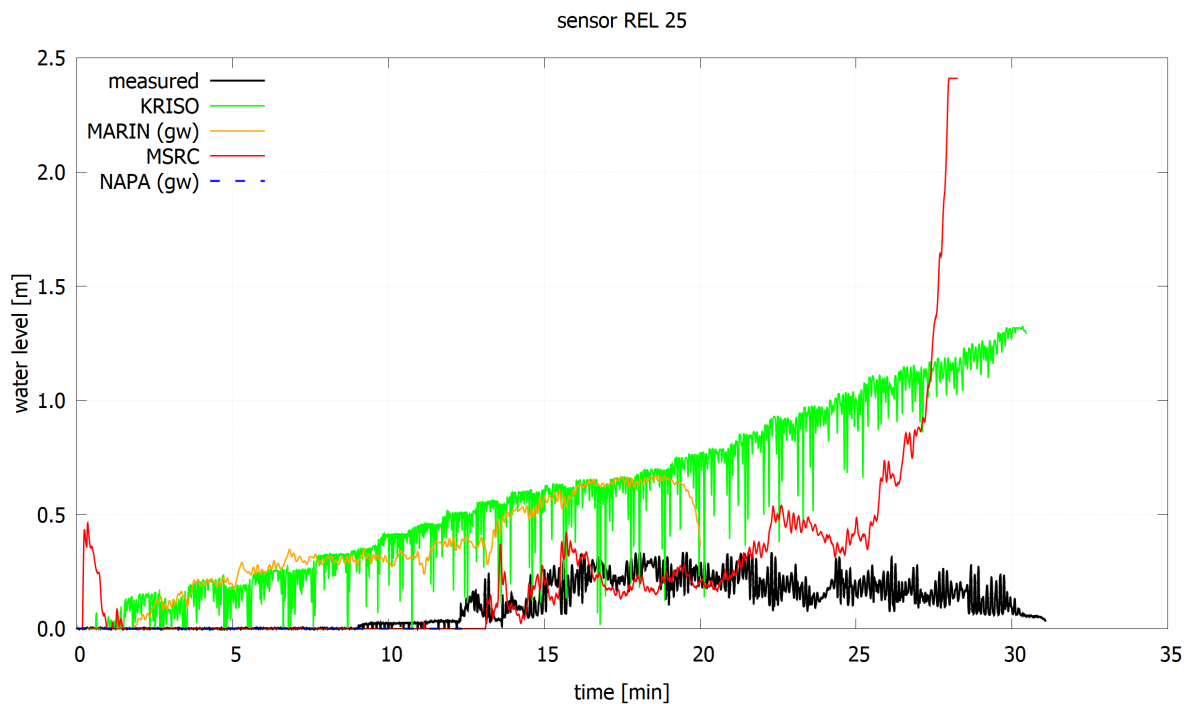


Figure 6.24 Comparison of water levels at sensor REL 25, indicating progressive flooding on the aft part of deck 4

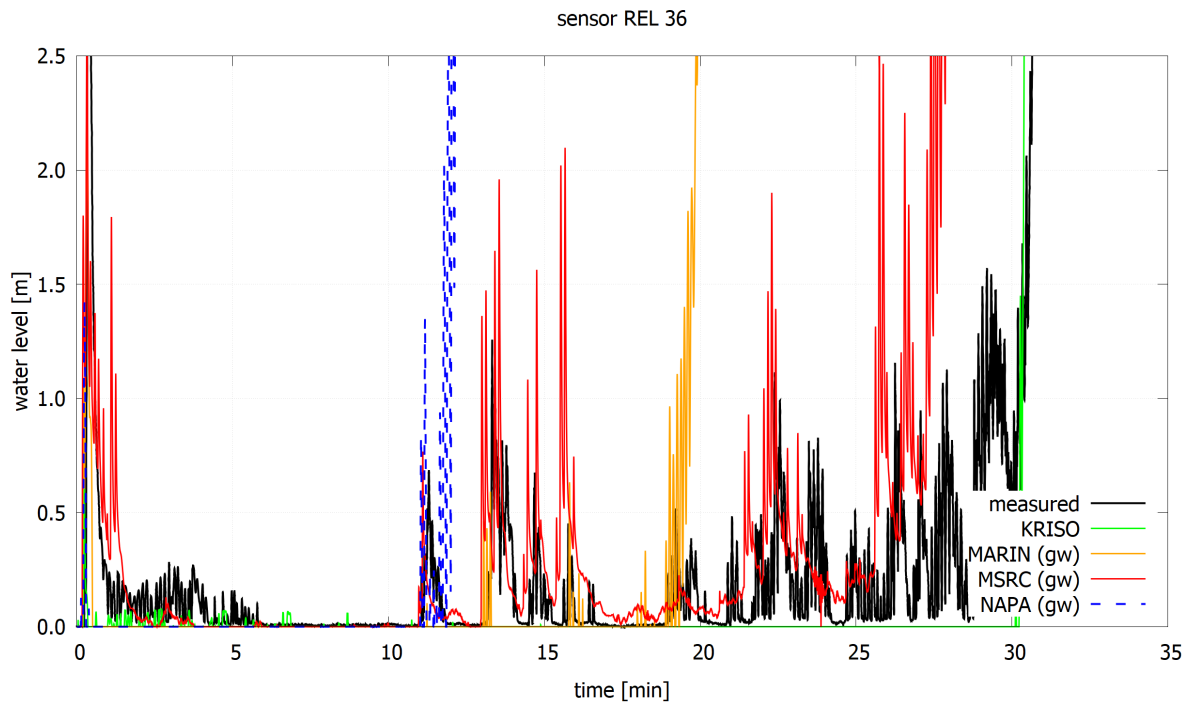


Figure 6.25 Comparison of water levels at sensor REL 36 on deck 6

### 6.5.3 On the Effects of Drifting

In the tests by MARIN the model was kept positioned by a soft spring mooring system. The mooring lines were connected at the bow and stern of the vessel. The angle of the mooring lines was 45 degrees with the centreline, Figure 6.26. Line stiffness was reported by MARIN to be 241 kN/m and the pretension 6516 kN.

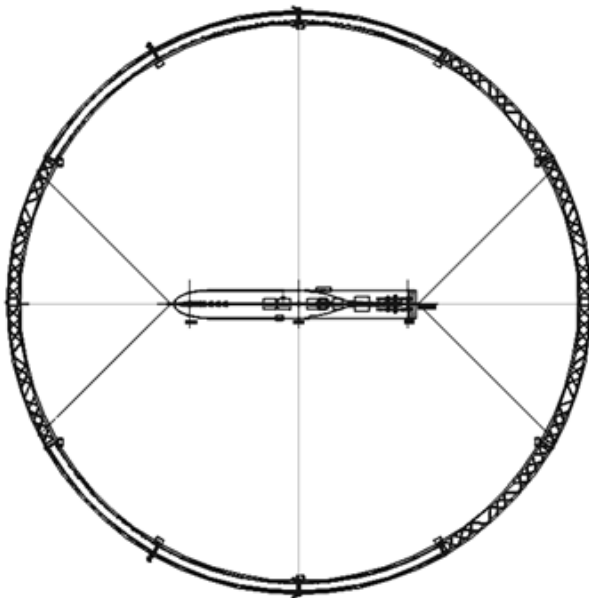


Figure 6.26 Soft mooring arrangement in model test (MARIN)

The development of sway motion, i.e. drift, is shown in Figure 6.27. In the following, the main related calculation features of the codes are briefly presented:

- CSSRC (Meth1) simulation with the code wDamstab is considering 4 degrees-of-freedom (DOF), namely sway, heave, roll and pitch. CSSRC also conducted 3 DOF simulations with zero sway motion, but the differences in the results were considered very small.
- SMTP code of KRISO does not use the 2nd order mean drift force due to waves. It calculates the wave forces by integrating the pressure on the wetted surface of the ship in its actual position, not the mean position. The drift forces arise in the case for which the phase of roll motion leads or that of heave motion lags that of waves. For the roll motion, the maximum drift comes in the case of  $90^\circ$ , when the wave crest is near the center of the ship, the roll motion is toward the weather side, and so the wetted surface area on the weather side is larger than in lee side. When the trough is near the center, the ship inclines towards lee side, and in this case the wetted area of the lee side is larger. The pressure near the wave crest is larger than in the trough. So the positive drift forces are come out. If in the phase lag, the negative drift can be come out. The same logic can be applied for heave motion, in this time the phase lag produces a positive drift. In short words, the drift takes place due to the non-linear effect of phase differences between the incoming waves and the roll/heave motion.
- MARIN considered the ship positioned in the four springs as per model test configuration. The surge, sway, roll and yaw damping characteristics were taken from the model tests and fine-tuned to match the decay tests of the intact ship. For the damaged ship the same coefficients were applied. The spring coefficients were slightly changed compared to the provided values to get the correct periods (which involves added mass, so this is most likely the reason why there is difference to the model tests).
- In PROTEUS, used by MSRC, the drift forces are modelled in a simplified way, not using QTF (Quadratic Transfer Function) but empirical formulations. The model is considered always in free-drifting mode, solving a 4 DOF system of equations (yaw and surge not modelled).
- NAPA simulation is based on the assumption of zero sway motion, which in this case corresponds fairly well with the experimental test condition.

There is a lot of variation in the magnitude of the drifting of the ship during the flooding process. CSSRC simulations resulted in minimal drift, and also MSRC predicts only a small drift, whereas in KRISO simulation the ship drifts 500 m (full scale) in 25 minutes. The drift in MARIN simulation is limited since the soft mooring lines were included in the model. The measured sway motion is also shown in Figure 6.27, showing that the used mooring lines effectively prevented drifting.

It should be noted that most flooding simulation codes are intended for simulation of ship motions in full scale, and thus a feature to include the mooring line effects is normally not included. Even so, completely restraining the sway motion does not fully represent the model test condition either.

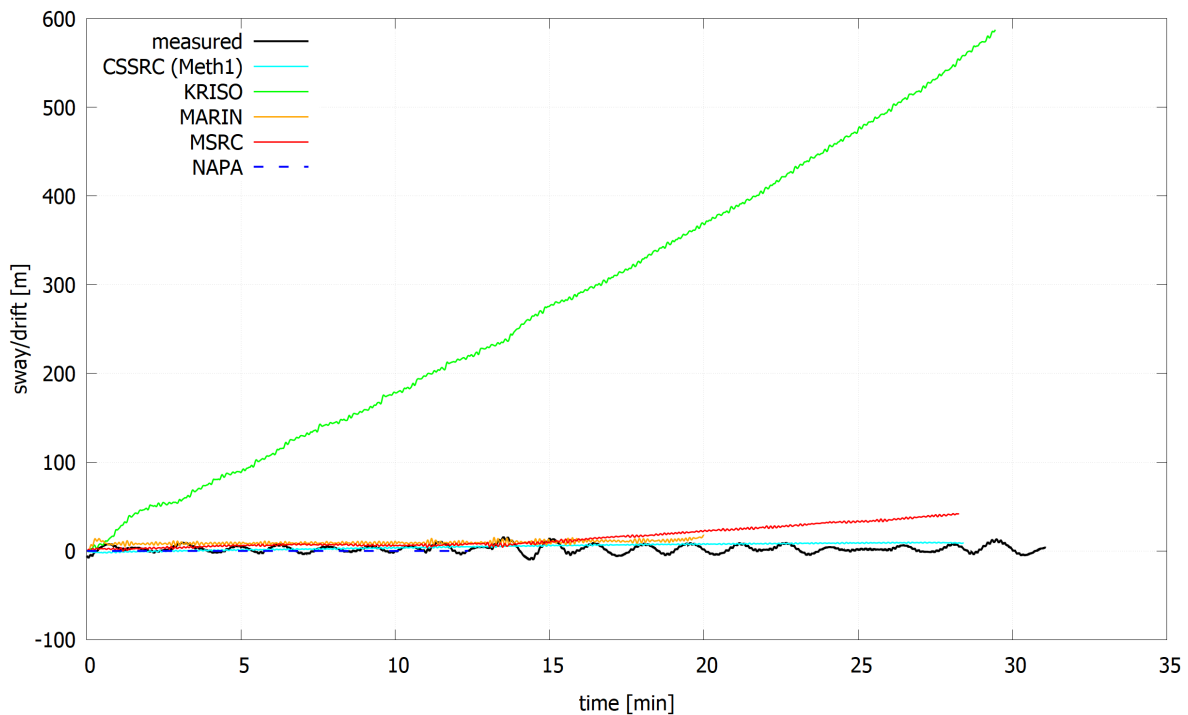


Figure 6.27 Comparison of sway motion in the case B2

## 6.6 Case B3 – Progressive Flooding in Calm Water

### 6.6.1 Description

The results of the benchmark case A1, up-flooding, indicate that progressive flooding through filled up rooms can be difficult to calculate, at least to some codes. Therefore, an additional benchmark case, with focus on progressive flooding in calm water is introduced. The initial condition is exactly the same as in case B1, but the breach size is smaller, representing a side grounding damage, as visualized in Figure 6.28. Because of the limited upper vertical limit of the breach, there will be up-flooding through the staircases, to the deck below the bulkhead deck. On the breached deck levels, the compartments will be filled up, thus resulting in a similar condition as in Part A1. However, this case has a more complex arrangement of compartments, and includes the motions of a freely floating ship.

It should be noted that at present, there is no experimental data for this case, and consequently, the numerical codes are compared to each other. However, additional model tests at MARIN are planned, and this part of the benchmark will be extended later. The updated results are planned to be published in a dedicated journal paper.

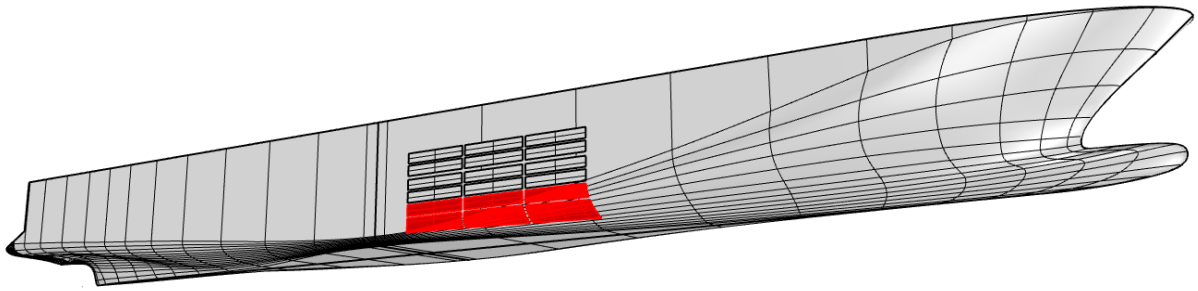


Figure 6.28 The vertically limited breach size (red) used for benchmark case B3

### 6.6.2 Results

Since no experimental data is available, only numerical simulation results are compared. There is quite a notable variation in the magnitude of both the transient roll angle and roll decaying, Figure 6.29. However, all codes converge to almost the same steady heel angle.

The OpenFOAM CFD results by DNV are preliminary, as proper assessment of convergence has not yet been finalized. Results are presented for a grid of about 5 million cells, using an overset mesh approach with a time step of 0.002 s. Model scale is used, and results have been converted to full scale for comparison with the other codes.

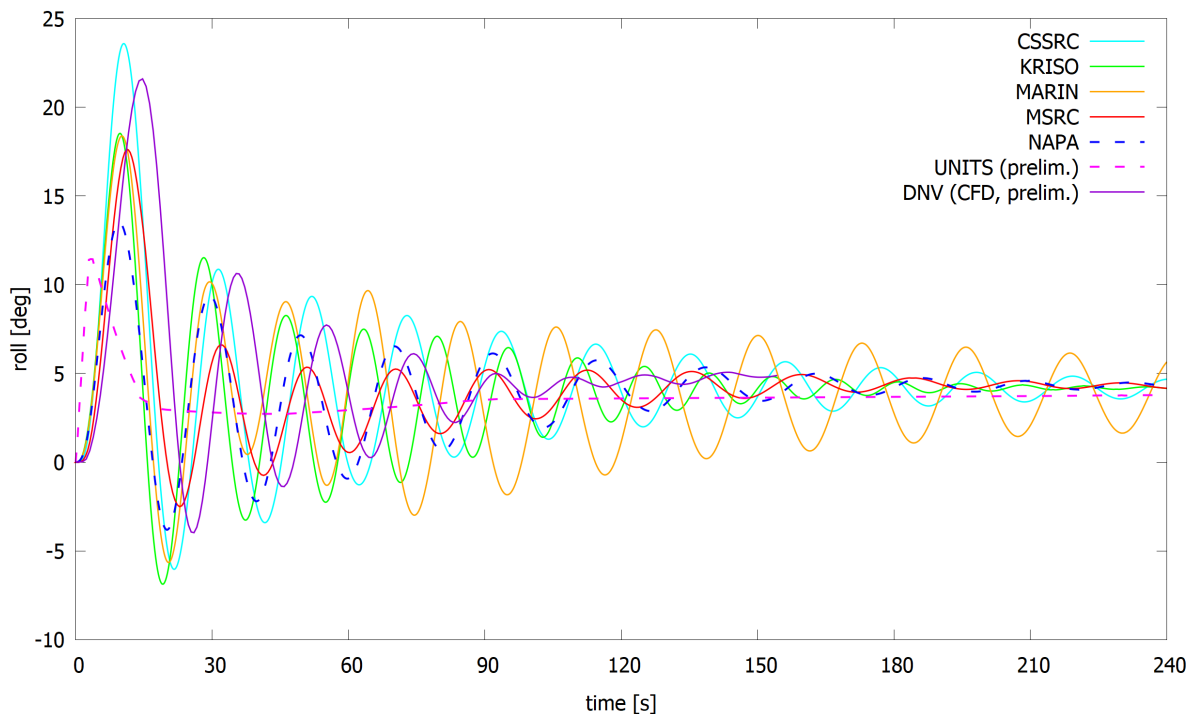


Figure 6.29 Comparison of the simulated roll angles for the small breach case B3

Since the full analysis of the CFD results is not yet available, the water levels are compared only for Bernoulli-based codes. The up-flooding to deck 3 from the breached deck 2 characterises this damage case, as visualized in Figure 6.30. Consequently, the water levels at sensors REL 11, REL 18 and REL 23 are of special interest.

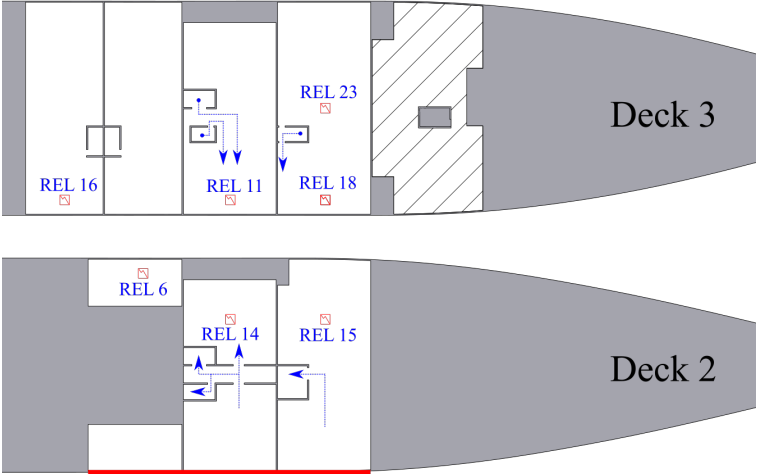


Figure 6.30 Routes of progressive flooding in case B3

KRISO, MARIN and NAPA predict a fairly consistent development of the water level at sensor REL 11, Figure 6.32. In the case of MARIN the fluctuations are much larger due to the larger roll amplitudes. UNITS simulation gives a notable slower flooding rate, possible due to the quasi-static assumption of the roll angle. However, UNITS results are considered preliminary since proper check of the applied geometric model have not yet been done.

MSRC simulation with the PROTEUS software predicts a notable peak of 0.3 m (full scale) water level about 10 s. MSRC modelled the up-flooding routes vertical trunk compartments, Figure 6.31. This modelling practice overcomes the up-flooding problems observed with PROTEUS in the benchmark Part A1, see Figure 5.4 on page 27.

The preliminary results of the CFD simulation by DNV indicate much smaller amplitude variation in the water level. In addition, the immersion of the sensor happens at about 50 s, which is somewhat later than with the other codes.

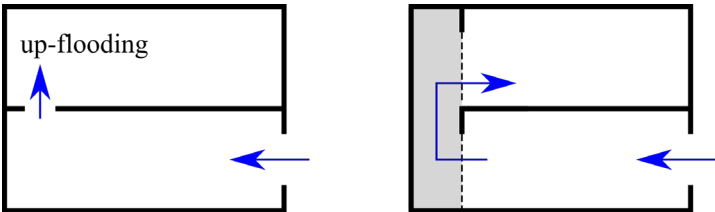


Figure 6.31 Schematic presentation of different modelling practices for up-flooding: simple opening on deck (left) and through a vertical trunk compartment (shaded area) on right

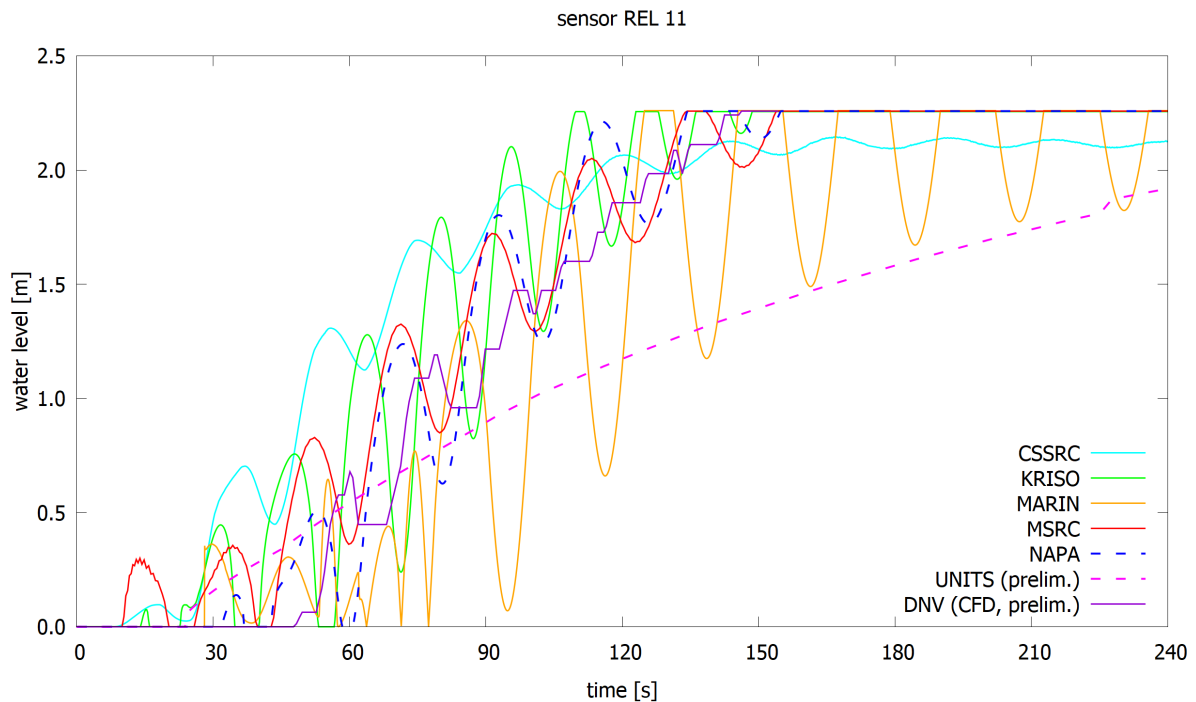


Figure 6.32 Comparison of water levels at the sensor REL 11 on deck 3 for case B3

At sensor REL 18 on deck 3 in the forward compartment, Figure 6.33, the development of the water level is rather similar to sensor REL 11.

The sensor REL 23 is in the same room as REL 18 but at the centerline. MARIN simulation predicts that this sensor is temporarily fully immersed, Figure 6.34, whereas other simulations result in more gradual flooding, although there are oscillations in the water level due to the roll motion.

Due to the large transient roll and slow decaying, MARIN simulation predicts also up-flooding to deck 4, whereas with the other codes up-flooding is limited to deck 3.

Although the CFD simulation by DNV reaches a quasi-steady roll angle in 115 s (full scale), the up-flooding still continues. In addition, a proper grid sensitivity study is not yet done, and therefore, the presents DNV results need to be considered as preliminary.

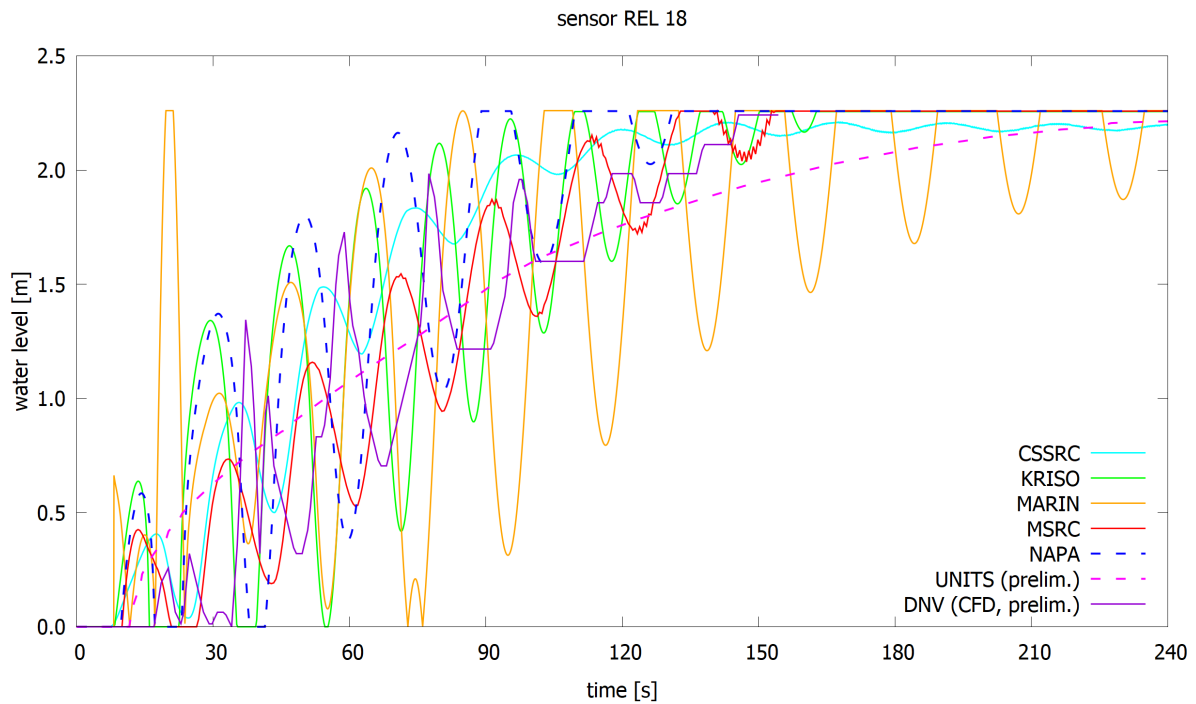


Figure 6.33 Comparison of water levels at the sensor REL 18 on deck 3 for case B3

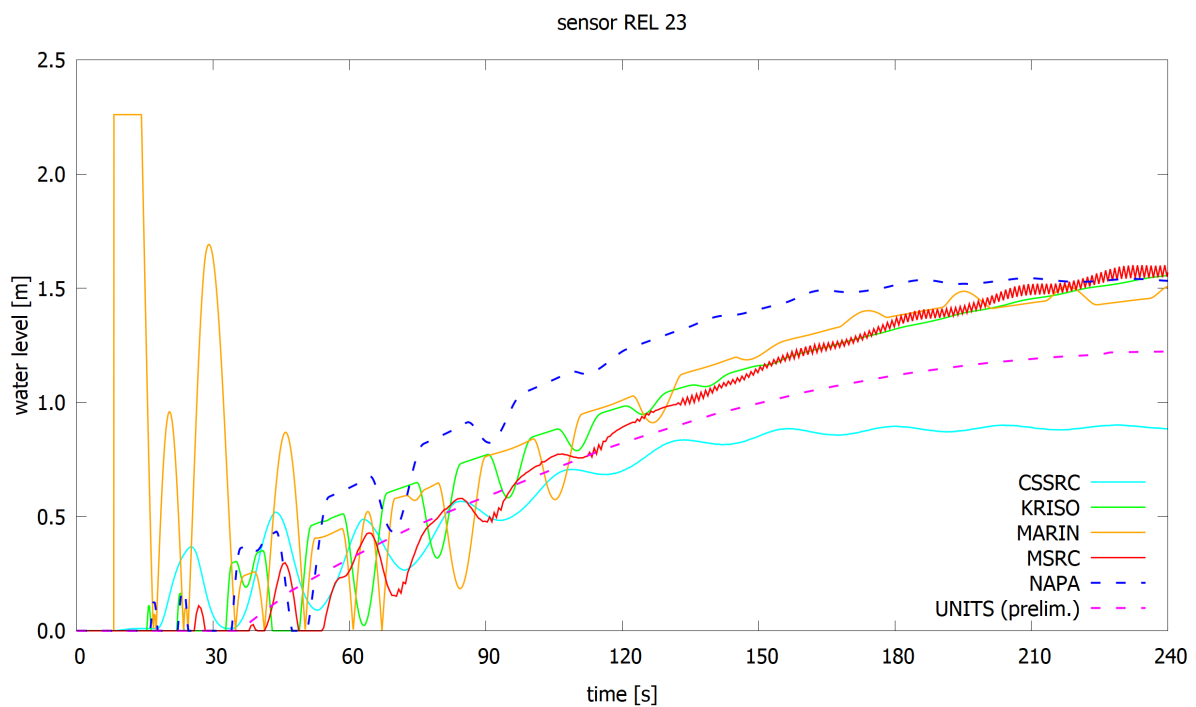


Figure 6.34 Comparison of water levels at the sensor REL 23 on deck 3 for case B3

## 6.7 Computational Performance

The computational performance of different simulation codes has been assessed based on relative computation time, i.e. the time spent in computations divided by the simulated time in full-scale. Results are presented on a logarithmic scale in Figure 6.35. Obviously, the used hardware and applied modelling practices, such as time step and number of calculation sections or panels, can have a significant effect. The applied time step and type of the hardware are listed in Table 6.6. Each participant selected the applied time step, and some participants may have emphasized computational efficiency.

With Bernoulli-based codes the simulations are typically running on real time, or somewhat faster. For some of the codes (KRISO, MSRC and NAPA) simulation in waves (case B2) is slower than in calm water (cases B1 and B3). In general, it seems that the code by KRISO is very efficient, at least with the settings applied in this benchmark study.

The preliminary CFD simulations for the case B3 by DNV turned out to be very slow, and the overset mesh update was identified as the main reason.

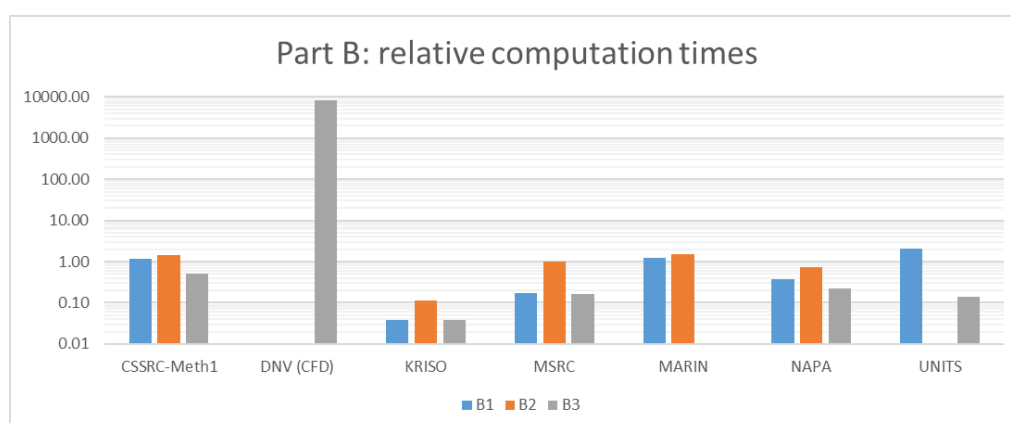


Figure 6.35 Relative computation times for cruise ship flooding cases (Part B)

Table 6.6 Summary of time discretization and hardware

ID	time step [s]	scale	Hardware
CSSRC-Meth1	0.05	ship	Intel i7 3rd gen
DNV (CFD)	0.002	model	Cluster with 128 CPUs
KRISO	0.02	ship	Intel i7 4th gen
MSRC	0.20	ship	Intel i7 8th gen
MARIN	0.05	ship	Intel i7 8th gen
NAPA	0.20	ship	Intel i7 8th gen
UNITS	0.07-1.90	ship	Intel i7 4th gen

## 6.8 Analysis on Air Compression Effects

Air compression in flooded compartments can notably delay the flooding progression. However, in model scale air is “too stiff”, and the compression effects are much larger than in full-scale, as noted e.g. in Ruponen et al. (2007). In the cruise ship flooding tests by MARIN the scale of the model was small (1:60), and therefore, proper ventilation of the model was essential to ensure usable results for benchmarking simulations performed for a full-scale ship.

The studied cruise ship model contains complex internal arrangement of the floodable compartments. In the experiments, the compartments were vented by large air pipes on the undamaged side of the model, as shown in Figure 6.36. The inner diameter of the pipes was 17 mm, and they extended up to the top of the model. In some cases, an additional bend of 90° was required.



Figure 6.36 Air pipes in the model for ventilating the flooded compartments (courtesy of MARIN)

In principle, the air pipes can have two different kinds of effects on the results:

- Air compression in flooded rooms, delaying flooding, especially in the beginning of the process if the pipes are not ventilating the compartments efficiently enough
- Submerged parts of the pipes provide some additional buoyancy, and eventually, also the pipes are flooded, thus potentially affecting the final equilibrium floating position

The volume of fluid (VOF) method, used in the CFD calculations by DNV, proved difficult without considering the air. Therefore, MARIN prepared a 3D model of the pipes, Figure 6.38. Preliminary results by DNV for the case B3 indicate that the air pressure peak reaches 900 Pa, corresponding to about 9 cm water height in model scale (5.4 m in full scale). Thus it seems likely that air compression inside the model did have some effect on the flooding process, especially during the transient stage.

MARIN simulated case B1 also by considering all compartments fully vented. A comparison of results is shown in Figure 6.37. The results fully vented results were obtained without any additional subdivision on deck 1 since adding this caused a rapid capsizing.

With air entrapment, the portside wing tank (sensor REL 06) does not fill completely and water level is somewhat less than in the model tests. When vented, this wing tank fills as in the model tests and the final steady heel angle is better captured. Overall, MARIN concluded that the air entrapment plays a role, but that it will be difficult to model this exactly as in the model tests due to the scale effects. The real case is somewhere in between fully vented and modelled air-entrapment case. In addition, the violent water ingress will lead to air-water effects that are very hard to model.

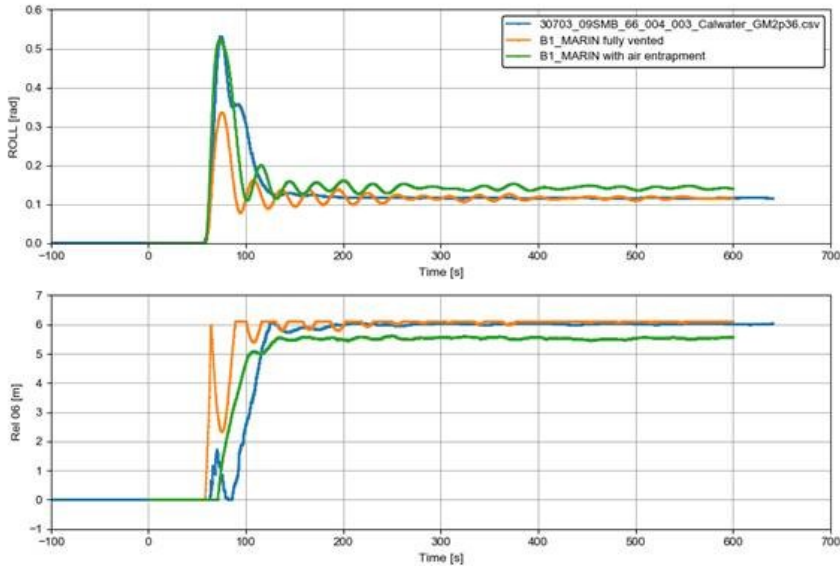


Figure 6.37 Comparison of B1 simulation results by MARIN with fully vented compartments and considering also air compression: roll angle (above) and water level at sensor REL 6 (below).

Also KRISO considered the air flow and compression effects, by identifying the ventilated compartments from the submitted material. At that time, the detailed ventilation arrangement was not available, and this may have had some effects on the results.

Although NAPA software can consider air compression and air flows, in these simulations full ventilation of all compartments was assumed since calculations were done in full scale. Similarly, also MSRC and UNITS ignored possible air compression effects.

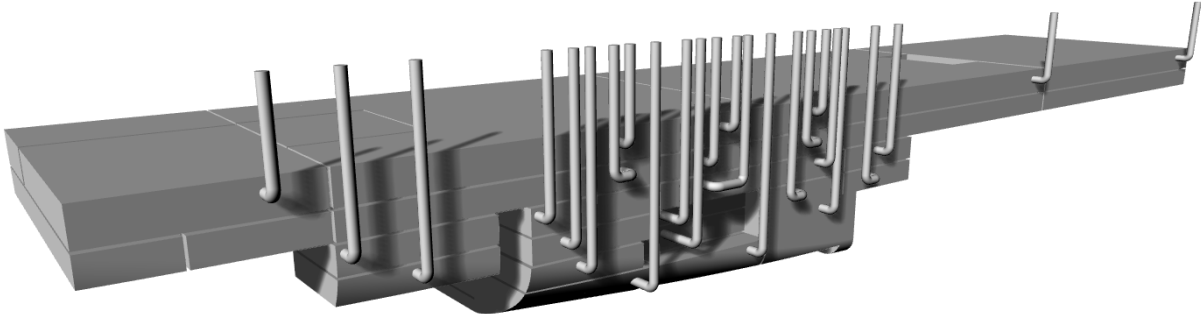


Figure 6.38 Rendering of 3D model of the air pipes, provided by MARIN

Based on an initial analysis, all benchmark participants were recommended to ignore the air compression effects, enabling better comparisons of the codes. Especially since many codes are not capable to calculate air compression. Considering the scale effects, air compression in model tests should be as small as possible. Due to the complex arrangement, no measurements of air pressure inside the model were done, and thus a final conclusion on the possible air compression effects cannot be done.



## 7 FLARE BENCHMARK C – ROPAX SHIP FLOODING

### 7.1 Model Geometry

The final part of the benchmark focuses on the accumulation of water on the vehicle deck, a characteristic stability failure mode for damaged ropax vessels. For this, an unbuilt ropax design (about 28 500 GT), provided by Meyer Turku, is used, Figure 7.1. Model tests were carried out at HSVA with a model in scale 1:28. The main parameters are listed in Table 7.1, both in full scale and in model scale. The lines drawing of the bare hull is shown in Figure 7.2.

The examined damage is a two-compartment damage scenario with a breach extending vertically to the vehicle deck. All damaged compartments were ventilated through ventilation pipes in the compartment corners. Consequently, full ventilation was recommended for the simulations.

Tests were conducted for a freely drifting model (contrary to the soft spring mooring used in Part B of the benchmark). A spring line from the bow was occasionally used to correct the model orientation back to a beam seas condition (in Parts C2 and C3).

Due to the large scale (1:28) of the model, the openings are quite large, and therefore, the industry standard discharge coefficient  $C_d = 0.6$  was recommended for all openings.

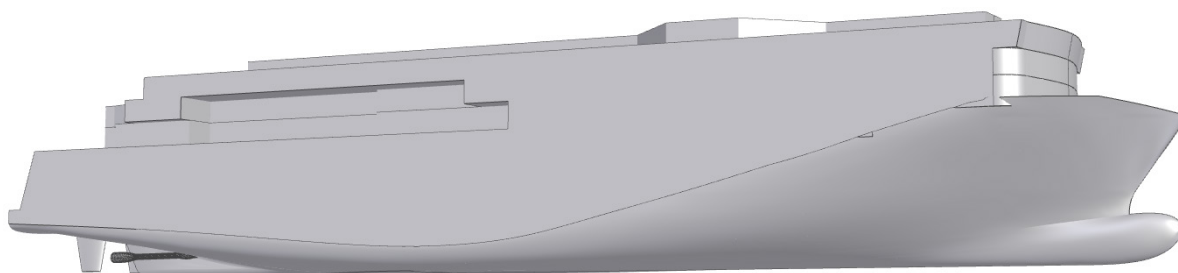


Figure 7.1 Visualization of the studied ropax ship

Table 7.1 Main parameters of the ropax ship (scale 1:28)

	Full scale	Model scale
Length over all	About 162 m	About 5.8 m
Length between perpendiculars	146.72 m	5.24 m
Breadth	28.0 m	1.00 m
Draught	6.1 m	0.218 m
Height of ro-ro deck from baseline	9.2 m	0.329 m
Gross tonnage	28 500	-

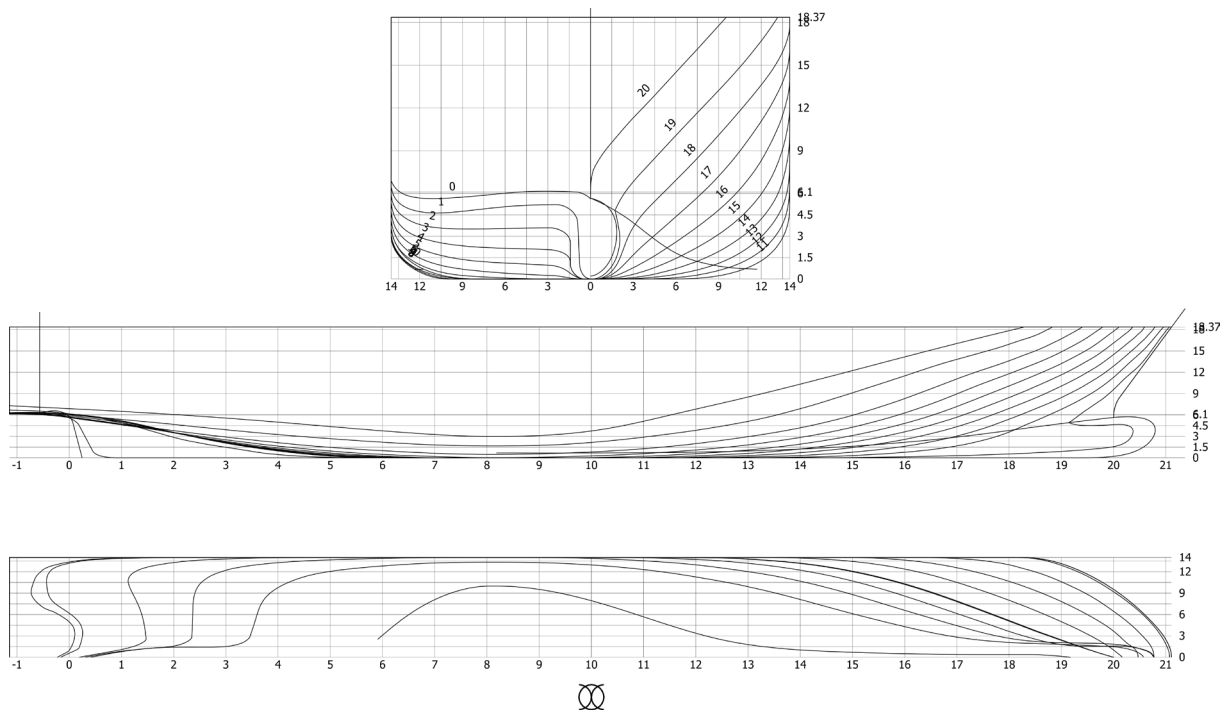


Figure 7.2 Lines drawing of the studied ropax ship

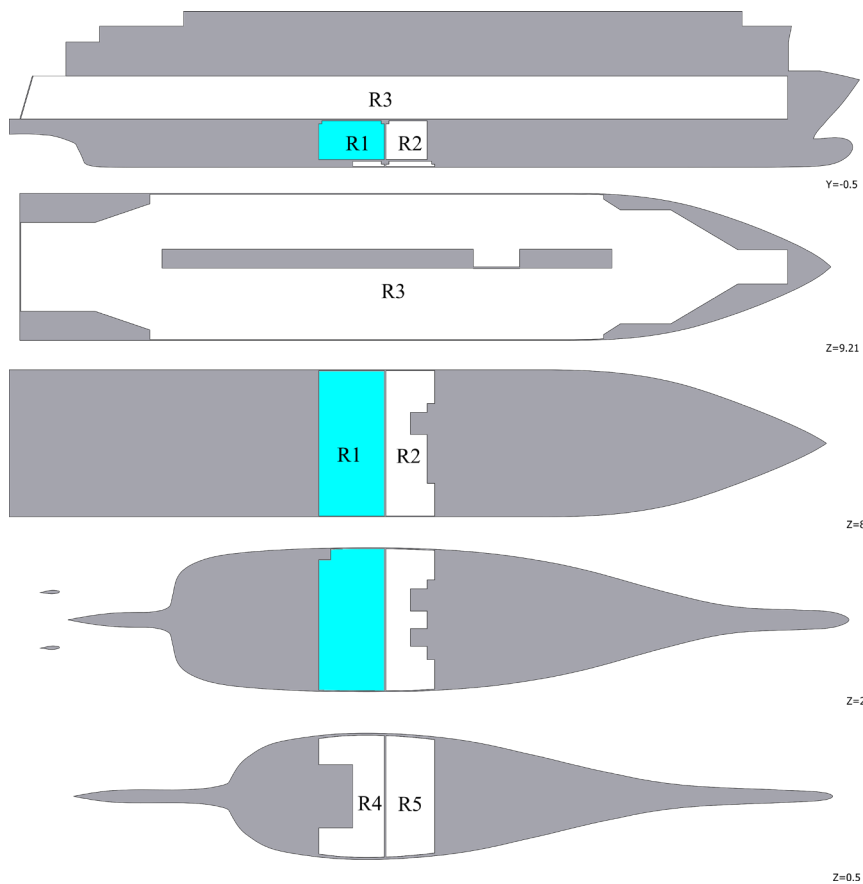


Figure 7.3 Arrangement of compartments of the ropax vessel, as modelled in NAPA, R1 is the "blue compartment" for which detailed experimental results are available

## 7.2 Comparison of Hydrostatics

In order to ensure that all participants had modelled the hull form and floodable compartments accurately, some basic hydrostatic results were collected and checked beforehand, as listed in Table 7.2 and shown in Figure 7.4. There is no significant deviation in either volumes or the centroids between the different codes. Consequently, the numerical models of the ship are considered very similar and suitable for benchmarking.

Table 7.2 Comparison of volumes, centroids and deck area

ID	Hull up to T = 17.4 m				Hull up to T = 6.1 m				Compartments				deck
	Vhull	Xhull	Yhull	Zhull	Vdisp	Xdisp	Ydisp	Zdisp	Vrooms	Xrooms	Yrooms	Zrooms	area
	m <sup>3</sup>	m	m	m	m <sup>3</sup>	m	m	m	m <sup>3</sup>	m	m	m	m <sup>2</sup>
BROO	61675	66.746	0.000	9.655	16186	67.851	0.000	3.456	29629	63.233	-0.135	12.012	3089.6
KRISO	61646	66.709	0.000	9.669	16084	67.963	0.000	3.458	29899	62.660	-0.131	12.031	3101.0
MARIN	61606	66.833	0.000	9.665	16118	68.019	0.000	3.457	29627	63.233	-0.135	12.013	3090.3
MSRC	61677	66.768	0.000	9.661	16163	67.817	0.000	3.458	29651	63.245	-0.129	12.003	3081.7
NAPA	61702	66.771	0.000	9.657	16189	67.838	0.000	3.455	29625	63.231	-0.135	12.013	3089.7
UNINA	61683	66.790	0.000	9.660	16170	67.910	0.000	3.460	29627	63.233	-0.135	12.013	3049.3

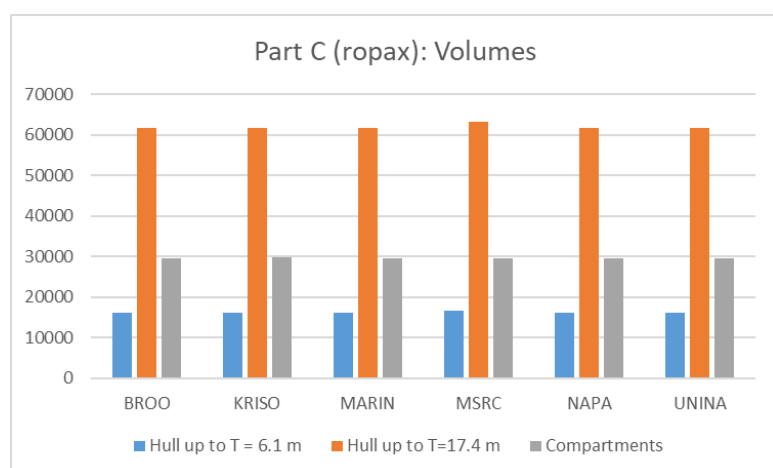


Figure 7.4 Comparison of modelled volumes of the ropax hull and compartments

A more detailed comparison was done for an intact condition with  $GM = 1.505$  m. The righting lever curves and related trim angles, calculated with different codes, are presented in Figure 7.5. Some small variation at large heel angles can be observed, especially regarding the trimming of the ship. However, in general, the restoring moment results are considered very unified. Moreover, the hull form is more conventional, and there are no significant discontinuities in the waterplane around the studied draft, as was the case for the cruise ship in benchmark Part B.

It should be noted that the hydrostatics from HSVA were based on pre-calculated hydrostatics using NAPA Software, and hence they are not included in the comparison.

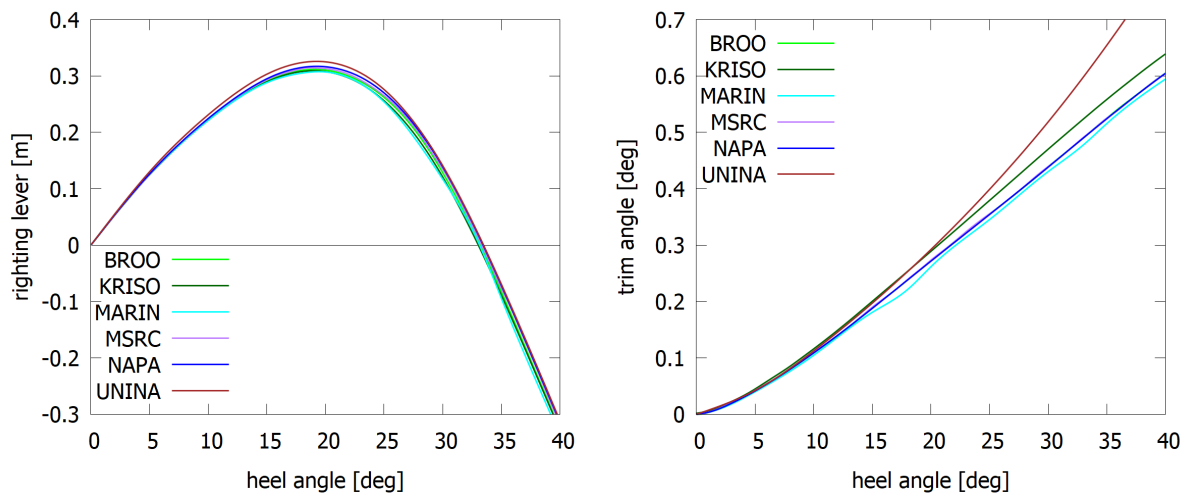


Figure 7.5 Comparison of the righting lever curve and trim angle for intact ship ( $GM = 1.505$  m) with different codes

### 7.3 Notes on Applied Simulation Codes

This part of the benchmark involves flooding of a large open vehicle deck of a ropax vessel. Consequently, the physics are somewhat different from the previous cases, and focusing more on progressive flooding. Moreover, different codes have different implementations on this matter, and therefore, a short summary provided by each participant is provided below:

#### BROO & MSRC

In the code PROTEUS ship motions are evaluated by solving a 4 DOF system of equation (yaw and surge not modelled) assuming the vessel is free drifting. Hydrodynamic forces are evaluated on a database approach, based on 2D strip theory calculations. Drift forces are modelled according to empirical formulations. Internal flow motions are modelled considering water as a lumped mass, assuming that the water level inside compartments/tanks is always parallel to the undisturbed sea water level. Compartments R1, R2, R3 and R4 have been considered as single rooms, the vehicle deck has been divided at the centreline. The code PROTEUS does not have an option for controlling the opening time of the breach, and thus instant opening was assumed. Consequently, BROO and MSRC did not provide results for part C1c.

#### HSVA

Shallow Water Equations (SWE) are used for the flooded compartments. Flow rates through the breaches is based on Bernoulli's equation. For damaged ship motions, roll motion + surge with ordinary differential equations, as well as linear strip theory and nonlinear hydrostatics in waves (based calculations from NAPA). Consequently, two non-linear DOFs and four linear DOFs in time domain. The SWE grid size was  $160 \times 30$  grid, altogether 3650 elements/cells for the vehicle deck and  $12 \times 28$  grid for both R1 (blue compartment) and R2. In all cases the dimensions of the grid were roughly 1.0 m for both longitudinal and transverse directions.

#### KRISO

The vehicle deck was divided into several compartments, connected internal openings, in order to model the vehicle deck appropriate to SMTP (inhouse code used by KRISO). the

floodwater is treated in two ways. One is a method in which the free surface remains horizontal. And another includes some dynamics of floodwater. The floodwater influences the ship dynamics by adding the mass and moving the center of gravity of the ship.

### **NAPA**

Flooding simulation in NAPA is primarily intended for progressive flooding analyses. All water levels are assumed horizontal, and therefore, the two damaged compartments below the vehicle deck were divided at the centerline (CL), and the parts connected by a large opening (size equal to the intersection of the room at CL).

### **UNINA**

The used numerical code is a Matlab/Simulink numerical code able to perform 6-DOF simulations of the ship behaviour both in intact and damaged conditions. The equations of motion in the time domain for a damaged ship account for all pertinent non-linearities. The hull is discretized to panels and the flooded water is modelled as a lumped mass, having a position that is restrained on a discrete three-dimensional path, depending on the amount of flooded water and free surface inclination in the longitudinal and lateral direction. The free surface of the floodwater is treated as a flat surface, but it can have different inclinations from the ship roll and pitch angles. The inclinations of the free surface are evaluated by the analogy with the pressure distribution in a liquid within a tank uniformly accelerated.

## **7.4 Case C1 – Transient Flooding in Calm Water**

### **7.4.1 Description**

The first case focuses on transient flooding of the ropax in calm water. A two-compartment collision damage amidships is studied, with three separate cases:

- C1a: transient flooding in calm water with intact  $GM = 1.505$  m (full-scale)
- C1b: transient flooding and capsize in calm water with smaller intact  $GM = 1.338$  m (full-scale)
- C1c: transient flooding when the breach is opened slowly,  $GM = 1.338$  m

The double bottom compartments (R4 and R5) are empty and are not open to the sea. The test setup is shown in Figure 7.6. The initial floating position and the breach opening times are given in Table 7.3 (in full-scale). These values were analysed by HSVA from the heave, roll and pitch signals averaged over the time range of 10 s just before the door opened. It should be noted that the small initial heel may be a result of remaining small amounts of water from the previous tests, and thus it might not be a clear indication of an asymmetric center of gravity of the model.

For the cases C1b and C1c the  $GM$  value at intact condition was considered as the largest  $GM$  still causing a capsize in calm water.



Figure 7.6 Test setup for transient flooding (courtesy of HSVA)

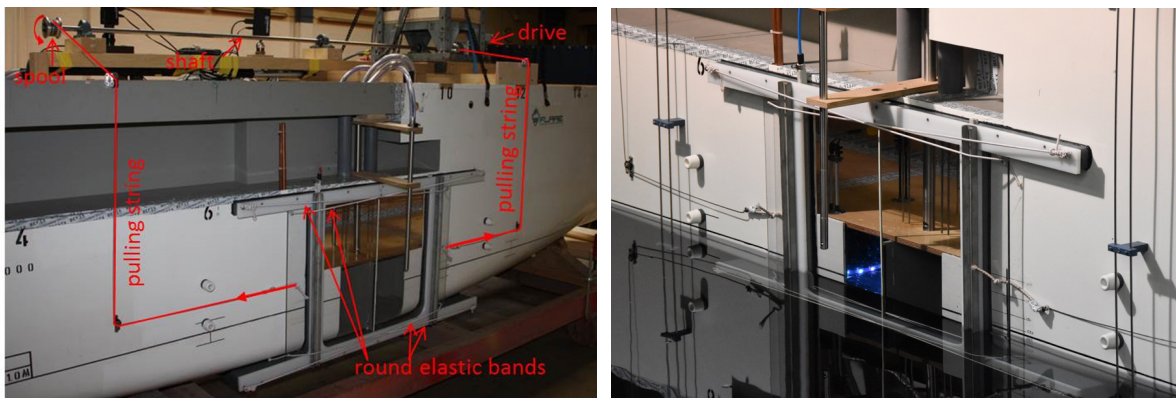


Figure 7.7 Sliding doors in front of the damage opening to allow transient flooding. Photo on the right was taken just before the door opening in the transient flooding tests in calm water (Courtesy of HSVA)

Table 7.3 Initial conditions for transient flooding in calm water

Case	HSVA test id	Initial heel (deg)	Initial trim (deg)	Opening time, lower comp. (s)	Opening time, upper comp. (s)
C1a (GM = 1.505 m)	2	-0.78	0.30	2.96	(3.81) <sup>1</sup>
C1b (GM = 1.338 m)	7	-0.52	0.30	1.80	(2.54) <sup>1</sup>
C1c (GM = 1.338 m)	17	-1.01	0.33	94.61	136.73

## 7.4.2 Results

Due to the momentum of the in-flow of water, the floodwater accumulates on the intact side, Figure 7.8, and the initial transient roll motion is also towards the intact side, with negative angles in Figure 7.9. The flooding case is very similar to the transient flooding of a box-shaped barge, studied by Manderbacka et al. (2015). This behaviour is characteristic for wide open compartments with a large breach opening, and thus very suitable for benchmarking.

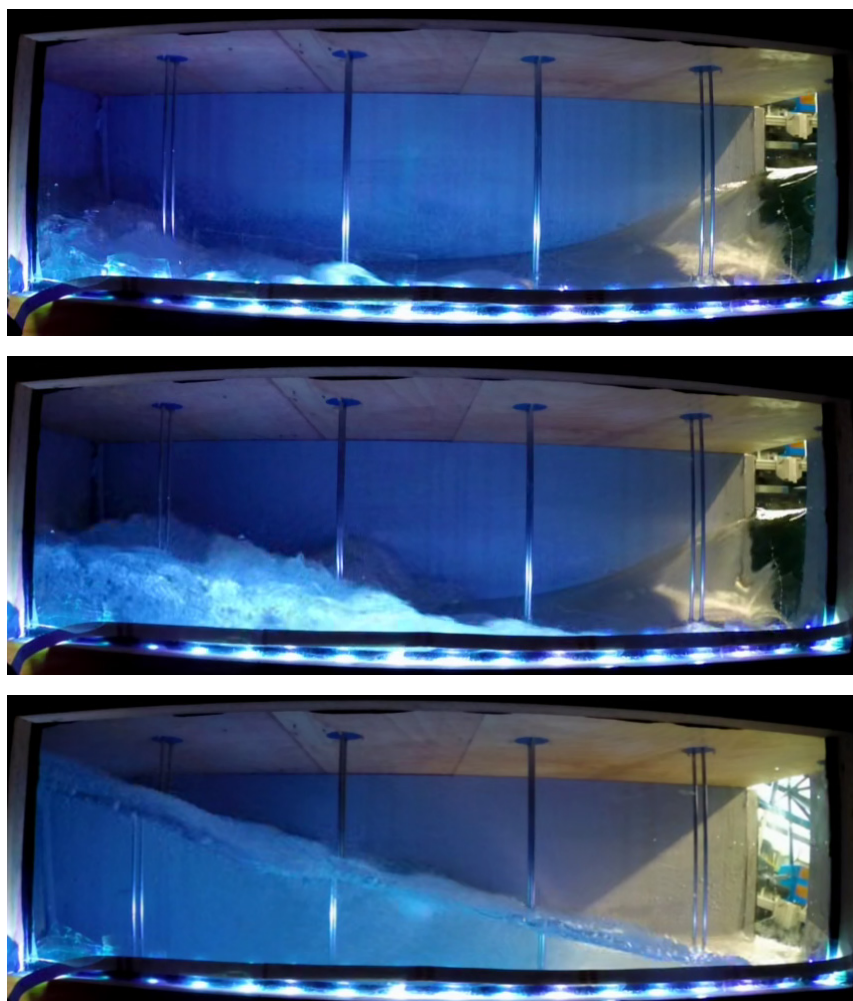


Figure 7.8 Transient flooding of the “blue compartment” R1 for case C1a, where water initially accumulates on the intact side (snapshots from video, courtesy of HSVA)

The code by KRISO predicts the development of roll motion very well, although the peak angle is slightly overestimated. HSVA and UNINA capture this transient heeling towards the intact side, but the magnitude is notably smaller. Also MSRC predicts the initial roll direction correctly, but this was found out to be very sensitive to the initial heel angle (with a zero initial heel, the roll direction was towards the damage). The quasi-static model in NAPA predicts a transient roll towards the damage.

Volumes of water in the compartments R1 and R2 are presented in Figure 7.10. Experimental data is available for R1, i.e. the “blue compartment”. Only KRISO and UNINA capture the

decrease in the volumetric flow rate after about 20 s. The center of floodwater in the “blue compartment” R1 is shown in Figure 7.11. For the first 120 s the variation in the transverse center of volume between the codes is very significant, clearly correlating with the observed differences in the roll angle. For the vertical center of volume all codes match rather well with the experimental result.

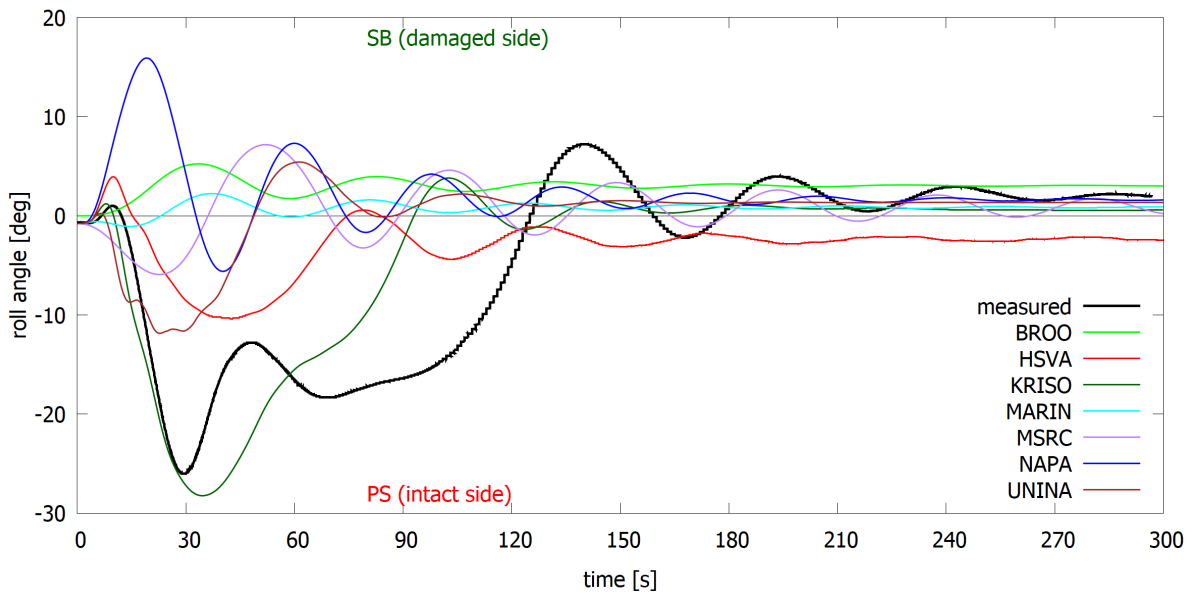


Figure 7.9 Measured and simulated development of roll angle for case C1a with  $GM=1.505$  m and rapid breach opening

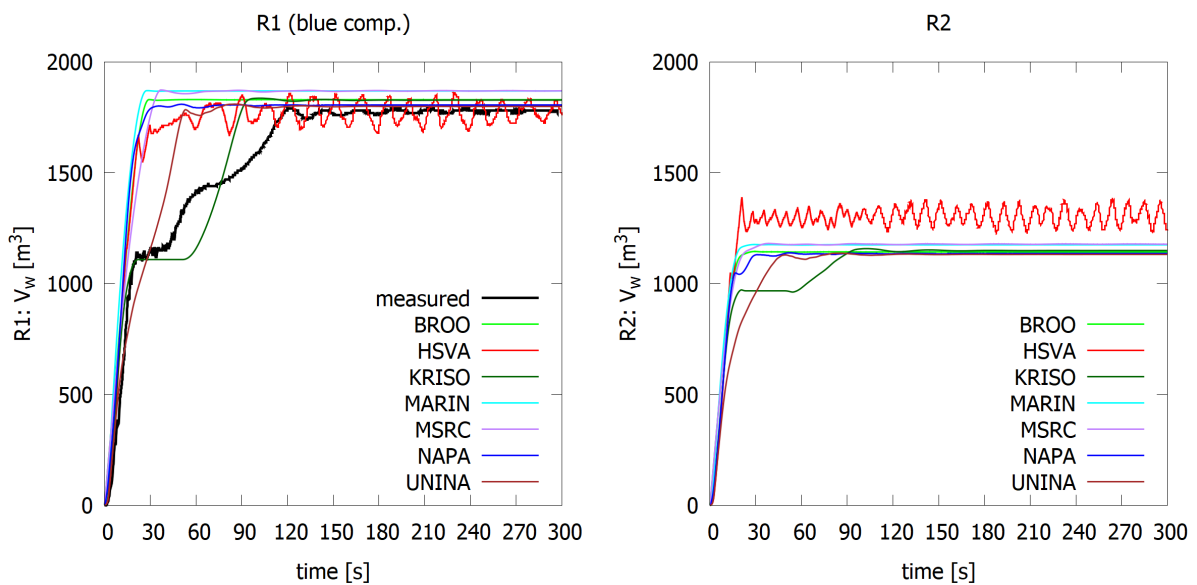


Figure 7.10 Volume of floodwater in the compartments for case C1a

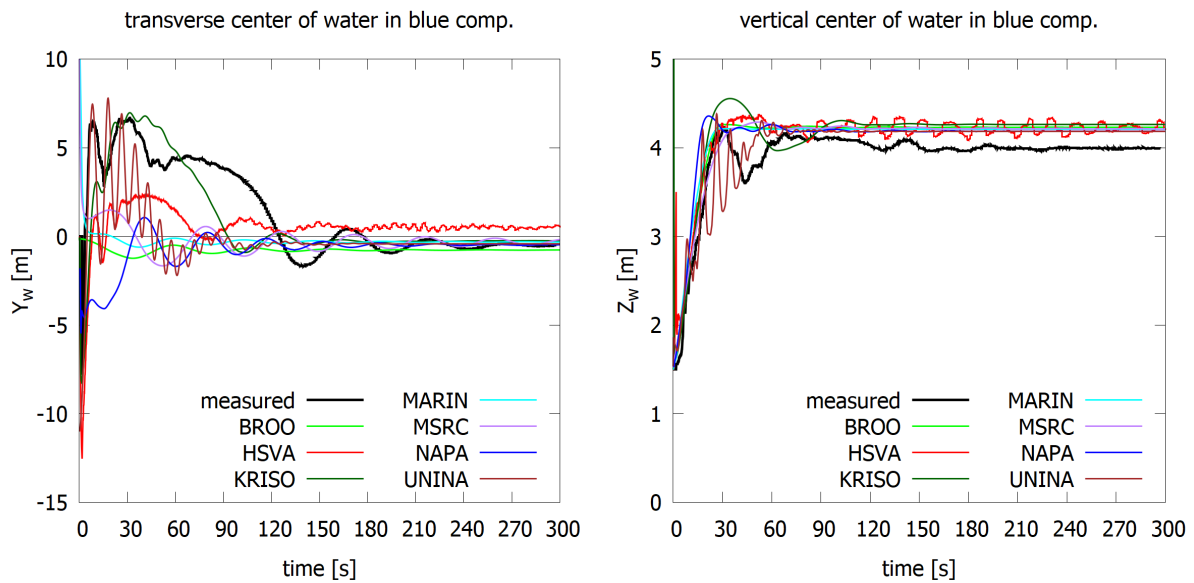


Figure 7.11 Transverse and vertical center of floodwater in the “blue compartment” R1 for case C1a

With a smaller GM value in the initial condition, the ship capsizes in transient flooding stage, Figure 7.12. All codes, except the one used by MARIN, correctly model that the ship capsizes. KRISO, UNINA and HSVA correctly predict that the ship capsizes to the intact side, whereas BROO, MSRC and NAPA simulations end in a capsize towards the damaged side.

There is quite a large variation in the time-to-capsize (TTC), and only KRISO simulation results matches very well the measured value of a roll angle up to almost 30°. Although, it should be noted that the capsize process is very rapid, and relatively large differences in TTC are not relevant for practical applications.

BROO and MSRC simulations result in roughly correct time-to-capsize, but the ship capsizes towards the damaged side. Both participants used the same PROTEUS code, and their difference in the TTC is likely due to the fact that BROO applied an upright initial condition, whereas MSRC considered the small initial heel angle.

The centroid of floodwater in the “blue compartment” R1 is presented in Figure 7.13. This explains the observed behaviour in the roll angle, as the codes predicting capsize to the damaged side have the transverse coordinate of the floodwater centroid on the wrong side of the ship. The results by KRISO match very well the measured value, which is obtained from the video recordings. HSVA predicts slower accumulation of the water in the intact side (positive Y-coordinate). UNINA results correspond well with the measurements but the fluctuations are much larger.

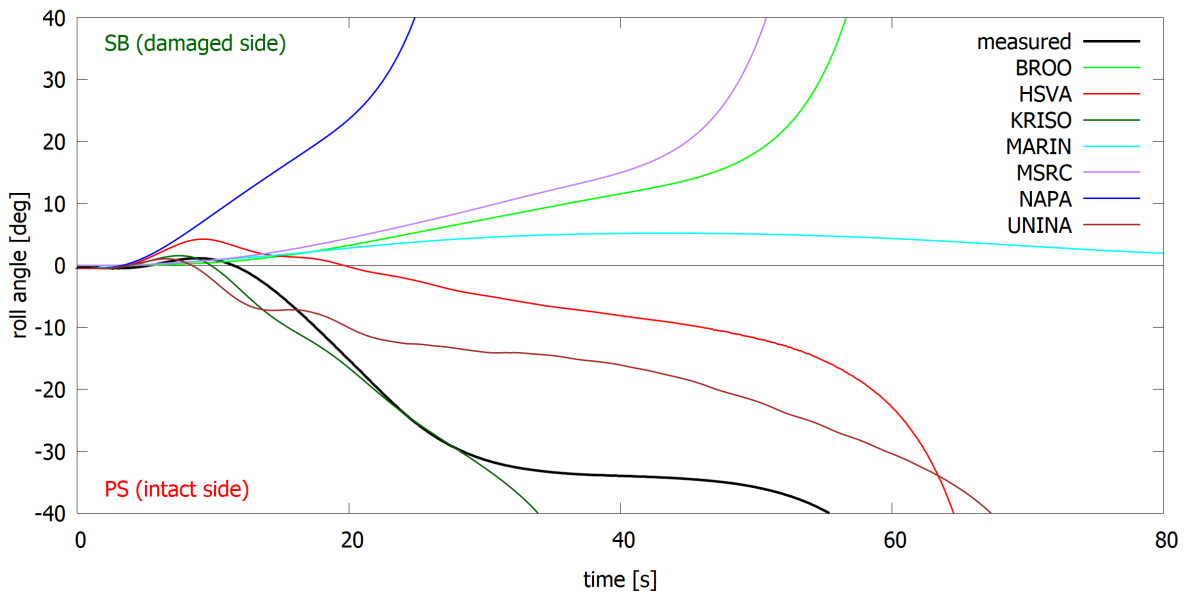


Figure 7.12 Measured and simulated development of roll angle for the case C1b with  $GM = 1.338$  m and rapid breach opening

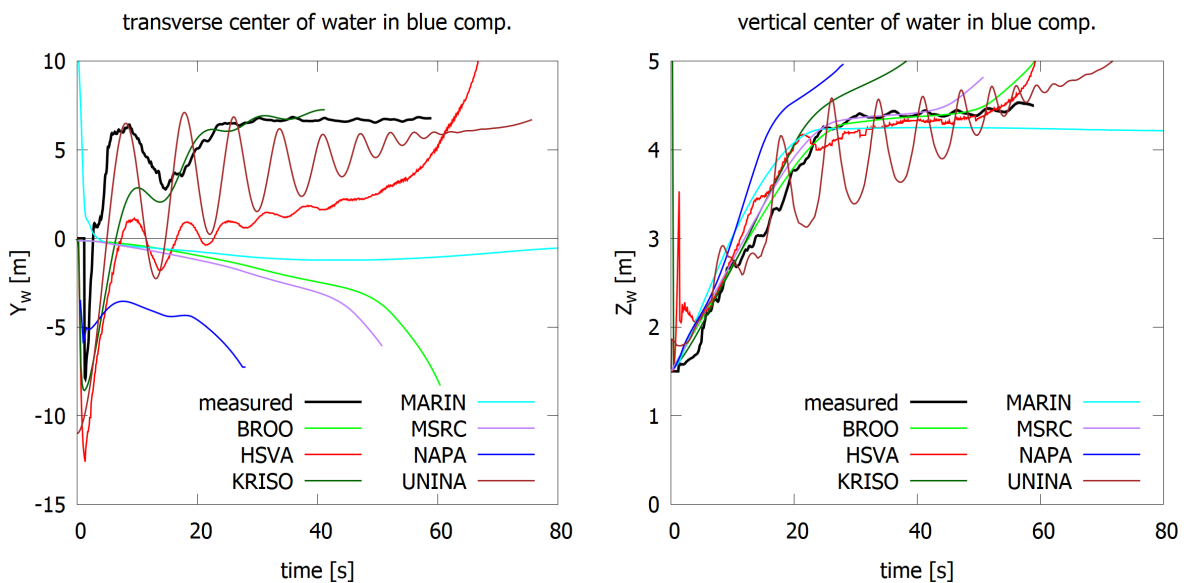


Figure 7.13 Transverse and vertical center of floodwater in the "blue compartment" R1 for case C1b

With the same lower initial GM value but when the breach is opened slowly, the time-to-capsize is much longer. The ship remains nearly upright for the first 45 s, and then starts to roll, and eventually capsizes, towards the intact side, Figure 7.14.

In the HSVA simulation the roll angle remains quite small for the first minute, although the angle is somewhat larger than measured. In addition, the capsize process is well predicted by HSVA. The code by KRISO predicts a faster transient heeling that is then temporarily decreased before the final capsize, which takes place somewhat faster than in the experiment. The simulation by

UNINA captures correctly initial flooding without a notable roll angle. The ship slowly heels towards the intact side, but instead of a capsize, a steady heel angle of about 20° is achieved. The simplified approach by NAPA predicts capsize towards the damaged side after about 40 s, due to the assumption of horizontal water levels in the flooded compartments.

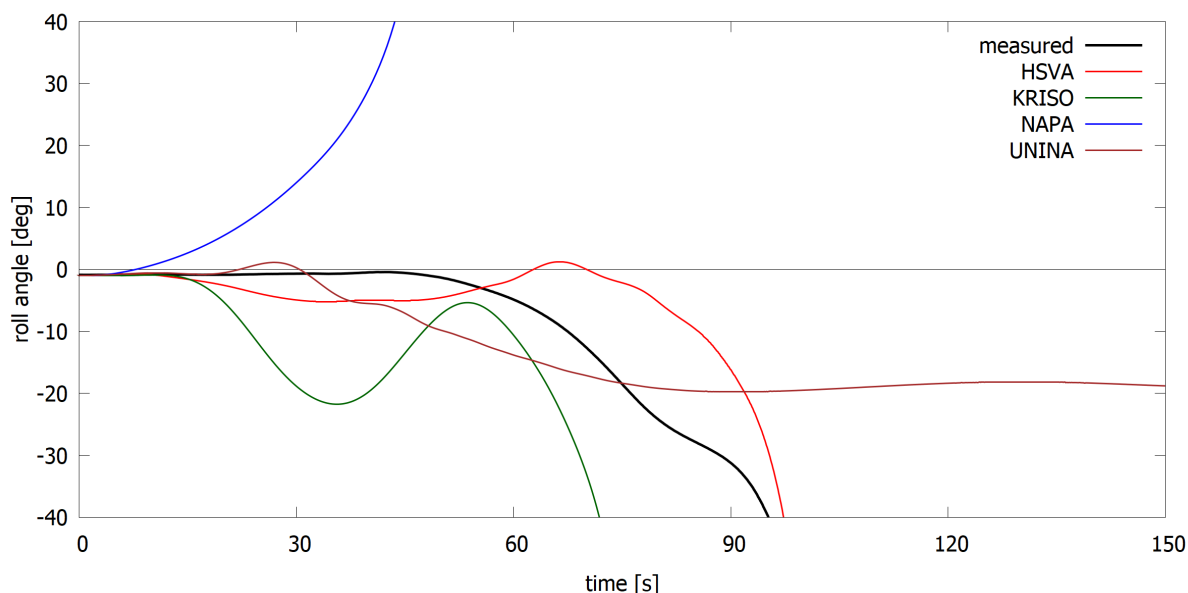


Figure 7.14 Measured and simulated development of roll angle for case C1c with  $GM = 1.338$  m and slow opening of the breach

## 7.5 Case C2 – Transient Flooding in Waves

### 7.5.1 Description

This part of the benchmark focuses on transient flooding in waves. In principle, the case is the same as in C1, but a slightly different initial GM value is used. The ship is in beam seas with the waves facing the damage. A JONSWAP wave spectrum with  $H_s = 4.0$  m and  $T_p = 10$  s is used. Participants were asked to provide results for 20 different wave realizations. Two variants of the initial condition are studied, as presented in Table 7.4.

The initial heel and trim values, Table 7.4, were analysed by HSVA from the heave, roll and pitch signals averaged over the time range of 10 s in calm water before the wave met the model for the tests in irregular seas. Two marginally different initial heel angles are studied. The breach is opened rapidly, and the measured opening times were provided to be used if the applied code has an option for this.

Contrary to the ITTC guidelines, a larger capsize limit of 40° was adopted, and consequently, also time-to-capsize (TTC) means the time frame from the beginning of flooding to reaching this roll angle.

Table 7.4 Initial conditions and breach opening times for benchmark part C2

Case	HSVA test id	Initial heel (deg)	Initial trim (deg)	Opening time, lower comp. (s)	Opening time, upper comp. (s)
C2a (GM = 1.425 m)	47,48,49	1.15	0.47	2.08	2.86
C2b (GM = 1.425 m)	43	-0.39	0.45	2.22	2.96

## 7.5.2 Results

The time histories of roll motions are presented in Figure 7.16 and Figure 7.17, for the 20 wave realizations by each simulation code for the two marginally different initial conditions. In addition, the measured roll is shown for the same initial conditions. In general, the capsizing of the ship is well captured, but the development of the roll angle is notably different and the time-to-capsize (TTC) is much shorter than measured.

As in the case of transient flooding in calm water (Part C1), there is a large transient heeling towards the intact side (negative roll angles), as shown in the video captures in Figure 7.15. Eventually, this is equalized, and in all test cases the ship capsized towards the damage.

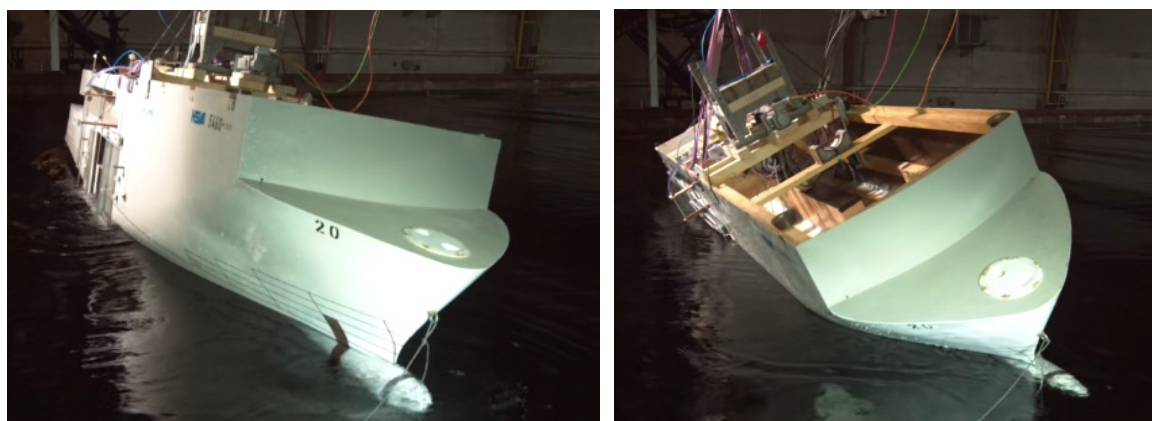


Figure 7.15 Video captures from the model test with transient roll towards intact side (left) and final capsize to damaged side (right), courtesy of HSVA

HSVA, NAPA and MSRC correctly capture the capsizing, but not the initial heeling away from the damage. However, one of the 20 simulations by MSRC capsizes towards the intact side. BROO used the same PROTEUS code as MSRC, but assumed the initial condition to be upright, and possibly because of this simplification the time-to-capsize is notably longer than in the simulations by MSRC. In fact, simulations by BROO predict well the TTC, but the transient roll towards the intact side is not captured.

KRISO simulation correctly captures the initial transient heeling, but only in 11 out of 20 simulations the ship capsizes, and always towards the intact side. Simulations by UNINA predict well the initial transient roll towards the intact side, and the eventual capsizing to the damaged side. In the case C2b several simulation results in a faster capsizing towards the intact side, which could be plausible since only one model test was conducted with the very a small initial heel towards the intact side, Figure 7.17.

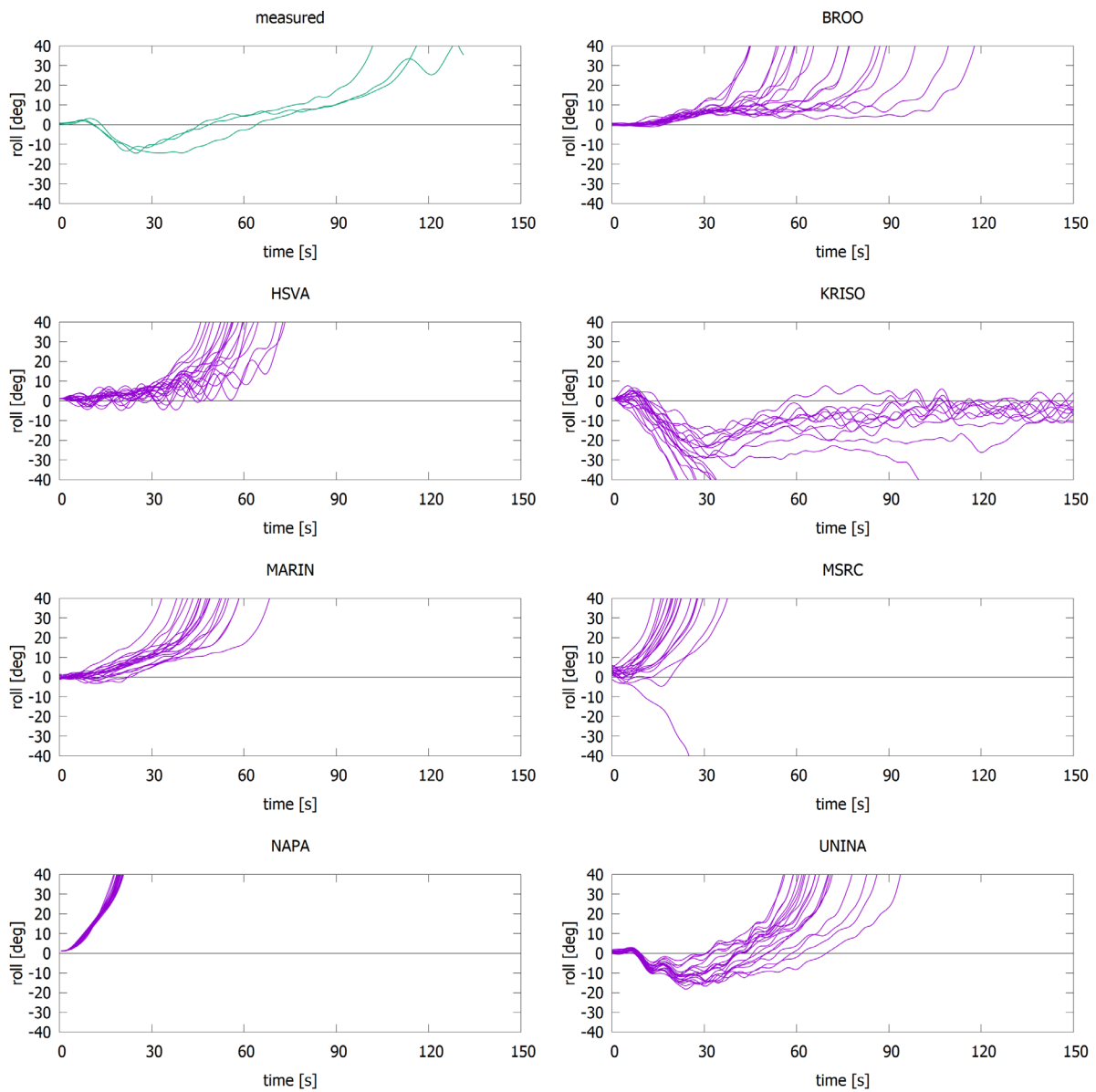


Figure 7.16 Time histories of roll motion for case C2a with 20 wave realizations using different simulation codes

In NAPA flooding simulation, currently only the wave pumping effects are considered, and direct impact of waves on ship motions are excluded. Therefore, a built-in limitation of significant wave height to half of the intact draught is applied. For the benchmark Part C2 simulations, this limitation was temporarily switched off. All 20 wave realizations resulted in a rapid capsizing. With the other codes, the dynamic ship motions in waves were considered.

It should be noted that a small change in the initial heel angle has a notable effect on the time-to-capsize. Cumulative density functions for both cases are shown in Figure 7.18. It should be noted that all simulation codes predict notably shorter time-to-capsizes than measured in the model tests.

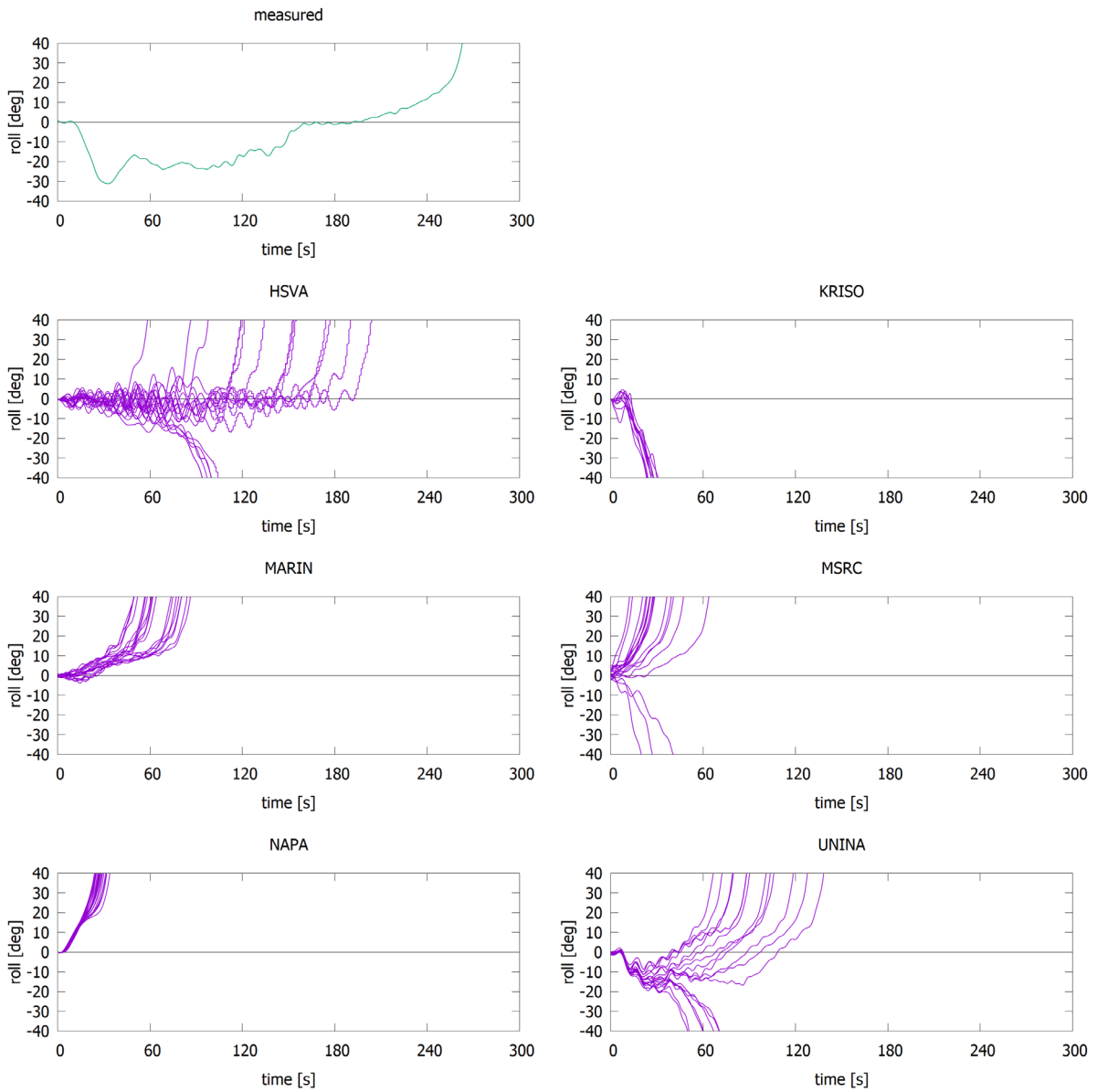


Figure 7.17 Time histories of roll motion for case C2b with 20 wave realizations using different simulation codes

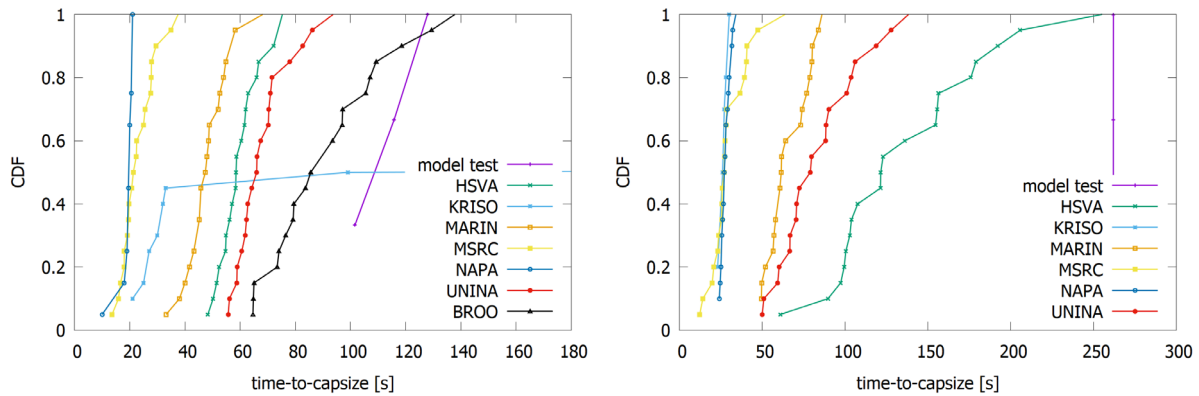


Figure 7.18 Cumulative density function for time-to-capsize for case C2a (left) and case C2b (right)

Table 7.5 Summary of results for time-to-capsize (TTC) in part C2

Participant	C2a					C2b				
	rep.	No. Caps	rate	TTC min	TTC max	rep.	no. Caps	rate	TTC min	TTC max
	-	-	-	s	s	-	-	-	s	s
measured	3	3	1.00	239.8	267.1	1	1	1.00	388.9	388.9
BROO	20	20	1.00	64.6	137.8	-	-	-	-	-
HSVA	20	20	1.00	48.3	75.3	20	20	1.00	60.8	255.2
KRISO	20	11	0.55	21.0	1517.0	10	10	1.00	24.0	30.0
MARIN	20	20	1.00	33.2	68.2	20	20	1.00	49.4	86.0
MSRC	20	20	1.00	13.6	37.5	20	20	1.00	12.2	63.7
NAPA	20	20	1.00	18.0	21.0	20	20	1.00	24.0	34.0
UNINA	20	20	1.00	55.7	93.7	20	20	1.00	49.9	138.3

The case C2 clearly demonstrate that in certain flooding scenarios the time-to-capsize can be very sensitive to the initial condition. A rather marginal difference in the initial heel angle between the cases C2a and C2b results in a large difference in the development of the roll angle, and especially on the eventual time-to-capsize. The details of the flooding and capsizing are not very well captured by the simulation methods, however, the final outcome, i.e. capsizing, is still correctly predicted.

## 7.6 Case C3 – Gradual Flooding in Waves

### 7.6.1 Description

The last part of the ropax benchmark focuses on a “Stockholm Agreement” type of damage case, where the ship is floating flooded in beam seas with the damage opening facing the waves. In this case also the double bottom compartments are open to sea. Since the transient flooding is not considered, the ship is first flooded in calm water before the waves are introduced, resulting in a fairly unrealistic condition, but the same approach has been used to study damage survivability of several ro-ro/passenger ferries over the past decades.

Two different sea states are investigated:

- C3a:  $H_s = 3.5\text{m}$  and  $T_p = 10\text{s}$
- C3b:  $H_s = 7.5\text{m}$  and  $T_p = 10\text{s}$

In both cases, JONSWAP wave spectrum is assumed, and simulations up to 30 min or capsizes (roll exceeds 40°) were performed for 20 wave realizations.

## 7.6.2 Results

In total five organizations provided simulation results. The capsizes frequencies and minimum and maximum observed time-to-capsize (TTC) are summarized in Table 7.6.

Time histories for roll motion are presented in Figure 7.19 for C1a with  $H_s = 3.5$  m, and in Figure 7.20 for C1b with  $H_s = 7.5$  m. Simulations by HSVA capture the capsizes frequency well for both cases. MSRC got good results for high waves in C3b, but in moderate waves the number of capsizes were underestimated. The same PROTEUS code was used by BROO with rather similar results in the case C3a. In moderate waves of C3a KRISO predicted zero capsizes, and in high waves of C3b the TTC was much shorter than in the model tests. MARIN simulations underestimated the capsizes frequency in C3a but the capsizes mechanism seems realistic.

Cumulative distributions for the time-to-capsize in both sea states are presented in Figure 7.21. In the case C3a, HSVA and MARIN simulations predicted a larger capsizes rate within 30 min and also a shorter TTC. Both BROO and MSRC underestimated the capsizes rate, whereas KRISO did not have any capsizes cases among the 20 samples. In extreme sea states with  $H_s = 7.5$  m, HSVA and MSRC both predict rather well the capsizes rate and TTC. In KRISO simulations the ship either capsizes rapidly or survives at least for the simulated 30 min. On the other hand, MARIN predicts longer TTC for the cases that end in capsizes, indicating that the capsizes rate could have been larger if the simulation time was longer.

It should be noted that in the model tests by HSVA the model was freely drifting, as assumed in the simulation codes (see section 6.5.3 on page 70).

Table 7.6 Summary of results for gradual flooding in waves in Part C3

Participant	C3a ( $H_s = 3.5$ m)					C3b ( $H_s = 7.5$ m)				
	rep.	no. Caps	rate	TTC min s	min roll deg	rep.	no. Caps	rate	TTC min s	min roll deg
measured	20	13	0.65	161.0	5.4	20	15	0.75	144.0	15.0
BROO	20	3	0.15	176.5	5.2	-	-	-	-	-
HSVA	20	15	0.75	64.7	2.7	20	18	0.90	164.1	30.4
KRISO	20	0	0.00	-	8.6	20	10	0.50	25.0	21.9
MARIN	20	17	0.85	0.0	8.8	20	6	0.30	19.0	2.1
MSRC	20	5	0.25	13.8	0.7	20	17	0.85	133.6	19.6

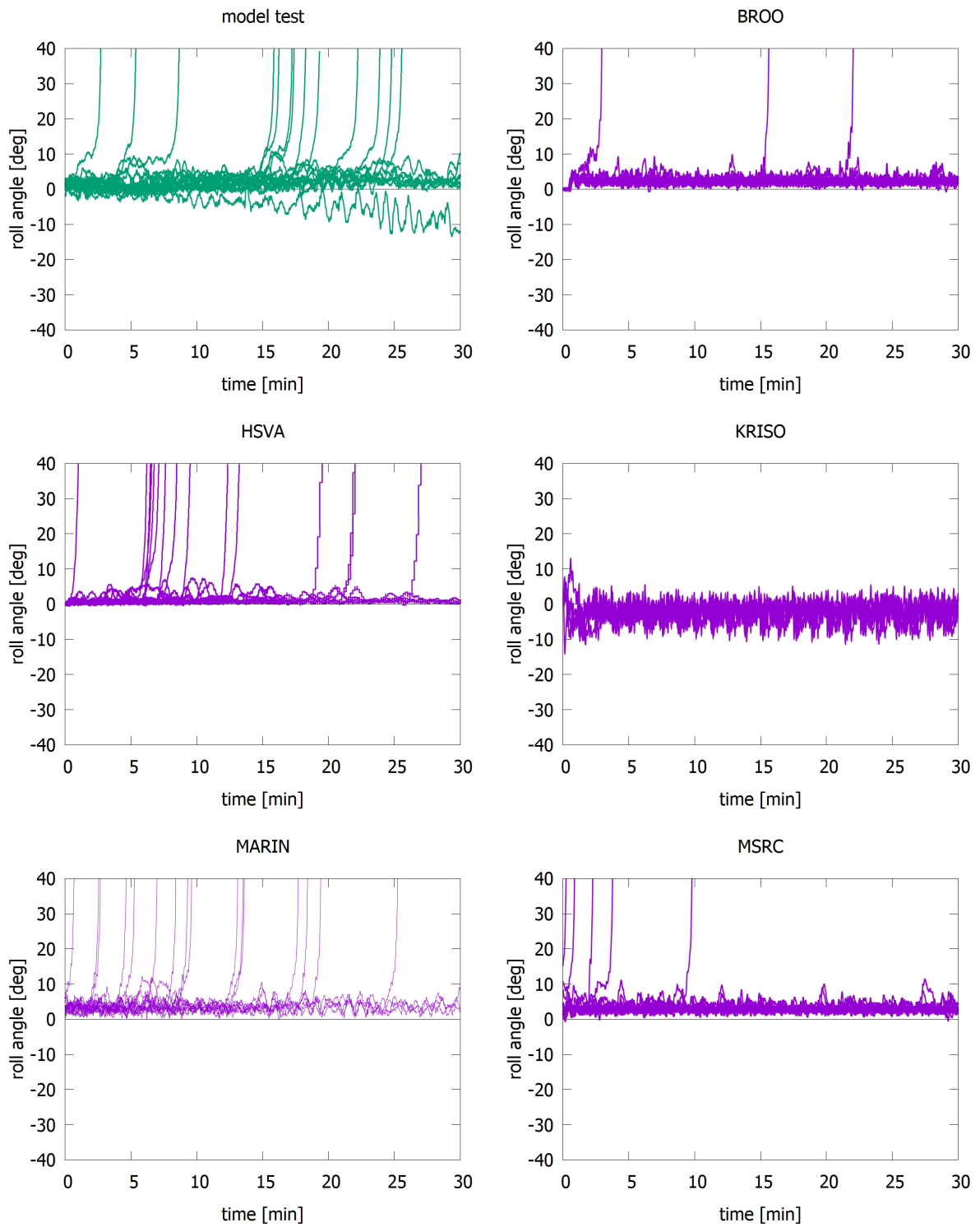


Figure 7.19 Measured and simulated roll angle for 20 wave realizations for case C3a with  $H_s = 3.5$  m

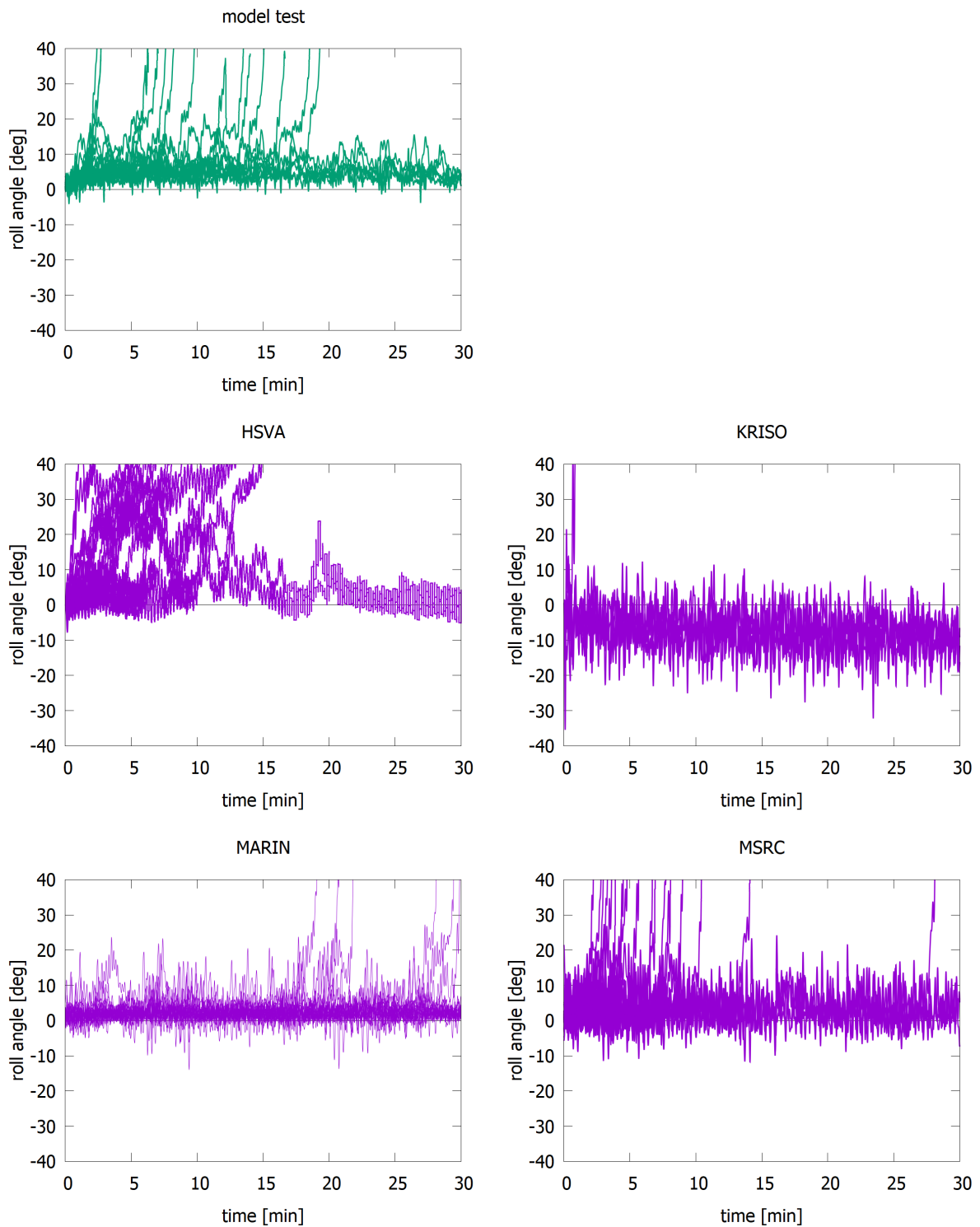


Figure 7.20 Measured and simulated roll angle for 20 wave realizations for case C3b with  $H_s = 7.5$  m

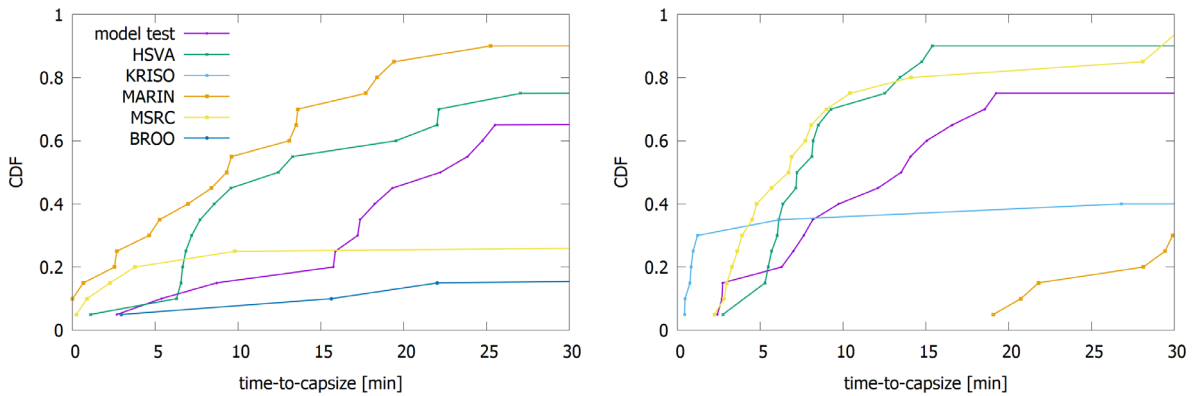


Figure 7.21 Cumulative distribution of time-to-capsize (TTC) for case C3a with  $H_s = 3.5$  m (left) and for case C3b with  $H_s = 7.5$  m (right)

## 7.7 Computational Performance

As in the previous parts of the benchmark, the computational performance of different simulation codes has been assessed based on relative computation time, i.e. the time spent in computations divided by the simulated time in full-scale. Obviously, the used hardware and applied modelling practices, such as time step and number of calculation sections or panels, can have a significant effect. The results for transient flooding in calm water (case C1a) and in irregular waves (case C2a) are presented in Figure 7.22 on a logarithmic scale. The differences are quite notable, and therefore, different hardware cannot be the only reason.

For some codes, namely KRISO, NAPA and UNINA, the simulation in waves seems to be notably slower than in calm water. However, it should be noted that at UNINA the cases were calculated with different hardware, and an older laptop was used for the cases in waves that most likely explains the much slower computation time.

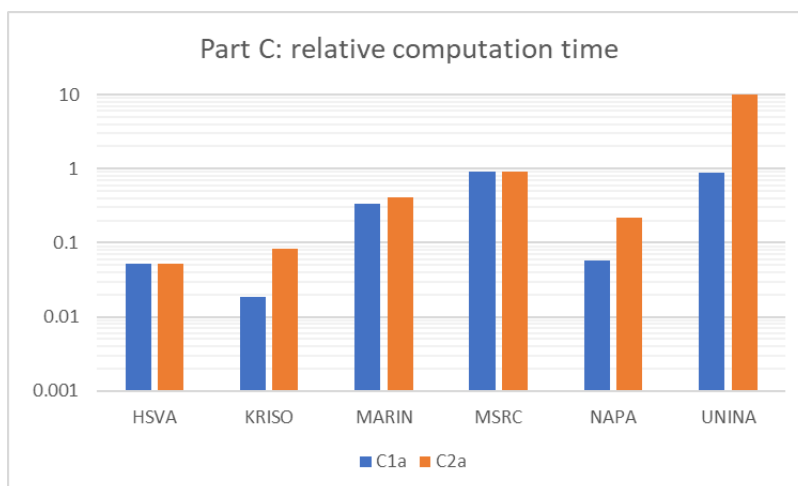


Figure 7.22 Relative computation times for the transient flooding of a ropax ship in calm water (C1a) and in waves (C2a)

## 8 SUMMARY AND CONCLUSIONS

Time-domain simulation of flooding and motions of damaged passenger ships is becoming a common practice for assessment of real survivability level in the event of a damage, especially for passenger ships. Within the project FLARE, these simulations have a significant role in the framework developed in WP5. Consequently, it is essential that such simulation codes are thoroughly validated against dedicated model tests. In order to get a wider perspective, also participants outside the FLARE consortium were invited to this benchmark study.

The study was organized in three separate parts, namely A, B and C, focusing on different aspects of the flooding and damaged ship motions. Some participants provided simulation results for all parts, while others concentrated on certain part only.

The first part of the benchmark focused on fundamental flooding mechanisms, with the following main conclusions:

- It was confirmed that most codes can satisfactorily simulate up and down flooding (A1 & A2). For such basic cases, the simple and fast, Bernoulli-based hydraulic simulation methods are in principle as accurate as computationally demanding CFD tools. Only one code had problems in calculation of simple up and down flooding, and it was identified that the problems were due to the implementation of the code, and not because of the applied Bernoulli-based simulation method.
- The deck flooding case (A4) demonstrated that progressive flooding along a long corridor cannot be captured by simple hydraulic models. With CFD codes this is properly modelled, but the computational time is extensive. The advanced approach by KRISO, considering also the momentum of floodwater, seems promising.
- The notable deviations in the simulation results between the Bernoulli-based codes when using same discharge coefficients indicates that different implementations of the time integration for the governing equations results in numerical error, at least for some codes. Naturally, also the applied time step may have an effect on this, but all participants should have ensured that a suitable time step is applied to minimize the numerical error.
- The computational performance of CFD codes is not suitable for practical assessment of survivability of damaged passenger ships. However, the detailed results on the flooding progression can be valuable for development and testing of simplified flooding simulation codes. Notable differences in the performance were also found between the Bernoulli-based simulation codes. When time-domain assessment of survivability is done for a large number of scenarios, the computational performance becomes more important.

The second part on cruise ship flooding provided more insight into the applicability of the simulation codes on flooding of a realistic geometry, considering both transient and progressive flooding stages. The results and observations are summarized in the following:

- An extensive three-compartment damage case was studied both in calm water (case B1) and in irregular beam seas with significant wave height of 4.0 m (case B2). In both cases, there was a large transient roll angle, and in waves the ship eventually capsized due to progressive flooding and accumulation of water on the upper decks due to the

waves. The last case (B3) had a smaller breach opening, and the case was characterized by notable up-flooding in the damaged compartments.

- The flooded compartments of the model reflected the general arrangement plan of the FLARE demo ship 3, prepared by Chantiers de l'Atlantique. Consequently, some compartments had very complex geometry, and some inaccuracies and differences between the numerical 3D models are quite likely. In addition, the pram type stern and large discontinuities in the waterplane area likely affected the inclining test, and resulted in uncertainties related to the initial condition for the model tests. For possible future benchmark study, a more simplified geometry of the compartments and a larger scale of the model should be considered. Also a simplified appendage geometry would have made it easier to ensure a consistent modelling of the buoyant hull form.
- Effects of air compression on the flooding and motions of the model could not be completely excluded, and consequently, in possible future model tests for benchmarking, measurement of air pressure in compartments that are rapidly flooded is considered essential.
- The qualitative behaviour of the transient roll motion and the capsize mechanism in beam seas was well captured, but there was a significant variation in the actual flooding progression for the compartments, also in calm water.
- The drifting effect during the flooding process was also identified as one potential explanation for the differences, since direct comparison of experiments with a softly moored model and numerical simulations with a freely drifting ship may not be reasonable.

The last part of the benchmark study consisted of transient flooding of a ropax vessel in calm water and in beam seas, including also a more conventional model test case with gradual flooding and capsizing in high waves.

- The final outcome (capsize or survival) of transient flooding in calm water was well captured by the codes. However, the floodwater inertia, and the resulting capsize towards the intact side could not be correctly modelled by the more simplified simulation methods.
- Also, capsize due to transient flooding in irregular beam seas was properly captured, but the capsize mechanism was in many cases very different from the model test. However, both the shallow water equations (SWE) and advanced pendulum models were found out to provide reasonably good results.
- It is worth noting that the benchmarking condition involves transient flooding of wide and empty compartments below the vehicle deck. This is somewhat unrealistic, since the various equipment and machinery in these compartments on real ships would have had an effect on the floodwater motions.
- The results for the capsize rate and time-to-capsize in the case of gradual flooding in high waves contained a lot of variation in the results.

Before drawing the final conclusions, it is essential to recall the main observations from the most recent ITTC benchmark studies:

- Papanikolaou and Spanos (2005) reported notable deviations between the numerical methods in the damage condition, which were considered to result from the different approaches to the effects of floodwater on ship motions.

- van Walree and Papanikolaou (2007) reported notable variation in the results for progressive flooding of a damaged box-shaped barge with simple internal geometry

Based on the results, the simulation tools have developed significantly since the last ITTC benchmark study, especially regarding fundamental flooding mechanisms, and most of the codes could correctly model both up- and down-flooding. The results for the deck flooding (case A4) were not very consistent, but the flooding progression was still fairly well captured by all codes.

The Benchmark parts B and C included extreme damage scenarios and transient capsizing cases that had not been included in previous studies. In general, the participating codes could properly reproduce the survival and capsize conditions, but especially regarding the transient flooding of large open compartments, the effects of the floodwater momentum can be essential, and many codes did not deal with this properly. Also, significant variation in the time-to-capsize was observed, for both the cruise and ropax ships.

The previous benchmark studies have considered only simulation tools based on Bernoulli's equation, but this time also CFD tools were included. The results show that such advanced methods can rather accurately model the flooding progression, but the computation times are much too long for use in practical work for survivability assessments for ships with complex internal arrangement and involving a large number of damage cases.

The wide participation in the benchmark study, including organizations outside the FLARE project consortium, shows that time-domain simulation tools are now more widely developed and used within the scientific community. The increased interest and wider expertise in dynamics of flooding and damaged ship stability pave way for further improvements.



## 9 ACKNOWLEDGEMENTS

In addition to the authors of the report (NAPA), the following people have contributed to the benchmark study by providing experimental data or simulation results, as well as comments to the draft versions:

- Maria Acanfora (UNINA)
- Henry Bandringa (MARIN)
- Rinnert van Basten Batenburg (MARIN)
- Luca Braidotti (UNITS)
- Shuxia Bu (CSSRC)
- Hendrik Dankowski (UAK)
- Katja Jakobsen (HSVA)
- Gyeong Joong Lee (KRISO)
- Francesco Mauro (MSRC)
- Alistair Murphy (BROO)
- Gennaro Rosano (UNINA)
- Eivind Ruth (DNV)
- Petri Valanto (HSVA)
- Riaan van't Veer (MARIN)

Especially the contributions from the external participants is gratefully acknowledged.

The CFD calculations by CSSRC were conducted in Wuxi National Computing Center.

Contributors from UNINA would also like to acknowledge the kind support of Prof. Riccardo Martino in updating the FloodW tool.



## 10 REFERENCES

- Acanfora, M., Cirillo, A. 2016. A simulation model for ship response in flooding scenario, Proceedings of the Institution of Mechanical Engineers, Part M: Journal of Engineering for the Maritime Environment, Vol. 231 (1), pp. 153-164. <https://doi.org/10.1177/1475090215627839>
- Acanfora, M., Cirillo, A. 2017. On the development of a fast modeling of floodwater effects on ship motions in waves, Proceedings of the Institution of Mechanical Engineers, Part M: Journal of Engineering for the Maritime Environment, Vol. 231(4), pp. 877-887. <https://doi.org/10.1177/1475090216687438>
- Acanfora, M., Begovic, E., De Luca, F. 2019. A fast simulation method for damaged ship dynamics, Journal of Marine Science and Engineering (Special Issue: Advances in Marine Dynamic Simulation), Vol. 7(4), pp. 1-14. <https://doi.org/10.3390/jmse7040111>
- Bandringa, H., Helder, J. A., & van Essen, S. 2020. On the Validity of CFD for Simulating Extreme Green Water Loads on Ocean-Going Vessels. In ASME 2020 39th International Conference on Ocean, Offshore and Arctic Engineering. American Society of Mechanical Engineers Digital Collection.
- Braidotti, L., Mauro, F. 2019. A new calculation technique for onboard progressive flooding simulation, Ship Technology Research, Vol. 66, no. 3, pp. 150-162. <https://doi.org/10.1080/09377255.2018.1558564>
- Braidotti, L., Mauro, F. 2020. A Fast Algorithm for Onboard Progressive Flooding Simulation, Journal of Marine Science and Engineering, 8(5):369. <https://doi.org/10.3390/jmse8050369>
- Bu, S., Gu, M., Lu, J. 2018. Prediction of damaged ship motions in waves in time domain [J]. Shipbuilding of China, 2018, Vol. 59, No.2, pp:80-89. (in Chinese)
- Bu, S., Gu, M. 2019. Study on damaged ship motion coupled with damaged flow based on the unified viscous and potential model, Proceedings of the 17th International Ship Stability Workshop, 10-12 June 2019, Helsinki, Finland, pp. 209-220.
- Bu, S., Gu, M. 2020. Unified viscous and potential prediction method for the coupled motion of damaged ship and floodwater in calm water, Ocean Engineering, Vol. 210, Article 107441. <https://doi.org/10.1016/j.oceaneng.2020.107441>
- Bu, S., Qi, J., Gu, M. 2020. Study on capsizing characteristics and influencing factors of damaged ship in regular waves. [J]. Shipbuilding of China, 2020, Vol. 61, No.4, pp:60-69. (in Chinese)
- Dankowski, H. 2013. A Fast and Explicit Method for the Simulation of Flooding and Sinkage Scenarios on Ships, PhD Thesis at Hamburg University of Technology.
- Dankowski, H., & Dilger, H. 2013. Investigation of the mighty servant 3 accident by a progressive flooding method. In International Conference on Offshore Mechanics and Arctic Engineering (Vol. 55317, p. V001T01A018). American Society of Mechanical Engineers. <https://doi.org/10.1115/OMAE2013-10342>
- Dankowski, H., Russell, P., & Krüger, S. 2014. New insights into the flooding sequence of the Costa Concordia accident. In International Conference on Offshore Mechanics and Arctic

Engineering (Vol. 45509, p. V08AT06A025). American Society of Mechanical Engineers. <https://doi.org/10.1115/OMAE2014-23323>

Dankowski, H., Krüger, S. 2015. Dynamic Extension of a Numerical Flooding Simulation in the Time-Domain, 12th International Conference on the Stability of Ships and Ocean Vehicles STAB2015, Glasgow, UK.

Idel'chik, I. E. 1960. Handbook of Hydraulic Resistance (translated from Russian), Published for the U.S. Atomic Energy Commission, Washington D.C.

ITTC 2002. The Specialist Committee on Prediction of Extreme Ship Motions and Capsizing – Final Report and Recommendations to the 23rd ITTC, Proceedings of the 23<sup>rd</sup> International Towing Tank conference, Volume II, pp. 619-748.

ITTC 2005. The Specialist Committee on Stability in Waves – Final Report and Recommendations to the 24th ITTC, Proceedings of the 24<sup>th</sup> International Towing Tank conference, Volume II, pp. 369-408.

ITTC 2008. The Specialist Committee on Stability in Waves – Final Report and Recommendations to the 25th ITTC, Proceedings of the 25<sup>th</sup> International Towing Tank conference, Volume II, pp. 605-639.

Jasionowski, A. 2001. An integrated approach to damage ship survivability assessment, PhD thesis, University of Strathclyde.

de Kat J., 2000. Dynamics of a Ship with Partially Flooded Compartment. Contemporary Ideas on Ship Stability, Elsevier, pp 249-263.

Katayama, T., Ikeda, Y. 2005. An Experimental Study of Fundamental Characteristics of Inflow Velocity from Damaged Opening, Proceedings of the 8th International Ship Stability Workshop, ISSW2005, Istanbul, Turkey, 6-7 October 2005.

Lee, G.J. 2015. Dynamic orifice flow model and compartment models for flooding simulation of a damaged ship, Ocean Engineering, Vol. 109, pp. 635-653. <http://dx.doi.org/10.1016/j.oceaneng.2015.09.051>

Manderbacka, T., Ruponen, P., Kulovesi, J., & Matusiak, J. (2015). Model experiments of the transient response to flooding of the box shaped barge. Journal of Fluids and Structures, 57, 127-143.

Papanikolaou, A., Spanos, D. 2001. Benchmark Study on the Capsizing of a Damaged Ro-Ro Passenger Ship in Waves – Final Report.

Papanikolaou, A., Spanos, D. 2005. The 24<sup>th</sup> ITTC Benchmark Study on Numerical Prediction of Damage Ship Stability in Waves – Final Report.

Papanikolaou, A., Spanos, D. 2008. Benchmark Study on Numerical Codes for the Prediction of Damage Ship Stability in Waves, ISSW2008.

Ruponen, P. 2007. Progressive Flooding of a Damaged Passenger Ship, Dissertation for the degree of Doctor of Science in Technology, TKK Dissertations 94, 124 p.

Ruponen, P., Sundell, T., Larmela, M., 2007. Validation of a simulation method for progressive flooding. International Shipbuilding Progress, Vol. 54, pp. 305-321.

- Ruoponen, P., Kurvinen, P., Saisto, I., Harras, J. 2010. Experimental and Numerical Study on Progressive Flooding in Full-Scale, Transactions of Royal Institute of Naval Architects, Vol. 152, Part A4, International Journal of Maritime Engineering, pp. A-197-207.
- Ruoponen, P. 2014. Adaptive time step in simulation of progressive flooding, Ocean Engineering, Vol. 78, pp. 35-44.
- Ruth, E., Olufsen, O., Rognebakke, O. 2019. CFD in damage stability, Proceedings of the 17th International Ship Stability Workshop, 10-12 June 2019, Helsinki, Finland, pp. 259-263.
- Santos, T.A., Winkle, I.E., Guedes Soares, C. 2002. Time domain modelling of the transient asymmetric flooding of Ro-Ro ships, Ocean Engineering, Vol. 29, Issue 6, pp. 667-688. [https://doi.org/10.1016/S0029-8018\(01\)00037-3](https://doi.org/10.1016/S0029-8018(01)00037-3)
- van't Veer, R., 2001. Model Test Results PRR02, Report (3-31-D-2001-07-0), European Commission research project on Harmonization of Rules and Design Rationale HARDER.
- Veldman, A. E., Luppens, R., van der Heiden, H. J., van der Plas, P., Düz, B., & Huijsmans, R. H. 2014. Turbulence modeling, local grid refinement and absorbing boundary conditions for free-surface flow simulations in offshore applications. In ASME 2014 33rd International Conference on Ocean, Offshore and Arctic Engineering. American Society of Mechanical Engineers Digital Collection.
- van Walree, F., Papanikolaou, A. 2007. Benchmark study of numerical codes for the prediction of time to flood of ships: Phase I, Proceedings of the 9<sup>th</sup> International Ship Stability Workshop ISSW2007, Hamburg, Germany.
- van Walree F., Carette, N. 2008. Benchmark study on numerical codes for the prediction of the time to flood of ships – phase II, ISSW2008.
- Ypma, E.L., Turner, T. 2019. An approach to the validation of ship flooding simulation models, Contemporary Ideas on Ship Stability. Springer, Cham, pp. 637-675.



## 11 ANNEXES

### 11.1 Annex A: Public summary

An extensive benchmark study on time domain simulation of flooding and motions of damaged ships was conducted with the project FLARE. In addition to the FLARE partners, also other organizations with recent publications on this topic were invited to participate. Eventually, a total of 11 organizations contributed to one or several parts of the study.

The benchmark study was organized between June 2020 and April 2021, and the test cases were divided into three separate parts:

- Part A: flooding fundamentals with simplified geometries and fixed floating positions
- Part B: transient and progressive flooding of a cruise ship in calm water and in irregular waves
- Part C: flooding of a ropax ship, considering transient flooding in calm water and in irregular waves, as well as gradual flooding of the vehicle deck in high waves

Most of the codes could correctly predict basic cases of up- and down-flooding. Even the extensive progressive flooding on a deck arrangement was well captured, although only CFD codes could capture the details accurately. Moreover, the variation in the results among the codes using Bernoulli's equation, and the same discharge coefficients, was larger than expected.

The motions of a damaged cruise ship in transient flooding were well captured in calm water, although significant deviation between different codes was observed, especially for the water levels in the flooded compartments. Progressive flooding in waves after transient flooding proved to be more problematic, and time-to-capsize was not accurately predicted.

The ropax ship flooding cases were challenging as floodwater momentum caused transient roll motions, and even capsizes, towards the intact side. Yet, some codes provided very good results. However, the final outcome of the transient flooding, either survival or capsizes, was correctly predicted, but the time-to-capsize varied significantly, especially in waves.

Calculation of flooding progression has significantly improved since the previous benchmark study. However, needs for further development were also identified, and the FLARE benchmark study results are considered an important step on the way for improving the flooding simulation tools of the future.

Name of responsible partner: NAPA

Name of responsible person: Dr. Pekka Ruponen

Contact info (e-mail address etc.): [pekka.ruponen@napa.fi](mailto:pekka.ruponen@napa.fi)



## 11.2 Annex B: Sensitivity Analyses for Cruise Ship Flooding Cases

The simulation results in Part B, cruise ship flooding, were found out to be rather sensitive to the applied vertical center of gravity. Consequently, some participants provided results with a slightly different input.

The cruise ship design used has a pram type stern, and there are large discontinuities in the waterplane area around the studied draft of 8.2 m (in full scale). Moreover, the concave hull, as shown in Figure 11.1, means “holes” in the calculated waterplane area Figure 11.2, and this affects the calculated metacentric radius. Depending on how the hull form is modelled, in some codes the holes may not be present, and thus the direct comparison of actual GM values is not very relevant.

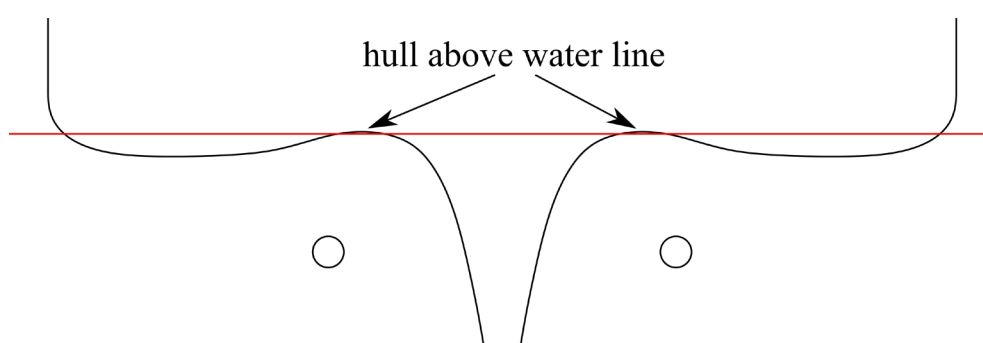


Figure 11.1 Section at  $X = 9.5$  m (full scale) from the NAPA model of the cruise ship in Part B showing the concave part that is partly above the water level at draft of 8.2 m



Figure 11.2 Waterplane area at draft of 8.2 m from the NAPA model of the cruise ship

Based on upright hydrostatics and location of transverse metacenter, MARIN obtained the vertical center of gravity for the given intact condition as  $KG = 17.63$  m. However, preliminary simulation of transient flooding in calm water, case B1, resulted in a too large steady heel angle, Figure 11.3, indicating that the applied  $KG$  is too high.

Based on analysis of the righting lever curve values in the inclining test condition, MARIN concluded that  $KG = 17.45$  m is likely representing well the actual test condition. With this  $KG$  value the final heel angle of the simulation matches well with the measurement, Figure 11.3.

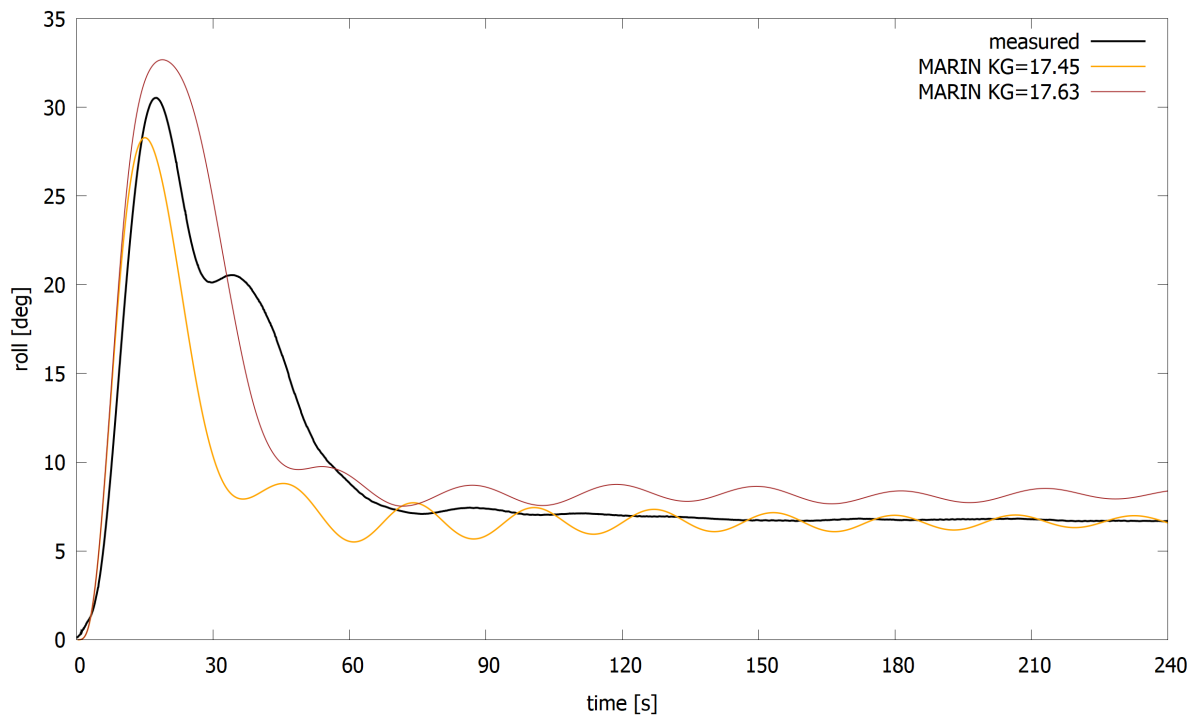


Figure 11.3 Preliminary simulation results for B1 by MARIN with two different KG values

MSRC conducted a similar analysis with simulations using different KG values, and different modelling approaches for the cross-flooded compartments on decks 0 and 1, Figure 11.4. With divided compartments and  $KG = 17.6$  m, calculated from the provided  $GM = 2.36$  m, the ship capsized immediately. With undivided compartments the final steady heel angle matched well with the experiments, but the transient roll motion was not properly captured. Moreover, since it seemed that the static righting moments at larger heel angles were much smaller than with other codes, a lower KG value of 17.50 m was adopted to be used for the benchmark simulations. With this KG value, only the large U-shaped room in the aftmost breached compartment needed to be undivided to avoid capsizing. Other cross-flooded rooms were divided at centerline with openings. Also, a low  $KG = 17.3$  m with all cross-flooded rooms divided was tested, but this resulted in a too small steady heel angle in the final condition.

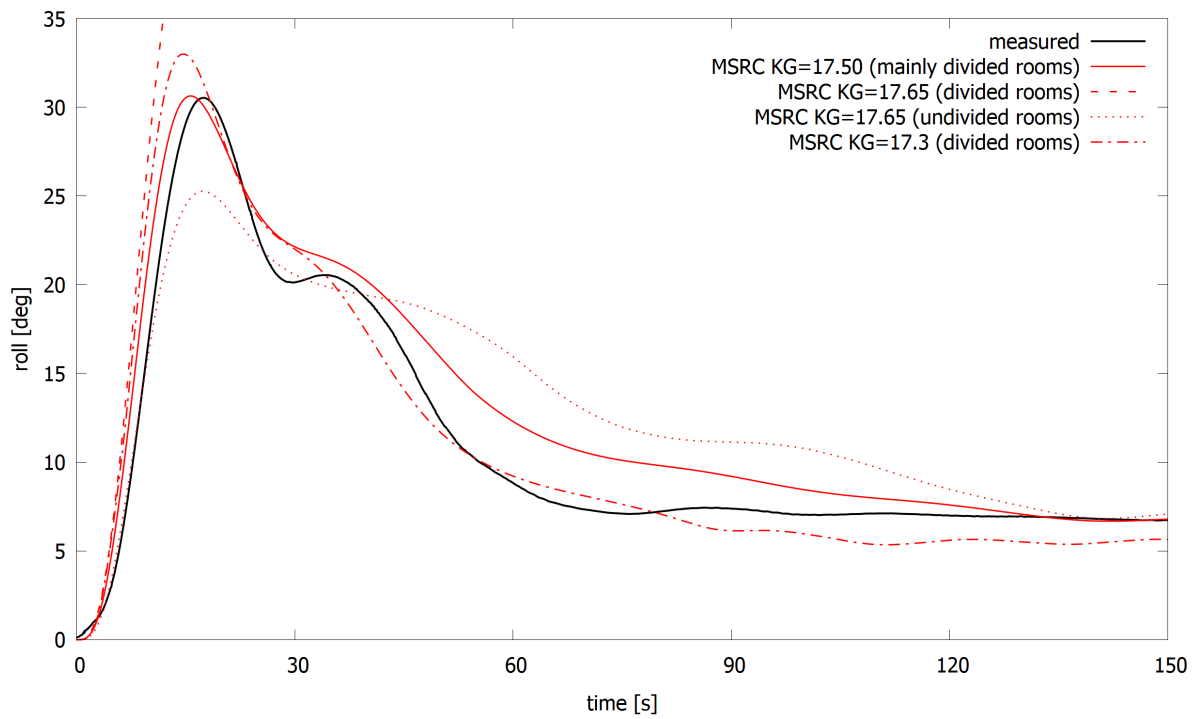


Figure 11.4 Simulation results for B1 by MSRC with different KG values and modelling of the compartments on Decks 0 and 1.